TRANSCRIPTIONAL PROFILING OF THE INFLAMED PERITONEUM

A Thesis submitted to Cardiff University in accordance to the requirements for the degree of Doctor Philosophy in the School of Medicine

by

Javier Uceda Fernández BSc (Hons)

March 2018

Declaration

This work has not been submitted in substance for any other degree or award at this or any other university or place of learning, nor is being submitted concurrently in candidature for any degree or other award.

Signed …… (candidate) Date ……

STATEMENT 1

This thesis is being submitted in partial fulfillment of the requirements for the degree of PhD.

Signed …… (candidate) Date ……

STATEMENT 2

This thesis is the result of my own independent work/investigation, except where otherwise stated, and the thesis has not been edited by a third party beyond what is permitted by Cardiff University's Policy on the Use of Third Party Editors by Research Degree Students. Other sources are acknowledged by explicit references. The views expressed are my own.

Signed …… (candidate) Date ……

STATEMENT 3

I hereby give consent for my thesis, if accepted, to be available online in the University's Open Access repository and for inter-library loan, and for the title and summary to be made available to outside organizations.

Signed …… (candidate) Date ……

STATEMENT 4: PREVIOUSLY APPROVED BAR ON ACCESS

I hereby give consent for my thesis, if accepted, to be available online in the University's Open Access repository and for inter-library loans after expiry of a bar on access previously approved by the Academic Standards & Quality Committee.

Signed …… (candidate) Date ……

Summary

Interleukin (IL)-6 is a pleiotropic cytokine associated with host defence, resolution of inflammation and chronic disease progression. During acute bacterial peritonitis, mice lacking IL-6 are unable to contain infection and display increased bacterial dissemination. To understand how IL-6 contributes to the local containment of infection, studies established an RNA-sequencing and bioinformatics pipeline to examine the role of the stromal tissue compartment in anti-microbial host defence. Investigations compared the host response to infection during both acute resolving peritoneal inflammation and under an inflammatory situation where pro-fibrotic CD4 T-cells contribute to the immune response. Molecular pathway analysis identified roles for IL-6 acting *via* the Jak-STAT signalling pathway in iron sequestration, complement regulation, and the control of leukocyte adhesion and activation. For example, stromal IL-6 signalling orchestrated responses relevant to the priming or activation of neutrophils, and infiltrating peritoneal neutrophils from infected *Il6*$^{-/-}$ mice displayed impaired phagocytic and respiratory burst capabilities. Previously we have shown that the IL-6-mediated expansion of peritoneal interferon (IFN)-γ-producing CD4 T-cells (Th1 cells) promotes peritoneal fibrosis in response to recurrent bacterial peritonitis. To mimic this environment, acute resolving inflammation was established in mice receiving *ex vivo* expanded Th1 cells. The presence of Th1 cells promoted IFN-γ-mediated STAT1 signalling in the peritoneum, which altered the expression of genes associated with the homeostatic turnover of extracellular matrix. Importantly, the presence of these cells also rescued the defective anti-microbial activities observed in the membrane of *Il6*$^{-/-}$ mice. This recovery was associated with a shift in the relative activation of STAT1 over that of STAT3. Taken together, these data provide a novel holistic view of IL-6 signalling in stromal tissue, and highlights the importance of STAT1 and STAT3 in shaping the course of inflammation and the host response to infection.

Acknowledgements

The past three and a half years have been incredibly intense, enjoyable and rewarding, and this thesis would not have been possible without the inestimable help of many people.

First, I would like to thank especially Professor Simon Jones for being a constant source of inspiration during my PhD; for giving me the opportunity to spend two months in his lab on the summer 2013, when this journey truly started, and for his professional and personal support and advice throughout all these years. Especial mention as well for Dr Gareth Jones, who convinced me that the weather in Cardiff would always be as nice as that summer, and who has always been incredibly helpful and keen on discussing any questions I had.

I would like to thank Dr Anna Cardus for showing me the insights of molecular biology and for helping me from the very first day: those sessions in "The Cave" won't be forgotten. Especial thanks to Dr Robert Andrews, with whom I spent countless hours waiting for script to run while sharing our experiences in dancing a singing. To Dr Jason Twohig, whose inquisitive questions always made me give a twist to any preconceived idea that I had. And to the rest of the members of the team: David Hill, for all the time spent swimming, playing squash and preparing libraries and talks; Alicia Derrac, for bringing light to the office; Ben Cossins, for his infinite patience teaching me 'R' and for coping with all the stuff that I've kept piling on his desk over the past months; Dr Rob Jenkins, who is the ultimate cause of that piling and a great opponent for epic snowball battles; and Dr David Millrine, for those endless 18 h sessions in the lab. Important mention as well to Dr Barbara Szomolay, for her time clustering the genes together, and all the people of the Haydn Ellis for taking me in during the sequencing period.

An essential part of this thesis belongs to all my friends, the ones I made here in Cardiff and the ones from back home and around the world. The constant laughs, dinners, beer sessions (either live of *via* skype), philosophical talks, dancing, trips and coffees have made these three and half years absolutely incredible. Thank you for making me realise that home is not a place, but a feeling. You have been part of each and every single experience I've had here, and I could not have done this without you.

Finally, to my parents, who have always encouraged me to follow my dreams and supported me in everything I have done, and whose constant source of strength have made the 1,231.01 km than separate Madrid to Cardiff feel like nothing.

I have left the PhD with the same enthusiasm for science than I had when I started it. And while some would say this is the end, it only feels like the beginning.

This one is for all of you…

Publications and presentations

PUBLICATIONS

Fielding, C.A., Jones, G.W., McLoughlin, R.M., McLeod, L., Hammond, V.J., **Uceda Fernández, J**., Williams, A.S., Lambie, M., Foster, T.L., Liao, C-T., Rice, C.M., Greenhill, C.J., Colmont, C.S., Hams, E., Coles, B.A., Kift-Morgan, A., Newton, Z., Craig, K.J., Williams, J.D., Williams, G.T., Davies, S.J., O'Donnell, V.B., Taylor, P.R., Jenkins, B.J., Topley, N., & Jones, S.A. **'IL-6 Signaling Drives Fibrosis in Unresolved Inflammation'**. Immunity 40: 40-50 (2014).

Catar, R., Witowski, J., Zhu, N., Lücht, C., Derrac Soria, A., **Uceda Fernández, J.**, Chen, L., Jones, S.A., Fielding, C.A., Rudolf, A., Topley, N., Dragun, D., & Jörres, A. **'IL-6 trans-signaling links inflammation with angiogenesis in the peritoneal membrane'**. Journal of American Society of Nephrology. November 11, 2016.

Isabel G. Azcárate, Sandra Sánchez-Jaut, Patricia Marín-García, María Linares, Susana Pérez-Benavente, Marta García-Sánchez, **Javier Uceda Fernández**, Ali N. Kamali, María-Josefa Morán-Jiménez, Antonio Puyet, Amalia Diez, José M. Bautista. **'Iron supplementation in mouse expands cellular innate defences in spleen and defers lethal malaria infection'**. BBA - Molecular Basis of Disease 1863 (2017) 3049–3059

Javier Uceda Fernández, David Millrine, Simon A. Jones. **'Tracking Competent Host Defence to Chronic Inflammation: An *In vivo* Model of Peritonitis'**. Methods in Molecular Biology**.** January 11, 2018.

Jason P. Twohig, Ana Cardus Figueras, Robert Andrews, Florian Wiede, Benjamin C. Cossins, **Javier Uceda Fernández**, Alicia Derrac Soria, David Hill, Xiao Liu, Barbara Szomolay, David Millrine, Christopher J. Pepper, Philip R. Taylor, Tony Tiganis, Nigel M. Williams, Gareth W. Jones & Simon A. Jones. **'Naïve T-cell activation re-tunes STAT signaling to deliver unique cytokine responses in memory CD4 T-cells'**. *In revision with Nature Immunology*

PRESENTATIONS

Javier Uceda Fernández, A. Cardus, G. W. Jones, S. A. Jones. Division of Infection and Immunity Annual Meeting (November 2015). **'Understanding the transition from competent host defence to inflammation-induced tissue damage'**. (Poster)

Javier Uceda Fernández, A. Cardus, G. W. Jones, S. A. Jones. Cardiff University School of Medicine Postgraduate Research Day (December 2015). **'Understanding the transition from competent host defence to inflammation-induced tissue damage'**. (Poster)

Javier Uceda Fernández, A. Cardus, C. M. Rice, R. Andrews, B. C. Cossins, J. P. Twohig, P. R. Taylor, N. M. Williams, G. W. Jones, S. A. Jones. 4th Annual Meeting of the International Cytokine and Interferon Society (ICIS)16-19 October 2016, San Francisco, CA, USA. **'Modification of Acute Inflammation as a Consequence of Recurrent Inflammatory Challenge'**. (Poster)

Javier Uceda Fernández, A. Cardus, C. M. Rice, R. Andrews, B. C. Cossins, J. P. Twohig, P. R. Taylor, N. M. Williams, G. W. Jones, S. A. Jones. Division of Infection and Immunity Annual Meeting (November 2016). **'Modification of Acute Inflammation as a Consequence of Recurrent Inflammatory Challenge'**. (Poster)

Javier Uceda Fernández. Division of Infection and Immunity Seminar Series, School of Medicine, Cardiff University November (November 2016). **'Modification of acute inflammation as a consequence of recurrent inflammatory challenge'**. (Oral)

Javier Uceda Fernández. Division of Infection and Immunity Annual Meeting (November 2017). **'Impact of IL-6 in the transcriptome profile of stromal tissue following acute resolving inflammation'**. (Oral)

Javier Uceda Fernández. Cardiff University School of Medicine Postgraduate Research Day (January 2018). **'Ups and Downs during your PhD: Discovery of a soluble form of gp130 in mice'**. (Oral)

Abbreviations

ADAM	Adamylsin and disintegrin-associated metalloprotease
ADAMT	A disintegrin and metalloproteinase with thrombospondin motifs
AP-1	Activator protein 1
APC	Antigen-presenting cell
APF	Aminophenyl fluoresceine
ATAC-seq	Assay for transposase accessible chromatin with high-throughput sequencing
BCR	B cell receptor
BSA	Bovine serum albumen
BSF-2	B-cell stimulatory factor 2
C5a	Complement component 5a
CAM	Cell adhesion molecules
cDNA	Complimentary DNA
cfu	Colony-forming units
ChIP-seq	Chromatin immuno-precipitation with high-throughput sequencing
ClO^-	Hypochlorite anion
CR3	Complement receptor 3
Ct	Comparative threshold cycle
CT-FR	Cell trace far red
DAMP	Damage-associated molecular patterns
dATP	Deoxyadenosine triphosphate
DC	Dendritic cell
dCTP	Deoxycytidine triphosphate
dGTP	Deoxyguanosine triphosphate
DNA	Deoxyribonucleic acid
DS	Differential splicing
dTTP	Deoxythymidine triphosphate
ECM	Extracellular matrix
EDTA	Ethylenediaminetetraacetic acid
ELISA	Enzyme-linked immunosorbent assay

ERCC	External RNA controls consortium
FCS	Foetal calf serum
Fe_3^+	Ferric cation
fMLP	N-formylmethionyl-leucyl-phenylalanine
FPKM	Fragments *per* kilobase of exon *per* million fragments mapped *per* sample
G-CSF	Granulocyte colony-stimulating factor
gp130	Glycoprotein 130
H_2O_2	Hydrogen peroxide
HA	Hyaluronic acid
HAS	Hyaluronic acid synthases
HDS	IL-6-siIL-6R chimeric fusion protein
HEV	High endothelial venules
HO^-	Hydroxyl radical
HOCl	Hypochlorite
HPGF	Hybridoma/plasmacytoma growth factor
HPMC	Human peritoneal mesothelial cells
HSF	Hepatocyte stimulatory factor
ICAM-1	Intercellular adhesion molecule-1
IFN-β2	Interferon-β2
IFN-γ	Interferon-γ
IFNGR	Interferon-γ receptor
IL-6	Interleukin-6
IL-8	Interleukin-8
IL-6Rα	Interleukin-6 receptor
ILC	Innate lymphoid cells
IPA	Ingenuity pathway analysis
ISP	Ion spheres particles
Jak	Janus-activated kinase
kDa	Kilo dalton
LOX	Lysyl oxidases
LPS	Lipopolysaccharides

LTB_4	Leukotriene b4
MAPK	Mitogen activated protein kinase
MCP-1	Monocyte chemotactic protein-1
MGI-2	Monocyte granulocyte inducer type 2
MMP	Matrix metalloproteinases
MPO	Myeloperoxidase
mRNA	Messenger RNA
NADP	Nicotinamide adenine dinucleotide phosphate
NET	Neutrophil extracellular DNA traps
NGS	Next-generation sequencing
NK	Natural killer
NO	Nitric oxide
NOX2	NADP oxidase 1
O_2^-	Superoxide
$ONOO^-$	Peroxynitrite anion
OSM	Oncostatin M
p300	Histone acetyltransferase p300
PAF	Platelet activating factor
PAMP	Pathogen-associated molecular patterns
PBS	Phosphate buffered saline
PC	Proteolytic cleavage
PCR	Polymerase chain reaction
PD	Peritoneal dialysis
PDGF	Platelet derived growth factor
PE	Paired-end reads
PI3K	Phosphatidylinositol-3-kinase
PIAS	Protein inhibitor of activated STATs
PKR	Protein kinase R
PRR	Pattern recognition receptors
PTP	Protein tyrosine phosphatases
PVDF	Polyvinylidene difluoride
QC	Quality control
qPCR	Quantitative polymerase chain reaction

RIN	RNA integrity number
RNA	Ribonucleic acid
RNA-seq	RNA-sequencing
ROS	Reactive oxygen species
rRNA	Ribosomal RNA
S. epidermidis	*Staphylococcus epidermidis*
S100A	S100 calcium-binding protein a1
SAA1	Serum amyloid a protein
SDS-PAGE	Sodium dodecyl sulphate polyacrylamide gel electrophoresis
SE	Singled-end reads
SES	*Staphylococcus epidermidis* cell-free supernatant
sgp130	Soluble glycoprotein 130
SHP-2	SH2 domain containing protein tyrosine phosphatase
sIL-6Rα	Soluble interleukin-6 receptor
SLC	Solute carriers
SMC	Submesothelial compact zone
SOCS	Suppressors of cytokine signalling
SOD	Superoxide dismutase
SOS	Son of sevenless
SP1	Specificity protein 1
SR	Scavenger receptor
STAT	Signal transducers and activators of transcription
TCR	T cell receptor
TGF-β1	Transforming growth factor-β1
Th0	Naïve T cells
Th1	T-helper 1 cells
TIMP	Tissue inhibitors of metalloproteinases
TLR	Toll-like receptors
TLS	Transcript level of support
TNF-α	Tumour necrosis factor
VEGF	Vascular endothelial growth factor
WT	Wild type
YAP	Yes-associated protein

Table of contents

List of Tables

List of Figures

Chapter 1. General Introduction

1.1. The Immune system

1.1.1. The Immune system

The immune system provides protection from infection, injury and trauma, and relies on cellular communication between leukocytes and cells located within tissues and organs. The primary role of the immune system is to recognise and distinguish between 'self' and 'non-self, and ensure the preservation of the body. This includes the provision of both immediate and more sustained forms of cellular and host defence. During infection, the immune system is designed to prevent the entry of infectious agents (e.g., bacteria, fungi, viruses and parasites), attack and destroy invading pathogens and minimize adverse tissue damage [1].

1.1.2. Mechanisms of anti-microbial host defence

To provide effective protection against such a broad range of pathogenic and environmental stimuli, the immune response has evolved into a highly coordinated process that incorporates several lines of defence. The first line of defence relies on exterior anatomical barriers including the skin and epithelial surfaces lining the lungs, intestines and genitourinary tract; and chemical secretions lubricating these sites. For example, the secretion of antimicrobial peptides and enzymes in the skin, respiratory track, saliva, tears and breast milk constitute an additional mechanism of defence, and the acidic environment of the gut provides an extreme chemical environment for the survival of pathogens. In addition, commensal microflora further restrict the colonisation of more pathogenic forms of bacteria at these sites [1]. However, periodic pathogenic infections are not always sufficiently contained and out-competed at these sites, and additional processes support the control of infection. For example, mechanical forms of protection including coughing and sneezing, which help to clear pathogens from the respiratory track, and the flushing of lining surface with tears or urine. In the airways and gastrointestinal track, cilia present on the epithelia surface removes pathogens that become trapped in the mucosal layer through peristaltic movements.

Pathogens that evade these barrier defences encounter cells of the immune system (leukocytes). These cells, together with other soluble mediators and communication molecules, orchestrate a response to invading pathogens that is termed inflammation. The main function of the inflammatory response is to recruit leukocytes from the bloodstream to the tissues, and direct the local immune response to infection, trauma or injury through the control of innate and adaptive immunity (see *Sections 1.1.3* & *1.1.4*) [1]. This control relies on soluble mediators such as cytokines, complement factors, bioactive lipids and acute phase proteins. The importance of these factors in host immunity is perhaps best illustrated by protein mimicry and decoy strategies employed by some viruses to evade immune detection [2]. Taken together, inflammation helps to combat and contain the infectious episode, and ensures restoration of normal tissue homeostasis (see *Section 1.1.5*).

1.1.3. Innate immunity

The innate immune response is defined as a rapid, non-specific mechanism that represents the first line of defence against invading microbes. The innate immune system shows remarkable evolutionary conservation in multi-cellular organisms, and has coevolved with microbes to protect the host from infection [3].

Activation of innate immunity is driven by several innate sensing mechanisms that recognise defined cell determinants on invading pathogens (termed pathogen-associated molecular patterns; PAMPs) or endogenous molecules produced by damaged cells (termed damage-associated molecular patterns; DAMPs). These sensing mechanisms include receptors for lipid derivatives, bacterial flagellin, viral RNA and oligodeoxynucleotide DNA, and are termed pattern recognition receptors (PRRs) [4]. Recognition of DAMPs and PAMPs by PPRs trigger cellular responses that promote antimicrobial and pro-inflammatory activities. These mechanisms aim to clear infections and limit host damage. The activation of these systems also provides a bridge to regulation of adaptive immune responses and sustained memory immunity [1, 5].

The cellular arm of the innate immune system is composed of specialised leukocytes that survey the tissue microenvironment and eliminate pathogens.

These include phagocytic cells (e.g., neutrophils, monocytes and macrophages, eosinophils, mast cells, basophils), dendritic cells (DCs), and innate lymphoid cells (e.g., ILCs including natural killer (NK) cells) [1]. The main function of phagocytes is to internalize and kill microbes. They also produce and secrete soluble mediators that promote the immune response. These activities include control of adaptive immunity and the release of resolution factors that dampen the inflammatory response and restore immune homeostasis. Here, resident tissue macrophages, dendritic cells and infiltrating monocytic cells play vital roles in the presentation of antigen to T-cells, and in the clearance of neutrophils from sites of inflammation [6] (*Section 1.1.8*). Similarly, mast cells, eosinophils and basophils provide host immunity against parasitic infections and various allergens [7]. Innate lymphoid cells are involved in the immune response against intracellular viruses and bacteria, and damaged and cancerous cells [8]. The immunological processes regulated by these leukocyte populations are supported by the activities of several soluble factors that support the detection by the immune system. These include natural antibodies (e.g., IgM, IgG3), components of the complement system, pentraxins, collectins and ficolins [1]. The binding of these soluble mediators to microbes facilitates their uptake by professional phagocytes and also promotes the progression of inflammation and the transition from innate to adaptive immunity [9].

1.1.4. Adaptive immunity

Adaptive immunity provides long-term protection against pathogens and other antigens (derived from the term *anti*body *gene*rating response). The mechanisms that control adaptive immunity are more elaborate than those described for innate immunity, and are an evolutionary feature of host defence in vertebrates [1, 10]. In this regard, adaptive immunity delivers three fundamental immune functions – (1) The capacity to distinguish between self and non-self antigens, (2) The generation of anti-microbial host responses that are tailored to eliminate specific extracellular or intracellular pathogens, and (3) The generation of immunological memory recall. These actions are mediated by specific subsets of lymphocytes known as B-cells, CD4 T helper cells and CD8 cytotoxic T cells.

Effector responses directed by the adaptive immune system rely on receptors expressed on B cells (the immunoglobulin BCR; B cell receptor formed from either membrane-bound IgM or IgD) and T cells (TCR; T cell receptor). Although functionally distinct, both receptors are members of the immunoglobulin superfamily. These are encoded by select combinations of specific gene clusters termed variable, diverse and joining (V(D)J) genes. The large repertoire of BCRs and TCRs is acquired by V(D)J recombination during B cell and T cell differentiation [11]. A complex array of inherent gene editing mechanisms gives rise to the generation of diversity, and the affinity binding characteristics for each receptor is unique to each individual T-cell or B-cell clone.

During the adaptive immune response, the interaction of antigen-presenting cells (e.g., B-cells, dendritic cells and other specialised monocytic populations) with lymphocytes promotes the development of antigen-specific responses and the survival and long-term maintenance of effector and memory subsets with defined inflammatory or regulatory characteristics [12, 13]. In this regard, immunological memory is a hallmark of the adaptive immunity and forms the basis of vaccination strategies against bacteria and viruses [14].

1.1.5. Inflammation

Inflammation is not a disease, but an active consequence of a disease process. It is therefore designed to offer protection. However persistent, recurrent or uncontrolled inflammation can promote various inflammatory or autoimmune diseases. The fundamental features of inflammation are defined by *rubor* (redness), *calor* (warmth), *dolor* (pain) and *tumor* (swelling) [15]. These hallmarks of inflammation arise from the accumulation of immune cells, plasma proteins and fluids at site of infection, injury or trauma. This response is however highly coordinated and ensures: (1) Recruitment of effector molecules and leukocytes to the inflamed tissue where they fight infection or damage; (2) Prevent the dissemination of the invading pathogen to other tissues; (3) Ensure the resolution of the inflammatory process to restore normal tissue homeostasis.

Acute inflammation refers to the initiation of a short-term response that develops quickly and resolves within 2-3 days. In this regard, a tight

communication between the local stromal compartment and the infiltrating effector cells during inflammation is essential to ensure the appropriate activation, maintenance and resolution of inflammatory cells (see *Sections 1.1.6-1.1.8*) (Figure 1.1) [9, 16, 17]. Persistent or recurrent acute inflammation leads to tissue damage and injury (e.g., fibrosis), and may give rise to chronic inflammatory disease [1]. These outcomes are regulated in a context-dependent manner, and are shaped by specific cytokines and soluble factors released as part of the disease process.

1.1.6. Induction and early phase of inflammation

Recognition of invading pathogens by the PPRs expressed by host cells (including tissue resident macrophages, dendritic cells and stromal epithelial cells) leads to the production of inflammatory mediators that initiate and amplify the inflammatory response – bioactive lipids (e.g., prostaglandins, leukotrienes), chemokines (chemotactic cytokines) and cytokines [18]. These include pro-inflammatory cytokines such as tumour necrosis factor (TNF)-α, interleukin (IL)-1β and IL-6, which control the expression of adhesion molecules and chemokines responsible for the trafficking of inflammatory cells from the blood into the inflamed tissue compartment [1, 16, 17] (*Section 1.2.1*). Here, changes in expression patterns of chemokines and adhesion molecules (e.g., selectins, integrins) ensure the timely recruitment of innate and adaptive immune cells to sites of inflammation. In particular, the early expression of neutrophil-activating chemokines by resident monocytic cells and stromal cells supports the rapid recruitment and activation of neutrophils to sites of bacterial infection [16]. Neutrophil recruitment, activation and effector activities will be extensively detailed in *Section 1.7*.

1.1.7. Maintenance and late phase of inflammation

The next stage in the inflammatory process is characterised by the clearance of the initial neutrophil influx and their replacement by a more sustained population of mononuclear cells [9]. This replacement is controlled by a shift in the

expression of neutrophil directing molecules, including chemokines (*Section 1.2.2*) and bioactive lipids (e.g., lipoxygenase-derived lipid mediators, lipoxins) [19], to monocyte [20] and lymphocyte directing molecules [21]. For example, the shift from leukotriene (e.g., LTB_4) to lipoxin production collectively inhibits neutrophil chemotaxis and promotes the extravasation of circulating monocytes and lymphocytes to the inflamed tissue [22]. This switch in leukocyte recruitment is supported by the selective expression of monocyte-specific cell adhesion molecules (CAMs) in the vascular endothelium [23, 24], and the clearance of apoptotic neutrophils through a mechanism known as nonphlogistic phagocytosis [25]. Importantly, this selective recruitment allows antigen presentation by inflammatory macrophages to lymphocytes and the generation of long-term immunological memory.

1.1.8. Resolution of inflammation

Finally, the inflammatory response has to cease in order to prevent tissue damage and injury. Resolution of inflammation relies in both cease of pro-inflammatory signals and induction in pro-resolving signals with the aim of: (1) Remove the microbes, dead cells and debris; (2) Restore the vascular integrity and perfusion; (3) Regenerate the inflamed tissue [26]. In this regard, the engulfment of apoptotic neutrophils by inflammatory macrophages induces a switch from pro- to anti-inflammatory macrophage phenotype that initiates their apoptosis [27] or egress from the inflamed local tissue to the nearest draining lymph node [28]. In addition, phagocytosis of apoptotic cells also induces the release of anti-inflammatory mediators such as transforming growth factor-β1 (TGF-β1), platelet derived growth factor (PDGF) and vascular endothelial growth factor (VEGF), which stimulate the proliferation of epithelial cells to surround the injury site and ensures the repair of endothelial and epithelial tissues [29]. Taken all together, these signals promote the resolution of the inflammatory process, tissue repair and restores normal homeostasis [6].

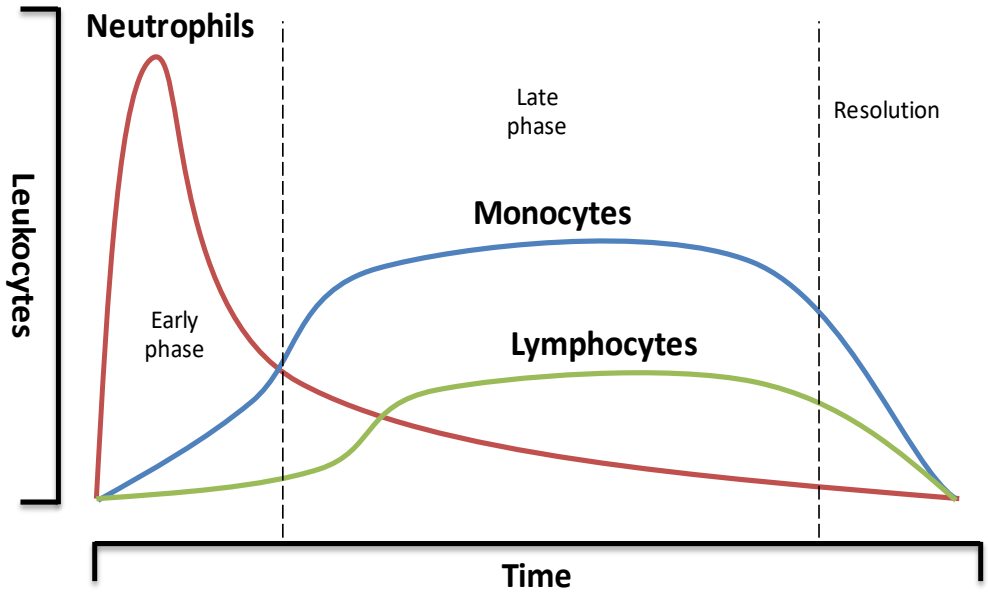

Figure 1.1. Stages of inflammation. The inflammatory response can be divided in three different stages attending the leukocyte population at the site of infection or injury. It is characterised by an initial influx of neutrophils during the early stage, followed by the recruitment of a more sustained population of monocytes and lymphocytes at the late phase. Finally, the inflammatory response is resolved, inflammatory leukocyte number reduce, and the tissue returns to homeostasis.

1.1.9. Acute resolving inflammation versus inflammation associated tissue damage

Inflammation induced tissue injury is often an unavoidable consequence of anti-microbial immune response, and ultimately is the result of the interaction between the host and the invading microorganism [30]. This is probably best illustrated in the case of bacterial commensalism versus infection, where commensalism is defined as a state of host–microorganism interaction that does not result in host damage [30]. While tissue injury arises from bacterial, fungal or viral infection, overt innate or adaptive immune responses have the potential to promote cellular damage and an alteration in tissue architecture. For example, processes that control oxidative stress or fibrosis. Thus, leukocyte infiltration and clearance during acute inflammation must be tightly regulated to ensure both competent host defence and correct resolution of inflammation [9].

Dysregulation of the inflammatory process can arise from persistent, recurrent or unresolved inflammation; allergy responses; autoimmune reactions and radiation [31]. Eventually, it leads to chronic inflammation and results in changes in local tissue architecture, tissue injury, cell death and the replacement of viable cells and parenchyma with fibrosis [30]. These events have been proposed to be useful in the containment of the early stages of infection [32]. For example, we have previously shown that recurrent episodes of resolving bacterial peritonitis lead to peritoneal fibrosis in a murine model of peritoneal inflammation [33]. This process relies on the local expansion and retention of effector CD4 T-cells in the peritoneal cavity. Here, fibrosis may similarly be a host response focused to limit bacterial dissemination.

Importantly, peritoneal fibrosis is a major cause of treatment failure in end stage renal failure patients in peritoneal dialysis. Here, treatment duration but also the incidence of bacterial peritonitis in these patients is linked with thickening of the sub-mesothelial compact zone and peritoneal fibrosis [34-36]. In particular, the onset of fibrosis after recurrent bacterial infection is strictly IL-6 depended [33]. While these observations present significant clinical relevance, they also illustrate the thin line between successful host defence and tissue damage, and will be the focus of the current thesis.

1.2. Cytokines and chemokines

As discussed previously in this Chapter, the inflammatory response is a process that must be tightly regulated. This control relies on complex signalling networks that include protein and lipid mediators, such as cytokines, chemokines, prostaglandins and leukotrienes. The following section will introduce the basic principles in chemokine and cytokine signalling, and will focus specially in the cytokine interleukin (IL)-6.

1.2.1. Cytokines

Cytokines are small molecular weight proteins that control cellular proliferation, differentiation and survival. They are produced by both haematopoietic (immune) and non-haematopoietic (stromal) cells to promote specific gene regulation through the activation of receptors expressed by target cells. They can act on the same cells that produce them (autocrine signalling), on cells in close contact (termed contact-dependent or juxtacrine signalling), on adjacent cells (paracrine signalling), or via the circulation to distant cells (endocrine signalling) [1, 37]. In addition, while one same cytokine can elicit multiple biologic effects in diverse cell types (termed pleiotropism), multiple cytokines can present overlapping activities (termed redundancy). For example, the IL-6 cytokine family includes several members that, despite being encoded in separate genes, induce the expression of hepatic acute phase proteins in addition to other unrelated biological properties [38].

Cytokines can be classified according two functional classes. Haematopoietic cytokines are secreted by tissue resident macrophages and stromal cells and provide local environment for haematopoiesis; whereas immune cytokines are produced by leukocytes, lymphocytes and stromal cells, and have activities relevant to immune homeostasis and disease [1, 37]. Importantly, some cytokines like IL-6 are responsible for both of these classifications.

In the context of immune homeostasis, cytokine signalling is essential for control of the inflammatory response, and they can act as pro- or anti-inflammatory mediators. Examples of pro-inflammatory cytokines are TNF-α or IL-1β [1],

which are produced at the early stages of inflammation and coordinate many aspects of the inflammatory response. Conversely, IL-10 or IL-27 have potent immuno-modulatory and anti-inflammatory properties [39, 40]. Finally, other cytokines such as IL-6 act as pleiotropic factors, and present both pro- or anti-inflammatory activity depending on the context in which IL-6 deeds [41]. As the present thesis focus on the impact of IL-6 signalling in educating the immune response, this cytokine will be discussed in detail in *Section 1.3*.

1.2.2. Chemotactic cytokines – Chemokines

Those cytokines that elicit chemotactic functions are termed chemokines. Chemokines are a family of structurally homologous cytokines that stimulate leukocyte trafficking and migration from blood to tissues in favour of their gradient [1]. These small proteins are divided in four subfamilies based on the number and location of N-terminal cysteine residues: CC family (e.g., monocyte chemotactic protein, MCP-1; CC-chemokine Ligand-1, CCL1), where the cysteine residues are adjacent; CXC (e.g., interleukin-8, IL-8; CXC-chemokine Ligand-8, CXCL8) and CX3C (e.g., fractalkine; CX3C-chemokine Ligand-1, CX3CL1) families, where the cysteine residues are separated by one or three amino acids, respectively; and C (e.g., lymphotactin; C-chemokine Ligand-1, CL1) family, with only one cysteine [1]. Systematic nomenclature designates each individual chemokine with their subfamily followed by a number and L or R, referring to ligand or receptor respectively [42]. Chemokine receptors show structural hallmarks of seven-transmembrane G-protein coupled receptors. Binding of a given chemokine to its respective receptors induces changes in the target cell's cytoskeleton and lipid membrane that induces movement along the chemokine gradient in a process known as chemotaxis [43].

Chemokines are involved in several biological processes, including lymphoid tissue organization and the recruitment of leukocytes involved in innate and adaptive immunity. During inflammation, time-dependent regulation of chemokine production ultimately dictates leukocyte trafficking, clearance and eventual resolution the inflammatory process. Among those regulators of chemokine expression are PRRs as well as cytokines. In the context of bacterial

peritonitis, IL-6 plays a pivotal role in controlling leukocyte recruitment by switching the production of different chemokines [9], which will be discussed extensively in *Section 1.3*.

1.3. Interleukin-6

The importance of IL-6 in innate immunity is perhaps best illustrated by the identification of a conserved IL-6-like cytokine system in *Drosophila melanogaster*. In particular, the binding of the secreted ligand unpaired-3 (IL-6-like) to the receptor Domeless (gp130-like) forms a signalling network that eventually promotes innate immunity [44-46]. Furthermore, several viruses have evolved to mimic or disrupt IL-6 signalling. For example, human herpesvirus 8 expresses a viral form of IL-6 that shares ~60% amino acid similarity with its human counterpart and can block the recruitment of neutrophils [47]. Taken together, these observations highlight the fundamental role of IL-6 in innate immunity and pathogen control [41].The following sections will review our current understanding of IL-6 signalling and its implication in health and disease.

1.3.1. Interleukin-6

Interleukin-6 (IL-6) is a cytokine of 26 kDa consisting of 4 long polypeptide α-helices (A, B, C and D) arranged in an up-up-down-down topology (Figure 1.2A) [48]. Prior to its naming as a single cytokine, IL-6 was characterised as β2-interferon (IFN-β2) [49], B-cell stimulatory factor 2 (BSF-2) [50], 26 kDa protein [51], hybridoma/plasmacytoma growth factor (HPGF or IL-HP1), hepatocyte stimulatory factor (HSF) [52] and monocyte granulocyte inducer type 2 (MGI-2). While these factors were discovered to be the same molecule in 1987 [53], these studies illustrate the characteristic of IL-6 of being a truly pleiotropic cytokine that has a broad impact in both stromal and immune cells.

Interleukin-6 is very promptly and transiently produced in response to infection and tissue injury. While the main cellular sources of IL-6 are monocytes and resident macrophages at the site of inflammation, mesenchymal cells, endothelial cells, fibroblasts, and many other stromal cells are also involved in the

production of IL-6 in response to various stimuli [54, 55]. Here, recognition of damage or infection by PRRs (e.g., toll-like receptors (TLRs) and retinoic acid-inducible gene-1-like receptors) trigger the activation of a range of signalling pathways that enhance the transcription of the mRNA of inflammatory cytokines, including IL-6. For example, peritoneal infection by gram positive bacteria activates TLR2 and the transcription factor NF-kB by resident peritoneal macrophages and stromal cells, which lead to the production and release of IL-6 – among other cytokines – to the peritoneal cavity [9, 56].

In the context of the immune response, IL-6 has been associated to promote the population expansion and activation of T-cells [57], the differentiation of B-cells [58] and regulation of acute phase responses [59, 60]. Interleukin-6 has also been shown to be essential for host defence against bacteria, viruses and parasites [61-65]. Unpublished observations in our laboratory are in close agreement with these findings. In particular, we have shown that *Il6*$^{-/-}$ mice have a reduced capacity to successfully clear infection during *Staphylococcus epidermidis* induced peritonitis.

The beneficial role of IL-6 in acute resolving infection is counteracted by its implication in chronic disease such as arthritis [66] and Crohn's disease [67], and cancer progression [68]. A more in-depth look at the role of IL-6 during inflammation will be discussed in *Sections 1.3.4* & *1.3.5*.

1.3.2. IL-6 receptor signalling

Interleukin-6 signalling relies on two receptors: the non-signalling α-receptor (CD126, IL-6Rα, encoded by the *Il6ra* gene) and the signal transducing β-receptor glycoprotein 130 kDa (CD130, gp130, encoded by *Il6st*) [48]. The stoichiometry of this interaction is 2:2:2 (Figure 1.2B), where each IL-6-IL-6R complex contacts two β-receptor subunits of gp130 [69]. This interaction allows the proximity of the two gp130 subunits and trigger the intracellular signalling [69], that will be detailed in *Section 1.3.3*.

Interleukin-6 can bind to both the membrane bound or soluble IL-6R (sIL-6R) in the site I (Figure 1.2A & 1.3) [70]. IL-6 signalling via the membrane bound receptor is referred as "classical IL-6 receptor signalling" [48] (Figure 1.3).

The expression of the membrane bound IL-6Rα is restricted to hepatocytes, leukocytes, megakaryocytes and some specialised stromal cells [41]. Therefore, only those cells are responsive to IL-6 classical signalling. IL-6 acting via its soluble receptor is termed "IL-6 trans-signalling" (Figure 1.3). Soluble IL-6R can be produced by proteolytic cleavage of the extra cellular domain by the enzyme adamylsin and disintegrin-associated metalloprotease (ADAM)-17 and -10 [71], or by differential splicing of *Il6ra* gene to produce a protein without the membrane anchor region. Both sIL-6R isoforms are termed proteolytic cleavage (PC)-sIL-6R and differential splicing (DS)-sIL-6R, and share similar structure and functional properties. IL-6R shedding is induced by several physiological activators, including C-reactive protein [72], complement component 5a (C5a) [73], platelet activating factor (PAF) [74], chemokines, such as CXCL8 [75], and other chemoattractants such as N-formylmethionyl-leucyl-phenylalanine (fMLP) [76]. In this regard, IL-6 binding to sIL-6R can initiate signal transduction in those cells not expressing IL-6R but expressing gp130. Another mechanism of IL-6 signalling has been recently proposed by Heink and colleagues, who showed that DCs using their membrane bound IL-6Rα trans-presented IL-6 to T cells during the process of cognate interaction [77]. This mechanism was termed IL-6 trans-presentation, and was found to be important for the generation of Th17 cells *in vivo* [77].

Both classical IL-6 receptor signalling and IL-6 trans-signalling rely on the membrane bound gp130 to initiate signal transduction (Figure 1.3). Here, IL-6 binds to each gp130 of the receptor complex via sites II and III respectively (Figure 1.2A) [70]. Gp130 is ubiquitously expressed in almost every cell type except red blood cells. A soluble form is gp130 (sgp130) is also generated by alternative splicing of the *Il6st* gene, and to a lesser extent by proteolytic cleavage [78, 79]. This sgp130 is an antagonist of IL-6 trans-signalling (Figure1.3) [78, 80], and an Fc-dimerized version of sgp130 (sgp130-Fc; olamkicept) has shown therapeutic efficacy in models of inflammatory disease and cancer [81-83]. The mechanisms of sgp130 production and its implications in disease will be detailed in Chapter 8.

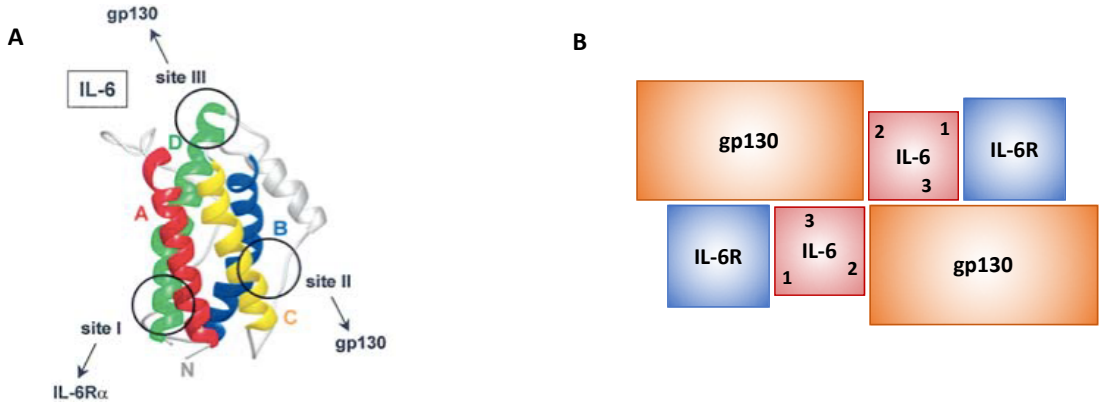

Figure 1.2. Interleukin-6 and its receptor complex form a trimeric dimer. A. The structure of IL-6 comprises 4 long alpha helices that are arranged in an up-up-down-down topology (Figure obtained from ref 48). **B.** The binding of IL-6 to IL-6R promotes the contact to the β-receptor subunits gp130 and the formation of a trimeric homodimer that allows the proximity of the two gp130 subunits (Figure adapted from ref 69).

1.3.3. IL-6 intracellular signalling – paradigm of Jak/STAT signalling pathway

Cytokine engagement of the IL-6 receptor complex promotes signalling via the Janus-activated kinase/signal transducers and activators of transcription (Jak/STAT) pathway. This pathway represents a landmark in cell biology and provides a direct mechanism to translate an extracellular signal (mediated by hormones, interferons, colony-stimulating factors, and interleukins) into a transcriptional response [84, 85]. The signalling mechanism is relatively simple and relies on very few principal components. Intracellular activation occurs when ligands bind to their respective receptors and induce their multimerization. This allows proximity of the intracellular domains of the receptors and the association of the Jak tyrosine kinases (Jak1, Jak2, Jak3 and Tyk2), which results in their intra- or intermolecular phosphorylation [85]. Tyrosine phosphorylation induces the activation of the Jaks catalytic domain, which now can phosphorylate several tyrosine residues in the carboxy-terminus of the cytoplasmic tail of the receptors. Here, tyrosine phosphorylation promotes the recruitment of STAT factors to the receptor complex and their subsequent activation by receptor-associated Jak

proteins. Activated STATs can now form homo- (e.g., STAT1-STAT1 dimers) and to a lesser extent hetero-dimers (e.g., STAT1-STAT3 heterodimers), which promotes translocation to the nucleus, DNA binding to defined DNA consensus binding motifs (e.g., GAS motifs) and the initiation of gene transcription [85].

In particular, IL-6 activates Jak1, Jak2 and Tyk2, and the latent transcription factors STAT1, STAT3 and to a lesser extent STAT5 [70] (Figure 1.3). In addition to STAT activation, IL-6 signalling also regulates activation of the mitogen activated protein kinase (MAPK) cascade [48]. This signalling pathway is initiated with the recruitment of the SH2 domain containing protein tyrosine phosphatase (SHP-2) to the tyrosine-759 (in humans; tyrosine-757 in mice) residue of gp130 [86]. SHP-2 is phosphorylated by Jak1 to initiate links with the Grb-SOS complex and the downstream activation of Ras, Raf and components of the MAPK cascade. Furthermore, phosphorylated SHP-2 can form a complex with Gab and PI3K that leads to the activation of the Akt pathway [48, 87]. Finally, IL-6 can activate the tyrosine kinases Src and Yes, which leads to the activation of the YAP-Notch pathway and promotes epithelial regeneration [88].

Interleukin-6 signalling is strictly regulated. One regulatory mechanism involves the hydrolysis of the phosphorylated tyrosine residues in Jaks, STATs and upstream receptors by a broad number of phosphatases, including SHP-2 and other protein tyrosine phosphatases (PTPs) [89]. Another mechanism involves proteins of the PIAS (protein inhibitor of activated STATs) family, which suppress STAT activities by allosteric interactions in the nucleus [90]. They also promote STATs sumoylation in a manner that resembles the action of RING-type ubiquitin E3 ligases [91]. Finally, activation of STAT1/3 respectively induces the transcription of suppressors of cytokine signalling (SOCS) 1 and 3, which act as negative feedback regulators for STAT signalling. For example, SOCS3 binds to the SH2 domain and inhibits the activation of SHP-2 and STAT pathways [92]. SOCS3 also limits the activation of STAT1 by IL-6 by ensuring that STAT3 has priority in binding to activated gp130 [93].

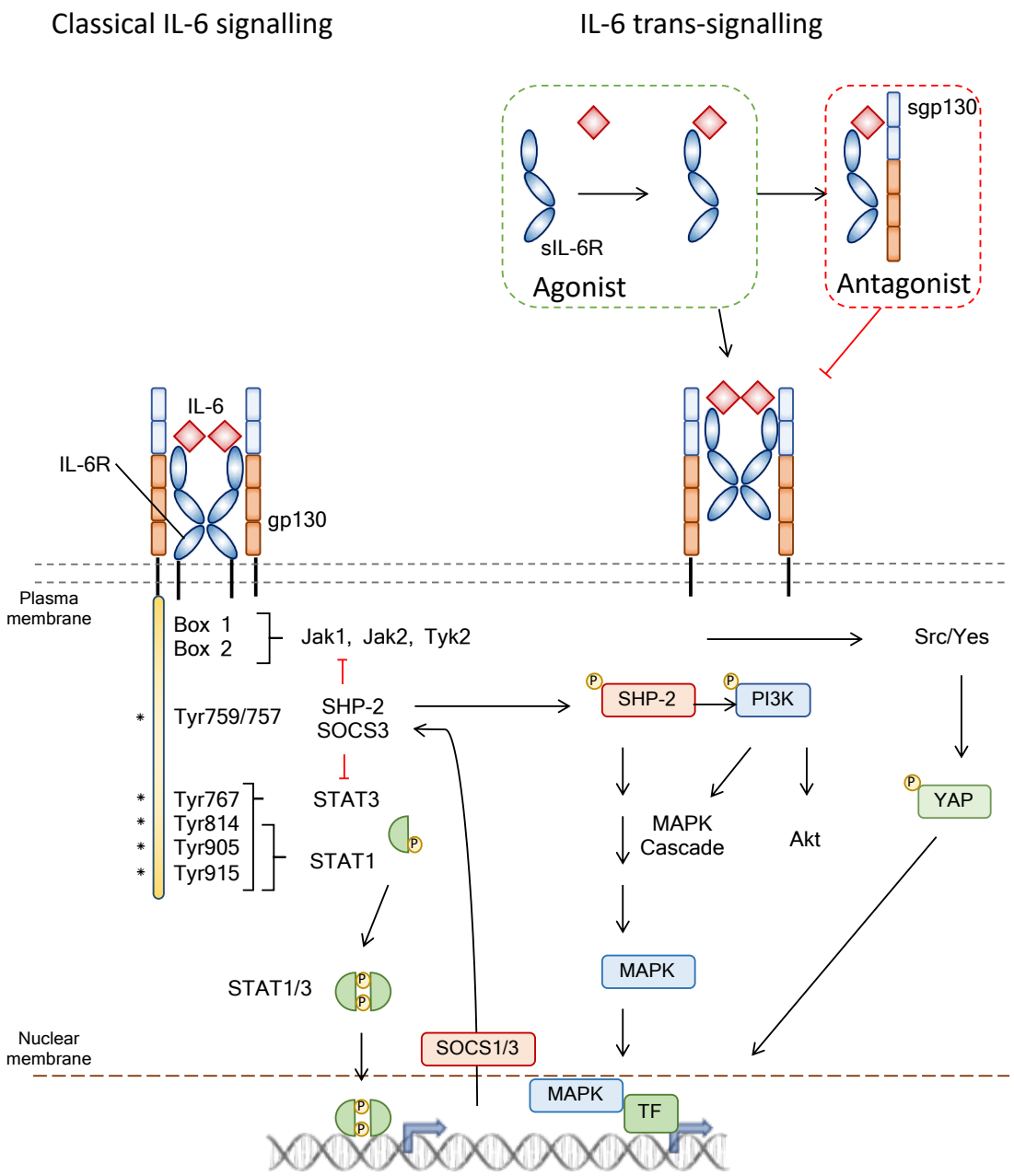

Figure 1.3. IL-6 signal transduction. The binding of two complex of IL-6-IL-6R to two molecules of gp130 allows the proximity of the cytoplasmic tails of gp130. This proximity leads to the activation of Jaks, which can now phosphorylate several tyrosine residues in the c terminus of the cytoplasmic tail of gp130. This phosphorylated Tyr acts as docking sites for the recruitment of several proteins including STAT1, STAT3 and SHP-2, where they become phosphorylated by the Jaks. Phosphorylation of STATs facilitates the formation of STAT dimers, which translocate to the nucleus to regulate gene expression. Alternatively, the activation of SHP-2 by phosphorylation leads to the activation of the MAPKs pathway or the Akt pathway. Finally, the activation of the kinases Src and Yes leads to the activation of the YAP-Notch pathway.

1.3.4. IL-6 in acute inflammation

The pleotropic properties of IL-6 are best illustrated by its key role in both the resolution of inflammation and chronic disease progression [41]. The following sections will discuss the contribution of IL-6 in directing competent host defence versus inflammation induced tissue damage in the context of peritoneal inflammation.

Interleukin-6 is rapidly induced during peritonitis in response to innate toll-like receptor signalling [9, 56]. The molecular and cellular events that characterise this model are depicted in Figure 1.4. Here, gram-positive bacterial (e.g., *S. epidermidis*) activation of TLR2 leads to the expression of the pro-inflammatory cytokines TNF-α, IL-1β and IL-6, and neutrophil-activating chemokines such as CXCL1 and CXCL8. Stimulation of human peritoneal mesothelial cells (HPMCs) with TNF-α and IL-1β also induces the production of IL-6 [94]. CXCL1 and CXCL8 mediate the recruitment of neutrophils to the peritoneal cavity, where they are activated to shed IL-6R [20].

While peritoneal mesothelial cells do not express IL-6R, the availability of sIL-6R promotes IL-6 trans-signalling in the mesothelium and the activation of STAT3 [21]. In this regard, IL-6 trans-signalling promotes the transition from the early influx of neutrophils to the more sustained mononuclear cell infiltrate. This transition is controlled through the induction of monocytic chemoattractants such as CCL2, and the inhibition of CXCL1 and CXCL8 [20]. This differential chemokine modulation was found to be STAT3 and not STAT1 dependent [95]. These responses are supplemented by the role of IL-6 in promoting angiogenesis and the differential expression of several adhesion molecules [76, 96, 97]. In addition, IL-6 suppresses the expression of pro-inflammatory cytokines and induces the release of the soluble p55 TNF-α receptor and the IL-1R antagonist [98, 99]. Finally, IL-6 also mediates neutrophil apoptosis [25], which facilitates neutrophil clearance by the infiltrating monocytes. Taken all together, these events illustrate the role of IL-6 in ensuring the correct progression of the inflammatory response (*Section 1.1.7*).

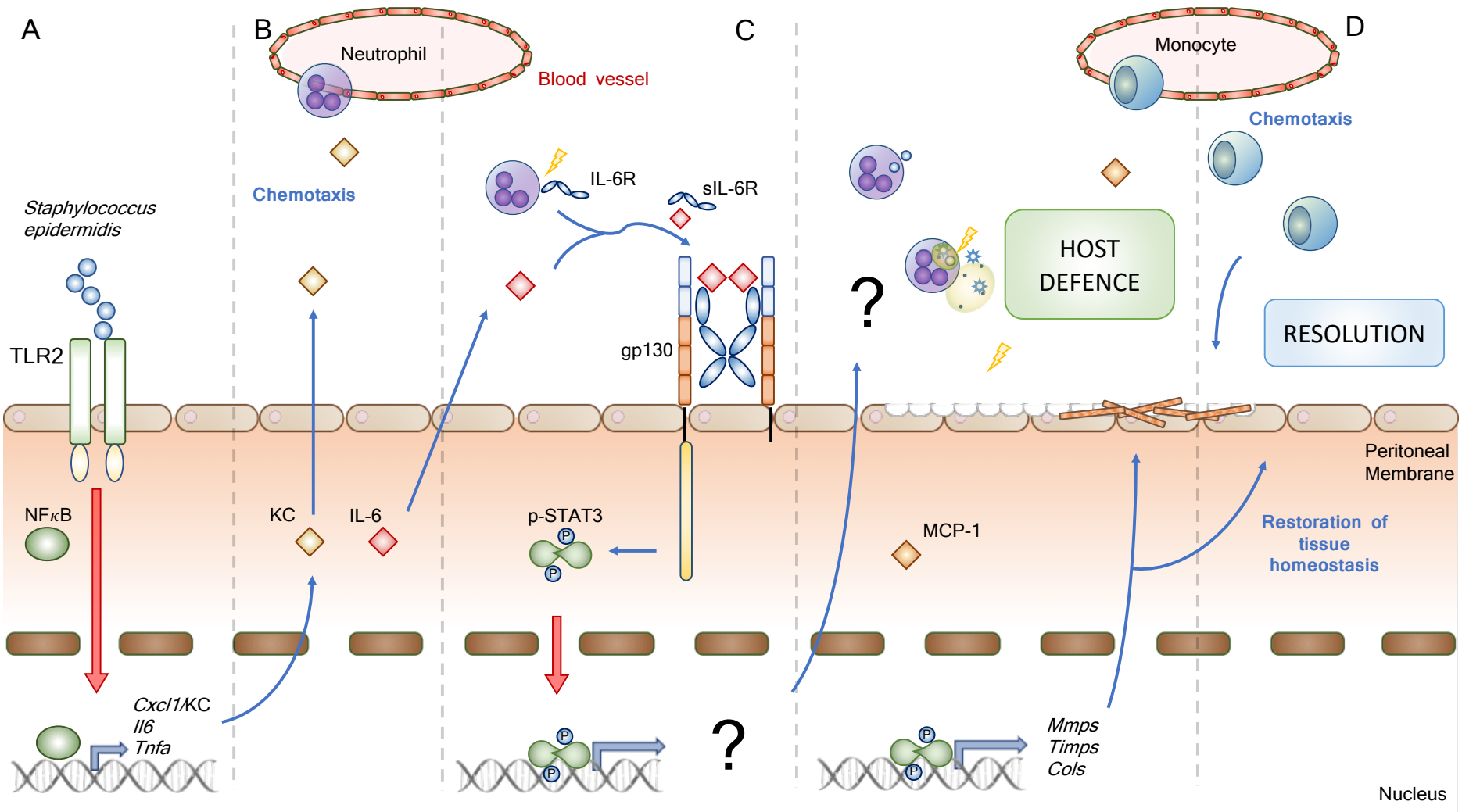

Figure 1.4. IL-6 governs leukocyte recruitment and clearance during acute peritonitis. A. TLR activation leads to the expression and release of several chemokines (CXCL1) and cytokines (TNF-α, IL6) to the peritoneal cavity. **B.** CXCL1 promotes the recruitment of inflammatory neutrophils, that rapidly shed their IL-6R upon transmigration. **C.** The complex IL-6-sIL-6R binds to gp130 in the peritoneal lining to induce the expression of several genes, including MCP-1, which promotes the recruitment of mononuclear cells and the eventual resolution of inflammation **(D)**. IL-6 is also essential for the correct clearance of the pathogen through mechanisms not yet determined.

The ability of IL-6 to dictate transition from innate to acquired immunity is represented by the ability of IL-6 to induce T-cell chemokines CXCL10, CCL4, CCL5, CCL11 and CCL17 in the peritoneal membrane [25]. This is accompanied by the IL-6-signalling mediated expression of CCR3, CCR4, CCR5, and CXCR3 on the $CD3^+$ infiltrate during the late stages of inflammation [21]. IL-6 trans-signalling also promotes the generation and maintenance of Th17 cells in the peritoneal cavity [100], which play an important role in the defence against bacterial infection [101].

In this regard, recent studies from our laboratory have shown that IL-6 is essential in the control of infection during acute bacterial peritonitis. Here, *Il6*$^{-/-}$ mice showed reduced bacterial clearance at the peritoneal cavity and increased dissemination to the blood stream. These results are accompanied by an impaired systemic acute phase response characterised by a reduction in the levels of serum amyloid a protein (SAA1) in the blood. These findings are in close agreement with other studies in the literature that highlight the importance of IL-6 in host defence against different pathogens [61-65]. For example, during gram positive bacterial infection, IL-6 promotes the expression of haptoglobin, serum amyloid A and other acute phase proteins in the liver [61]. In addition, IL-6 enhances antibody responses that provide long-term protection against influenza virus [64]. Importantly, reconstitution of IL-6 trans-signalling in the peritoneal cavity correlated with improved bacterial clearance and reduced dissemination in a dose dependent manner. In line with these studies, Onogawa and co-workers have demonstrated that local delivery of sIL-6R improved bacterial clearance during *S. aureus* induced peritoneal infection in mice [102]. Taken together, this data stresses the pivotal role of IL-6 in directing a successful host defence during acute inflammation.

1.3.5. IL-6 in chronic inflammation

The beneficial role of IL-6 during acute inflammation is darkened by its involvement in the onset of chronic inflammation. For example, early studies have shown that IL-6 is present in the synovial fluids of patients with rheumatoid arthritis [103] and the psoriatic plaques of patients with psoriasis [104]. In addition, elevated IL-6 levels have been found in the serum of patients with various forms of chronic diseases including colitis and systemic juvenile idiopathic arthritis [105, 106]. These

findings are supported by other studies that demonstrated that *Il6*$^{-/-}$ mice are resistant to the development of experimental models of chronic disease such as arthritis [107, 108] and autoimmune encephalomyelitis [109]. Interestingly, the pro-inflammatory properties of IL-6 seem to be mediated by IL-6 trans-signalling in many of these conditions [110]. Here, blockade of IL-6 trans-signalling using sgp130-Fc has been beneficial in several models of chronic inflammatory bowel disease [111]. In rheumatoid arthritis, reconstitution of IL-6 trans-signalling (but not classical IL-6 receptor signalling) promotes disease progression. Here, changes in leukocyte recruitment, synovial hyperplasia and joint erosion are inhibited by action of sgp130 [107]. These findings have led to the clinical development of a specific IL-6 trans-signalling inhibitor under the drug name olamkicept [112].

In the context of end stage renal failure patients in peritoneal dialysis, repetitive episodes of bacterial infection and treatment duration lead to peritoneal fibrosis, which a major cause for treatment failure [34, 113]. Using a murine model of peritoneal inflammation, we have demonstrated that this process is strictly IL-6 dependent [33]. After four episodes of acute resolving peritonitis, IL-6 mediates the expansion of IFN-γ producing Th1 cells at the site of infection. IFN-γ signalling in the peritoneal membrane via STAT1 promotes fibrosis, which was not observed in mice deficient in IL-6, IFN-γ or STAT1 [33] (Figure 1.5). In this model, a relative increase in stromal STAT1 activity led to fibrosis through an alteration in the physiological turnover of extracellular matrix (ECM) by proteases [33]. The mechanisms of fibrosis will be further discussed in *Section 1.5*. Overall, this setting illustrates the importance of IL-6 in determining transition from competent host defence to inflammation induced tissue damage.

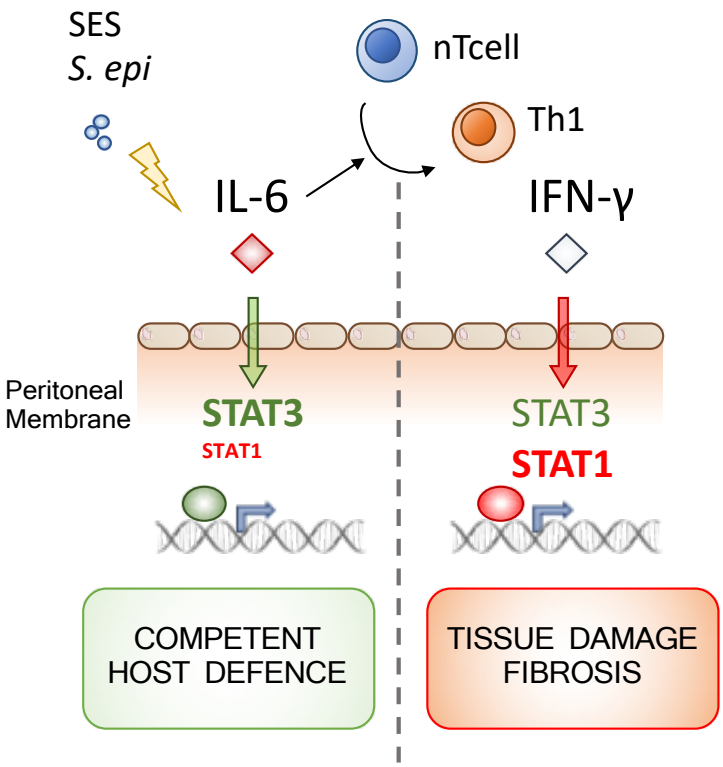

Figure 1.5. IL-6 as a key cytokine in determining the transition from competent host defence to inflammation induced tissue damage. While acute resolving peritonitis relies in IL-6 for the successful resolution of the infection, repetitive episodes of bacterial peritonitis leads to the IL-6 mediated expansion of Th1 cells and the production of IFN-γ in the peritoneal cavity. IFN-γ signalling *via* STAT1 in the peritoneal lining leads to peritoneal fibrosis, which is a major cause of peritoneal dialysis failure as replacement treatment for end-stage renal failure patients. nTcell, naïve T cell; *S. epi*, *Staphylococcus epidermidis*.

1.4. Interferon-γ

Interferon (IFN)-γ is a dimerized soluble cytokine that is the only member of the type II IFN. Each monomer consists of a core of six alpha helix and an unfolded sequence in the C-terminal region [114]. IFN-γ is produced by many cell types, including NK cells, B cells, professional antigen-presenting cells (APCs; e.g., macrophages and dendritic cells), $CD4^+$ Th1 cells and $CD8^+$ cytotoxic T lymphocytes [115]. Such broad expression illustrates the importance of this cytokine in both innate and adaptive immunity. For example, secretion of specific cytokines such as IL-12 by APCs mediates naïve $CD4^+$ T-cell differentiation to Th1 [116]. In return, Th1-derived IFN-γ promotes the activation of APCs to enhance Th1 differentiation. What is more, IFN-γ inhibits IL-4 secretion and Th2 polarization [117]. Thus, both IL-12 and IFN-γ coordinate the link between pattern recognition by innate immune cells and the induction of specific adaptive immunity by mediating a positive feedback loop to amplify the Th1 responses [118].

As well as IL-6, IFN-γ elicits a broad variety of biological functions, including antiviral, immunoregulatory and anti-tumour activities [117]. For example, IFN-γ derived antiviral mechanisms rely on the induction of key antiviral enzymes such as protein kinase R (PKR), which also presents anti-proliferative activity and suppress tumour progression [119]. In the context of peritoneal inflammation, we have previously shown that IFN-γ controls the initial recruitment of neutrophils to the peritoneal cavity [120]. Together with IL-6 acting via its soluble receptor, IFN-γ also regulates neutrophil clearance [25]. Finally, IFN-γ activation of STAT1 signalling in the peritoneal membrane disrupts the correct turnover of ECM by matrix metalloproteinases (MMPs), which eventually leads to peritoneal fibrosis (*Section 1.3.5*) [33]. Taken all together, these studies emphasise the importance of the interplay between IL-6 and IFN-γ in controlling every stage of the inflammatory response.

1.4.1. IFN-γ signalling

IFN-γ signalling relies on two receptors: a ligand-binding subunit, termed IFNGR1, and a signal transducing subunit, termed IFNGR2. Both subunits belong to the class II cytokine receptor family [117]. The stoichiometry of this interaction is 2:2:2, where each IFN-γ dimer binds to two subunits of IFNGR1, that then associate to two subunits of IFNGR2 [121] (Figure 1.6).

Downstream receptor signalling can be divided into canonical and non-canonical signalling pathways. Canonical signalling refers to IFN-γ acting via the Jak/STAT pathway (*Section 1.3.3*) [122]. In particular, IFN-γ binding to the constitutively assembled IFNGR1-IFNGR2 leads to recruitment and activation of Jak1 and Jak2, and the latent transcription factor STAT1. Recruited STAT1 undergoes tyrosine phosphorylation, dimerization and nuclear translocation in response to Jak activation [122]. Alternatively, recruitment of adaptor proteins associated to IFNGR2 such as MAL [123] and Fyn [124] results in non-canonical signalling that activates alternative pathways including PI3K pathway and others [125].

Negative regulation of IFN-γ signalling occurs at every level of the signalling cascade. Following signal transduction, the ligand-receptor complex internalizes and dissociates [126]. Also, STAT1 induces the transcription of SOCS1, which acts as a specific feedback inhibitor of STAT1 signalling [127]. Finally, IFN-γ signalling is controlled by the action of several phosphatases at every level of the pathway. For example, SHP-2 can dephosphorylate both Jaks and IFNGR1 [128], or STAT1 can be dephosphorylated in the nucleus by nuclear tyrosine phosphatases [129].

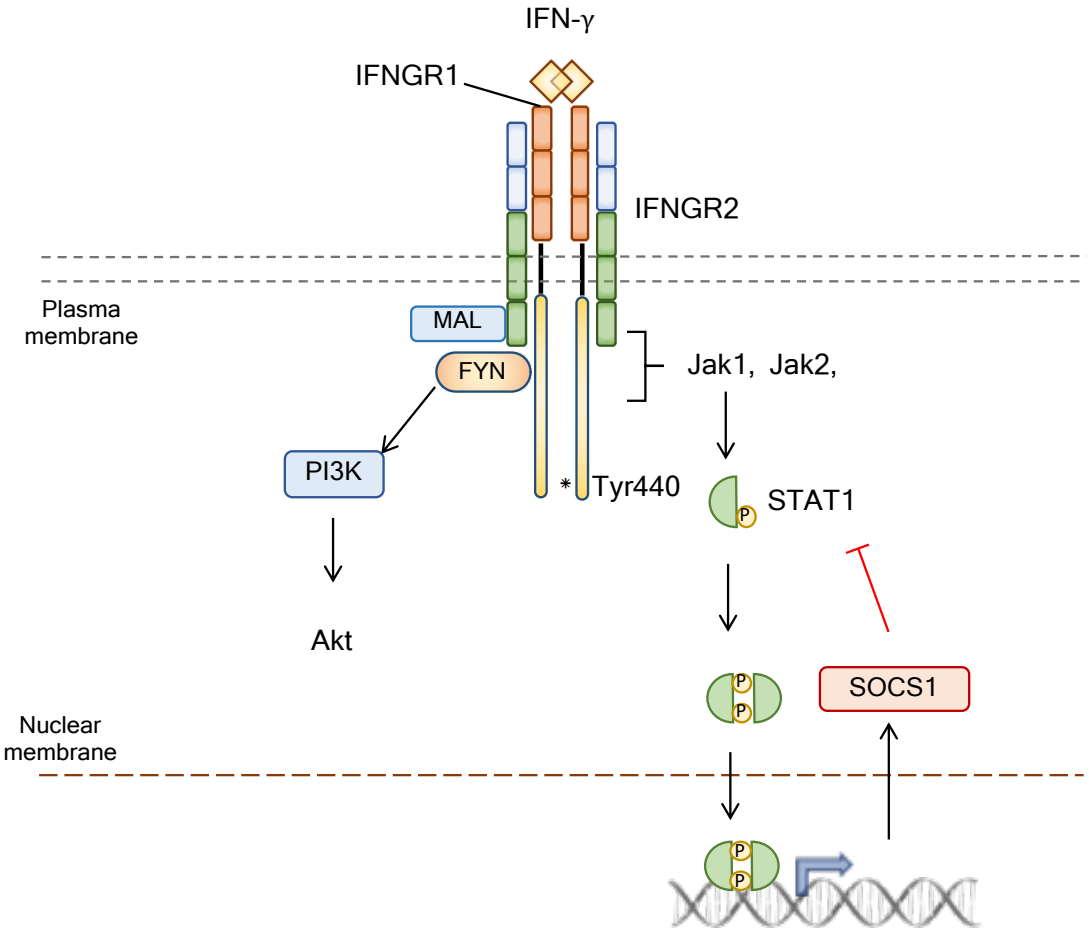

Figure 1.6. Interferon-γ signalling pathways. IFN-γ is a dimer that binds to two subunits of IFNGR1 and two subunits of IFNGR2. This leads to the recruitment and activation of Jaks, which become active and phosphorylate specific tyrosine residues in the cytoplasmic tail of each IFNGR1. This leads to the recruitment of STAT1 and their phosphorylation by the Jaks. Phosphorylated STAT1 dimerize and enter the nucleus, where they control the expression of several genes. Receptor dimerization can also lead to the recruitment of other adaptor proteins such as MAL of Fyn, the eventually results in the activation of the Akt pathway, among others.

1.5. Fibrosis

Fibrosis is a pathological hallmark of many chronic degenerative diseases and is characterised by the deposition of extracellular matrix following tissue damage or persistent inflammation [130]. While the inflammatory processes responsible for the onset of tissue fibrosis are context dependent, the clinical features are often similar. Most fibrotic disorders are caused by persistent irritants that sustain the production of growth factors, pro-inflammatory cytokines and angiogenic factors that promote the accumulation of connective tissue components (e.g., hyaluronic acid, fibronectin, and interstitial collagens), and eventually alter the normal tissue architecture [31].

The molecular mechanisms that drive fibrosis are intrinsically linked with those that promote wound healing. In the late phase and resolution of inflammation, inflammatory macrophages secrete different growth factors such as TGF-β1 and PDGF so as to regenerate the tissue and return to homeostasis (*Sections 1.1.7* & *1.1.8*). These factors stimulate the proliferation of epithelial cells to surround the injury site and the formation of new blood vessels [31]. For example, TGF-β1 acting *via* the transcription factors Smad promotes the differentiation of fibroblasts and resident epithelial cells into collagen-producing myofibroblasts [131, 132]. In addition, the IL-6 family cytokine oncostatin-M (OSM) has also been shown to promote myofibroblast differentiation via Jak/STAT pathway activation. [133]. Activated myofibroblasts stimulate wound contraction and sustain the migration of endothelial and epithelial cells to regenerate the damaged tissue and complete the wound healing process [31].

However, during persistent or unresolved inflammation this repair process becomes dysregulated and contributes to scarring. Several cell types can be responsible of the onset of fibrosis. In particular, myofibroblasts are one of the main stromal cells implicated in the production of pathological ECM proteins, including collagen type I [130, 134]. They also modulate the ECM properties by expressing cross-linking enzymes such as lysyl oxidases [135] and transglutaminases [136], which are responsible for collagen and elastin cross-linking and support their stability

against metalloproteases [135]. For example, OSM-mediated myofibroblast differentiation promotes idiopathic pulmonary [137] and kidney fibrosis [133].

In addition to myofibroblasts, macrophages also contribute to the onset and regulation of fibrosis [138]. However, their precise role in the pathology is controversial. Here, some studies have shown macrophages to promote the differentiation and activation of myofibroblasts, and changes in the relative expression of MMPs and tissue inhibitors of metalloproteinases (TIMPs) in macrophages at the site of injury ultimately dictates the outcome of fibrosis [138]. Other studies have linked macrophage activity with the resolution of fibrosis in a mechanism involving arginase-1 and the inhibition of myofibroblast survival [139]. Therefore, it is likely that specific subpopulations of macrophages dictate pro- or anti-fibrotic outcomes. Ultimately, these involvements are likely to be context dependent, and specific to tissue microenvironment.

Effector cytokine production by CD4 T-cells plays an integral role in the development of fibrosis. For example, the Th2-derived cytokines IL-4 and IL-13 promote myofibroblast differentiation and activation [140], and stimulate the expression and function of several pro-fibrotic genes including collagen [141], arginase [142] and several MMPs and TIMPs [143, 144]. While these pro-fibrotic Th2 type responses often support signalling through TGF-β/Smad3 pathway, these activities may also arise in the absence of TGF-β [145].

While Th2 activities have historically been regarded as pro-fibrotic, Th1 responses are frequently considered protective or anti-fibrotic [31, 146]. Indeed, Th1 and Th2 effector cytokine responses often oppose each other [146]. In this regard, several studies have shown that the Th1 cytokines IFN-γ and IL-12 decrease collagen deposition in models of schistosomiasis [147], pulmonary [148, 149], liver [150] and kidney fibrosis [151]. However, these activities are typically context dependent, and several recent investigations challenge this Th1/Th2 paradigm. For example, in our model of recurrent peritoneal inflammation, fibrosis is Th1-dependent [33]. In this model, IFN-γ-mediated STAT1 signalling in the peritoneal membrane alters the correct turnover of the ECM and leads to fibrosis [33] (*Section 1.3.5*). Importantly, in this context fibrosis onset does not rely on the traditional pro-fibrotic cytokines OSM, IL-4, IL-13 or TGF-β1 [33, 152]. The involvement of

IFN-γ in tissue remodelling has further been supported by observation in double *Tcra*$^{-/-}$*Socs1*$^{-/-}$ mice, where the development of colitis is promoted by excessive IFN-γ-mediated STAT1 signalling [153]. In addition, recent studies have shown that Th1 cells locate in close proximity to activated hepatic stellate cells and areas of fibrosis in patients with biliary atresia [154]. Here, IFN-γ secretion by Th1 cells promotes a STAT1-mediated proliferation and secretion of pro-fibrogenic markers by hepatic stellate cells [154]. Collectively, these studies suggest that the involvement of Th1 cells in fibrosis is specific to the local tissue microenvironment, and dependent on the inflammatory context.

1.6. The peritoneal membrane

The peritoneal membrane is a heterogeneous, serous membrane that overlies the surface of all intra-abdominal organs, the diaphragm, and the parietal peritoneal wall. It is formed from a superficial mesothelial layer attached to a basement membrane. Underneath the basal membrane is a submesothelial compact zone consisting of connective tissue, fibroblast, peritoneal resident macrophages and blood vessels, and the underlying abdominal wall muscle (Figure 1.7) [155].

The peritoneal membrane has long been used as a dialysis membrane for renal replacement therapy in end-stage renal failure patients [156]. Under optimal conditions, the peritoneum acts as semi-permeable membrane that allows the efficient removal of metabolites, uremic toxins, salt and water from the patient. In this regard, peritoneal dialysis (PD) presents several advantages when compared to haemodialysis, including protection of residual renal functions [157]. However, it also presents major obstacles to sustain a long-term treatment. Here, repetitive infections and deleterious functional alterations in the peritoneal membrane after exposure to dialysis solutions are linked with thickening of the sub-mesothelial compact zone and peritoneal fibrosis [34-36, 158]. The ultimate consequence of these alterations are loss of ultrafiltration and treatment failure, which is responsible of increased mortality and morbidity in patients with end-stage renal failure [158].

During the past few decades, several animal models have been developed to understand the aetiology, mechanisms and stages involved in the exacerbation of

peritoneal tissue injury [159, 160]. These include both acute and chronic animal models [161-163]. Acute models describe experiments of short duration that study the impact of a single dwell in the peritoneal membrane (*Sections 2.3.2* & *2.3.3*). Chronic models such as the catheter implantation and peritoneal dialysis exposure model evaluate the impact of peritoneal dialysis fluids used in human therapy. These models are designed to replicate the events associated with prolonged exposure to a dialysis regime [163]. Such models provide opportunities to test the impact of uraemia on local and systemic inflammatory outputs [164].

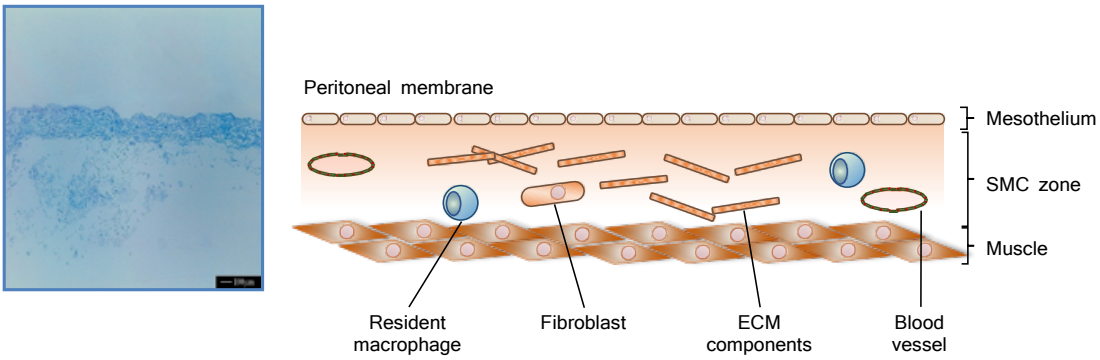

Figure 1.7. Peritoneal membrane structure. The peritoneum is a serous membrane formed by a superficial mesothelial layer followed by a submesothelial compact zone (SMC) consisting of connective tissue, fibroblast, peritoneal resident macrophages and blood vessels. Underneath the SMC zone lies the abdominal wall muscle.

1.7. Neutrophils

Neutrophils are polymorphonuclear leukocytes with a nucleus segmented in three to five connected lobules that constitute the most abundant population of circulating blood cells in humans. Their cytoplasm is characterized by the presence of "specific" granules filled with enzymes such as lysozyme, collagenase and elastase; and "azuphilic" granules, which are lysosomes containing enzymes and diverse microbicidal substances, including defensins and cathelicidins [1].

Neutrophils are produced in the bone marrow from a common lineage with mononuclear phagocytes. These precursors mature into neutrophils by the action of

granulocyte colony-stimulating factor (G-CSF) [1], and they are released to the circulation where they last for around 3-5 days [165]. Upon pathogen invasion, neutrophils are quickly recruited to the site of the infection and they constitute the main effector cells during the early stages of inflammation (*Section 1.1.6*).

Historically, neutrophils have been regarded as a homogeneous cell population with specific functions. However, investigations by Tsuda and co-workers have shown that different neutrophil subsets present distinct effector characteristics as defined by specific cytokine production, an ability to control macrophage activation, and the expression of TLRs and other surface antigens [166]. The effector characteristics of this cells, as well as the mechanisms involved in their activation will be discusses in the following sections.

1.7.1. Neutrophil recruitment

Neutrophil recruitment to the inflammation site is a multistep process that requires their tethering and rolling along the endothelial surface followed by an arrest and transmigration into the inflamed tissue. Collectively, these processes are known as the leukocyte adhesion cascade, and have been extensively reviewed by Ley and colleagues [167]. Briefly, inflammatory activation leads to the expression of P- and E-selectins on the surface of activated endothelial cells [168]. Shear-stress mediated interactions between selectins and their ligands on the surface of circulating neutrophils allow them to adhere to the endothelium and roll [169]. Selectin engagement to their ligands as well as chemokine signalling induce integrin activation in the rolling neutrophil [170]. Here, interaction of the activated β2 integrin in the neutrophils with intercellular adhesion molecule (ICAM)-1 in the endothelium promotes neutrophil arrest [171] and subsequent crawl inside the high endothelial venules (HEV), seeking optimal sites for transmigration towards the chemoattractant gradient [172, 173]. Once at the site of inflammation, neutrophils become fully activated – or primed – to elicit their effector functions in order to eliminate the invading pathogens.

1.7.2. Neutrophil priming

Neutrophils in circulation are quiescent so as to minimize the release of reactive oxygen species (ROS) and proteolytic granules that otherwise would induce tissue damage [174]. Neutrophil activation is therefore required so that these cells are fully effective at the site of infection or injury. Neutrophil priming is usually a two-step process that is initiated during their extravasation from the blood to the inflamed tissue. This is subsequently followed by a full neutrophil activation by pro-inflammatory stimuli local to the site of disease [174]. These priming factors can be divided into early-phase cytokines (e.g., TNF-α and IL-1β) and PAMPs (e.g., endotoxin); or late-phase chemoattractants and growth factors, including CXCL1, CXCL8 and LTB_4 [175, 176]. Priming can also occur by interaction between the neutrophils and endothelial surfaces during extravasation [177], and is essential to ensure the optimal production of reactive oxygen species, bioactive lipid mediators [177] and degranulation [175, 178].

1.7.3. Neutrophil effector functions

Neutrophils deliver a microbicidal response through several mechanisms. The following section will discuss the capacities of neutrophils to undergo phagocytosis, respiratory burst, degranulation and NETosis – the formation of extracellular DNA traps (NETs) (Figure 1.8).

Phagocytosis

Phagocytosis is a form of endocytosis performed by specialised cells in which solid particles including microorganisms, dead or dying cells and cell debris are engulfed from the extracellular space. To do so, neutrophils express a broad range of receptors capable of recognizing these solid particles. For example, Fc-receptors, complement receptors, scavenger receptors, integrins, lectin and TLRs [179]. Some receptors such as TLRs directly recognise conserved PAMPs expressed in the surface of invading pathogens and mediate phagocytosis. Other receptors, such as Fc-receptors and complement receptors, rely on the recognition of pathogens by different host molecules to undergo phagocytosis (Figure 1.9). For example, binding of FcγR1 to the conserved Fc regions of IgG [180], and binding of complement

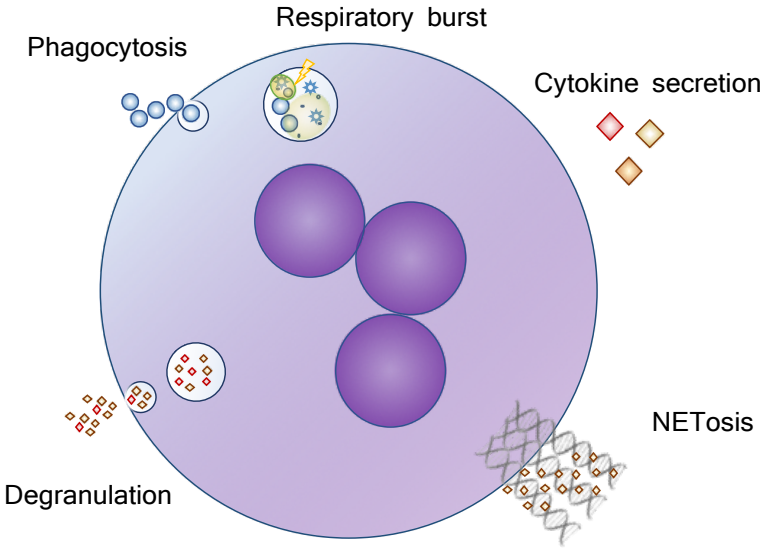

Figure 1.8. Neutrophils elicit their antimicrobial activities by different mechanism. Neutrophil effector functions against pathogens include their ingest by phagocytosis and their degradation through the generation of free radicals (respiratory burst), which oxidize a broad range of organic molecules. Degranulation releases contents of the secretory granules, including antimicrobial peptides, iron binding proteins and enzymes. Neutrophils can also produce and release cytokines that further amplify the inflammatory cascade; and they can undergo NETosis, where the release of decondensed chromatin together with antimicrobial peptides trap the pathogens and promote their degradation.

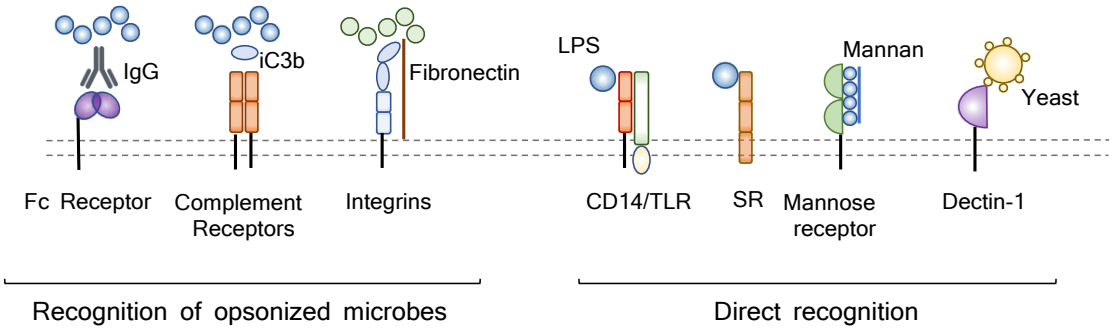

Figure 1.9. Neutrophil can recognize and engulf invading pathogens using several phagocytic receptors. Some of these receptors (e.g., Fc receptors) rely on the previous opsonisation of the pathogen by different host molecules, such antibodies and the complement protein iC3b. Other receptors (e.g., TLRs) directly recognize conserved determinants in the surface of the microbes, resulting in the engulfment of the pathogen. Adapted from ref 179.

receptor CR3 to iC3b [181] mediates the phagocytosis of the respective IgG- and iC3b-opsonized particles.

After internalization, microbes are contained within a phagosome, which then fuses with lysosome granules to form a phagolysosome. The release of the digestive and antibacterial compounds into the phagolysosome permits the degradation of the engulfed pathogens [182]. In addition, the assembling of the NADPH oxidase complex at the phagosome membrane allows the production of superoxide and other ROS within the vesicle and the killing of microbes [183]. Therefore, phagocytosis and the production of ROS are two processes strongly related. For a more detailed review of phagocytosis, referrer to [179].

Respiratory burst

Phagocytosis by neutrophils is accompanied by an increase in oxygen consumption termed respiratory burst, which is caused by the assembly and activation of the NADPH oxidase complex in the membrane of the phagosomes [184]. There are seven members of the NADPH oxidase family (also termed NOX), which are implicated in different events including host defence, cellular signalling and the regulation of gene expression. Their structure and functions have been extensively reviewed before [185]. The NAPDH oxidase present in phagocytes is the complex NOX2, which comprises six different subunits: the catalytic subunit $gp91^{phox}$ (a flavocytochrome) and the regulatory subunits $p22^{phox}$, $p40^{phox}$, $p47^{phox}$, $p67^{phox}$, and RAC2. Altogether, the complex mediates the transference of an electron from the reduction of the substrate NADPH across the phagosome membrane to molecular oxygen inside the phagosome to generate superoxide (O_2^-) ion (Figure 1.10) [185]. Eventually, this O_2^- can also be converted into other ROS either spontaneously or by the action of several enzymes (Figure 1.11).

Collectively, ROS can oxidase non-specifically a broad range of organic molecules, damaging DNA, carbohydrates, lipid cell membranes and proteins, and they constitute an essential mechanism for killing microbes. The importance of the respiratory burst as a major antimicrobial mechanism is perhaps best illustrated in inherited deficiencies of the enzyme NOX2, such as chronic granulomatous disease. Here, genetic mutations that affect any of the 4 genes encoding protein

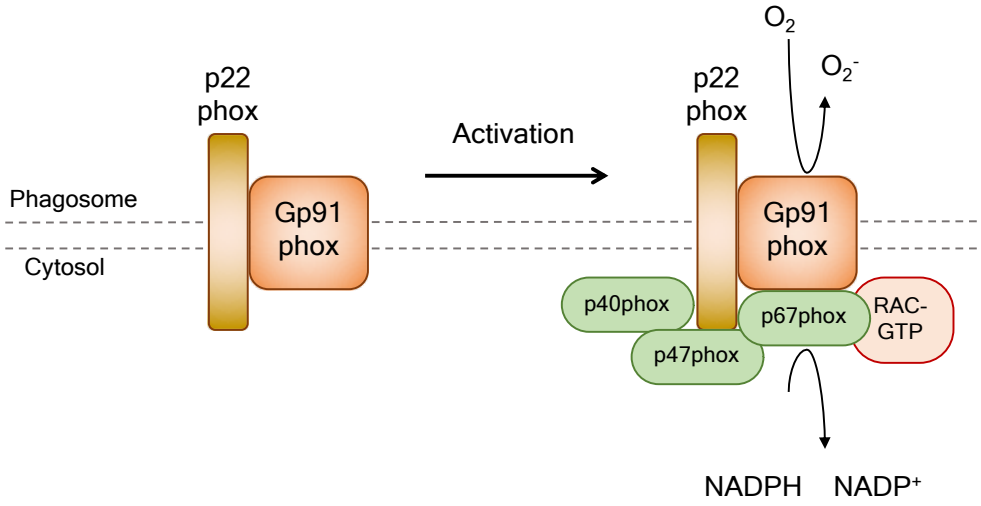

Figure 1.11. NAPDH oxidase complex initiates the production of superoxide. Upon neutrophil activation, the cytosolic subunit p47phox becomes phosphorylated and translocates to the membrane of the phagosome, where it interacts with the integral membrane proteins gp91phox and p22phox (cytochrome b558). This leads to the binding of the subunits p40phox, p67phox and RAC-GTP, which form the active NAPDH oxidase complex. The active complex transfers an electron from NAPDH across the phagosome membrane to molecular oxygen inside the phagosome to generate superoxide (O_2^-).

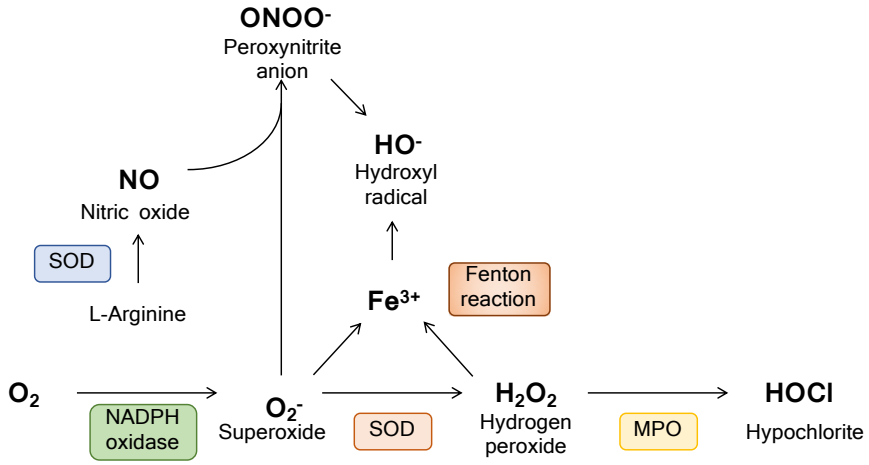

Figure 1.10. Summary of the generation of free radicals by neutrophils. Superoxide produced by the NADPH oxidase complex can be further catalysed to hydrogen peroxidase by the enzyme superoxide dismutase. Hydrogen peroxide can be converted to hypochlorite by myeloperoxidase, or together with superoxide and transition metal ions can be spontaneously converted into hydroxyl radical. Nitric oxide synthase catalyses the formation of nitric oxide from L-arginine. Together with superoxide, nitric oxide can for peroxynitrite anion.

components of NOX2 are associated to the inability of patients to deal with pathogens, resulting in chronic and often fatal infections [186]. In particular, the X-linked form of chronic granulomatosis disease arise from mutations of the catalytic subunit $gp91^{phox}$ [187], while the autosomal recessive forms are associated to mutations of the genes for $p22^{phox}$, $p47^{phox}$, or $p67^{phox}$ [188, 189].

Degranulation

Degranulation is another neutrophil antimicrobial mechanism consisting in the release of cytoplasmic granules into the extracellular space or the phagosome [190]. Neutrophils contain four different types of granules: (1) primary granules (azuphilic granules), that contain toxic mediators such as elastase, cathepsins and defensins; (2) secondary granules (specific granules), and (3) tertiary granules, that contain lactoferrin and MMP9, respectively, together with other molecules; and (4) secretory vesicles [190].

Upon receptor stimulation by a secretagogue, cytoplasmic granules are released following a four-step mechanism [191]: (1) the granule is recruited from the cytoplasm to the plasma or phagosome membrane in a process that relies on the actin cytoskeleton remodelling; (2) the secretory vesicle outer lipid bilayer contacts the inner surface of the target membrane by tethering and docking; (3) a fusion pore is formed between both membranes, which finally (4) expands and completes the fusion of the granule to the target membrane and the release of the granular content [192].

Degranulation must be a tightly regulated process in order to prevent tissue damage, as neutrophils granules are highly enriched in tissue-degrading proteases. Thus, the release of granules depends on non-redundant receptor-mediated activation of intracellular pathways, including β-arrestins, the Rho guanosine triphosphatase Rac2, and others. In addition, initiation of NADPH oxidase activity coincides to degranulation, and occurs after the fusion between the cytoplasmic granules into the phagosome [193, 194]. Here, NADPH oxidase activity may control the pH within the granule to support optimal proteolytic activity. For a more in depth review on degranulation, see [190].

NETosis

NETosis is a form of cell death characterised by the release of decondensed chromatin and other granules to the extracellular space following nuclear and granule membrane disintegration [174]. It is a relative slow antimicrobial process whose mechanism of activation depends on a broad variety of stimuli, including cytokines such as TNF-α and IL-8, or PAMPs from different pathogens. For example, NETosis stimulated with microbial products requires NADPH oxidase activity to function [195], whereas the induction of NETosis by soluble immune complexes can be also achieved in the absence of ROS [196].

Extracellular traps provide antimicrobial activities by several mechanisms. First, the stickiness of the decondensed chromatin acts as a net that traps pathogens, which are then exposed to the different antimicrobial peptides linked within the chromatin, including myeloid peroxidase, neutrophil elastase, S100 calcium-binding protein A1 (S100A), and lactoferrin-chelating proteins [174]. In addition, histones themselves present significant antimicrobial activity [197]. Conversely, the abundance of pro-inflammatory mediators within the NETs have some detrimental effects, and excessive NET formation has been associated with several pathologies such as sepsis [198] and systemic lupus erythematosus nephritis [199].

1.8. Aims and hypothesis

Previous studies in the Jones laboratory have demonstrated that IL-6 acting *via* its soluble receptor is essential for competent host defence in a model of acute resolving peritonitis. This effective antimicrobial response is associated with STAT3 activation in the peritoneal lining. Conversely, repetitive episodes of bacterial infection lead to peritoneal fibrosis, which is a major cause of treatment failure in end-stage renal failure patients in peritoneal dialysis. Here, fibrosis is driven by the IL-6-dependent proliferative expansion of Th1 cells and the activation of IFN-γ-mediated STAT1 signalling in the membrane (Figure 1.5).

We hypothesise that changes in the relative activities of STAT1 and STAT3 in the peritoneum will alter the outcome of inflammation to dictate transition from successful resolution to deleterious tissue damage. The aim of this thesis is to provide a holistic interpretation of the genes regulated within the peritoneal membrane following inflammatory activation. Specifically, this thesis aims to:

1.8.1. Optimise an RNA-sequencing pipeline and library preparation from tissue

Experiments will optimise RNA extraction from peritoneal tissue and cDNA library preparation for subsequent high-throughput RNA-sequencing. Studies aim to establish a comprehensive pipeline for downstream RNA-seq analysis and interpretation.

1.8.2. Identify gene targets that influence the course of inflammation during a "resolving" and a "pro-fibrotic" environment

Adopting a holistic approach, experiments will explore changes in gene expression during acute resolving inflammation and during a pro-fibrotic setting in WT and *Il6*$^{-/-}$ mice. Molecular pathways analysis will be used to identify potential mechanisms by which the stromal compartment shapes the outcome of immune response against infection.

1.8.3. Understand the mechanisms by which IL-6 activates the local stromal compartment to direct a successful host defence

Studies will assess the impact of IL-6 trans-signalling within the stromal microenvironment to direct neutrophil effector function at the early stages of infection. Experiments will focus on how stromal derived signals indirectly contribute to neutrophil phagocytosis and respiratory burst.

1.8.4. Identify a potential novel form of murine soluble gp130

RNA-sequencing will be used to identify a potential new form of murine soluble gp130 arising from alternative splicing of the *Il6st* gene. Experiments will aim to purify and characterize this novel form of this protein.

Chapter 2. Materials and Methods

2.1. Reagents

All the reagents used in this thesis were purchased from Sigma unless otherwise specified.

2.2. Bacterial cultures

2.2.1. Bacterial strains

Staphylococcus epidermidis (strain ATTC 12228) was used to induce bacterial peritonitis *in vivo* (*Section 2.3.3*), and to perform *in vitro* phagocytosis assays (*Section 2.4.3*). A clinical isolate of *S. epidermidis*, termed SH, was used to produce *S. epidermidis* cell free supernatant (SES) (see *Section 2.3.2*). Both bacterial stocks were stored in glycerol at -80°C.

2.2.2. Growth of bacterial cultures

Using a sterile inoculating loop, a sample of dormant *S. epidermidis* stock was streaked onto an LB agar plate (OXOID). Bacterial growth was promoted by incubation at 37°C for 48 h. Single colonies were captured and used to inoculate 125 ml flasks containing 10 ml of nutrient broth n°2 (OXOID). The culture was incubated for 6 h at 37°C with gentle agitation (180 rpm) unless otherwise specified. To standardize the growth phase of the bacterial cultures, 60 µL of culture were transferred to 250 ml flasks containing 60 ml of fresh nutrient broth n°2, before incubation for 18 h at 37°C with gentle agitation.

2.2.3. Fluorescent labelling of bacteria

The optimal inoculum of bacteria for *in vivo* and *in vitro* experiments has been empirically determined by previous studies in the Jones laboratory [200]. For *in vitro* assays, cultures were diluted to an OD of 0.5 at 650 nm (corresponding to $5.0x10^8$ cfu/ml). For *in vivo* experiments, cultures were diluted to an absorbance of 1.10-1.15 at 650 nm ($1x10^9$ cfu/ml). The suspension was then centrifuged

(2000xg, 5 min) and the pellet resuspended to the same inoculum volume containing Cell Trace Far Red (CT-FR) (Life Technologies) (1 µM or 8 µM for *in vitro* and *in vivo*, respectively) in pre-warmed phosphate buffered saline (PBS; pH7.4) for 20 min at 37°C. The reaction was stopped by diluting the suspension in 5 volumes of RPMI 1640 (Gibco) containing 1% (w:v) of bovine serum albumen (BSA), before incubation at 37°C for 5 min. Cultures were opsonized (*Section 2.2.4*, for *ex vivo* experiments) or centrifuged and washed 3 times in PBS, before re-suspending to the initial inoculum volume in sterile PBS (for *in vivo* experiments).

2.2.4. Bacterial opsonisation

Cell Trace Far Red stained bacteria were opsonized with serum corresponding to the neutrophil genotype from which they were isolated (e.g., neutrophils from Wild Type (WT) mice were incubated with serum obtained from these mice). Briefly, fluorescently labelled bacteria (*Section 2.2.3*) were resuspended in PBS containing 10% (v:v) serum and incubated for 15 min at 37°C. Bacteria were pelleted by centrifugation (2000xg, 5 min) and washed 3 times in PBS before re-suspending in serum-free RPMI 1640.

2.3. *In vivo* experiments

2.3.1. Mouse strains

8-12 weeks old WT C57Bl/6 mice were purchased from Charles River. In-house C57Bl/6 interleukin-6 (*Il6*$^{-/-}$) and interleukin-6 receptor knock out (*Il6ra*$^{-/-}$) mice were bred in accordance with UK Home Office regulations and procedures (PPL 30/2938 and PPL P05D6A456). *Il6*$^{-/-}$ and *Il6ra*$^{-/-}$ mice were generated as previously described [61, 100].

2.3.2. Preparation of *Staphylococcus epidermidis* cell-free supernatant (SES) and induction of sterile inflammation

SES was prepared from a clinical isolate of *S. epidermidis* as described previously [20, 25]. *S. epidermidis* (SH strain) cultures were grown as described in *Section 2.2.2*. Bacterial growth was monitored until the culture medium went turbid. Bacteria were pelleted by centrifugation (2000xg for 20 min) and re-suspended in Tyrode's salt solution to an OD of 0.5 at 560 nm (corresponding to $5x10^8$ cfu/ml). The culture supernatant was collected 18-24 h later and filtered using a 0.22 µm Stericup filter bottle (Millipore). The bacterial extract was dialysed against deionized H_2O at 4°C for 8-12 h, with four changes of H_2O in total. The dialysate was divided into 10 ml aliquots in universal tubes (gbo) and frozen at -20°C overnight. Finally, aliquots were lyophilized in a freeze-drier (Edwards) and stored at -80°C for up to one year.

The bioactivity of SES was assessed *in vitro*. Briefly, resident peritoneal mononuclear cells were recovered by peritoneal lavage in complete RPMI 1640 (RPMI 1640 supplemented with 10% (v/v) heat-inactivated foetal calf serum (FCS), 2mM L-glutamine, 1mM sodium pyruvate, 100U/ml penicillin, 100µg/ml streptomycin, and 55µM 2-mercaptoethanol; all from Life Technologies), and cultured as detailed in *Section 2.4.1*. Each vial of lyophilised SES was reconstituted in 1 ml of complete RPMI 1640. Cells were stimulated in a final volume of 1 ml containing serial dilutions of the prepared SES (1/1, 1/2, 1/4, 1/8, 1/16, 1/32). Control cells received complete RPMI 1640 alone. SES-conditioned media (SES-

CM) was rendered cell free by centrifugation (500xg, 5 min), and the production of IL-6 and p40IL-12 measured by ELISA (*Section 2.5.9*) (Figure 2.1).

Acute peritoneal inflammation was induced in WT and *Il6*$^{-/-}$ mice through the intraperitoneal (i.p.) administration of SES. Lyophilised SES was reconstituted in 0.75 ml of sterile PBS/vial (Gibco) and filtered using a 0.22 μm syringe filter unit (Millipore). Mice were treated with a 0.5 ml dose of the re-suspended SES [20, 25]. At defined time points, peritoneal lining tissue and lavage fluids were collected for analysis (*Section 2.5*) (Figure 2.2A).

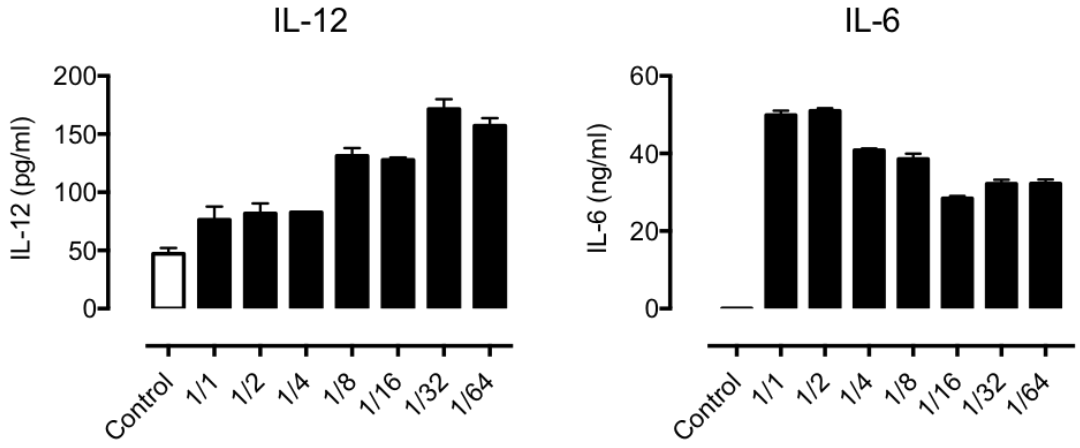

Figure 2.1. Validation of SES bioactivity in peritoneal monocytic cells. Peritoneal monocytic cells (1x10^6 cells/well; *Section 2.4.1*) were stimulated overnight in serial dilutions of SES (highest concentration, 1 part reconstituted SES to 1 part of 1 x 10^6 cells in complete RPMI 1640). IL-6 and p40-IL-12 production was quantified using ELISA in cell-free culture supernatants. Representative data from a single SES batch preparation is shown.

2.3.3. Live model of *S. epidermidis*-induced peritonitis

Live bacteria peritonitis was induced using a commercial strain of *S. epidermidis* (ATTC 12228 strain; *Section 2.2.1*). A single colony of *S. epidermidis* was isolated from a streaked agar plate and cultured as described in *Section 2.2.2*. The growth rate was periodically assessed by monitoring OD at 600 nm – OD of 1.10-1.15 corresponding to $1x10^9$ cfu/ml. Bacterial cultures ($1x10^9$ cfu/ml) were then centrifuged and resuspended in sterile PBS.

Bacterial infection was induced in WT and *Il6*$^{-/-}$ mice through intraperitoneal injection of a non-lethal dose of $5x10^8$ cfu/mice of *S. epidermidis* delivered in a volume of 0.5 ml of sterile PBS (Figure 2.2B).

2.3.4. Adoptive transfer of interferon-secreting CD4 T-helper cells

$CD4^+$ T-helper 1 cells were polarized and expanded according to *Section 2.4.2*. For *in vivo* adoptive transfer, $0.5\text{-}1.0x10^6$ Th1 cells were administered to WT, *Il6*$^{-/-}$ and *Il6ra*$^{-/-}$ mice (i.p.) in combination with 0.5 ml of SES (*Section 2.3.2*). Control mice received the same amount of sorted naïve $CD4^+$ (Th0) T cells. At 3 and 6 h after injection, peritoneal lining tissue and lavage samples were collected for subsequent analysis (*Section 2.5*) (Figure 2.2C).

2.3.5. *In vivo* neutrophil effector function assay

To assess the activation and effector characteristics of infiltrating neutrophils in response to bacterial infection, mice were treated with CT-FR fluorescently labelled *S. epidermidis* (*Section 2.2.3*). WT and *Il6*$^{-/-}$ mice were administered (i.p.) with $5x10^8$ cfu/mice of labelled *S. epidermidis* in 0.5 ml of sterile PBS.

At desired time points, the peritoneal cavity was lavaged with 2 ml of RPMI 1640 containing 5 µM of aminophenyl fluoresceine (APF, from Life Technologies), a reactive oxygen species indicator that is sensitive for hydroxyl radical, hypochlorite or peroxynitrite anion (Figure 2.3). The lavage was incubated at 37°C for 15 min and placed in an iced water bath. Cells were then collected by

centrifugation (500xg, 5 min), and stained for flow cytometry analysis using fluorochrome-labelled antibody for Ly6G (*Section 2.5.8*).

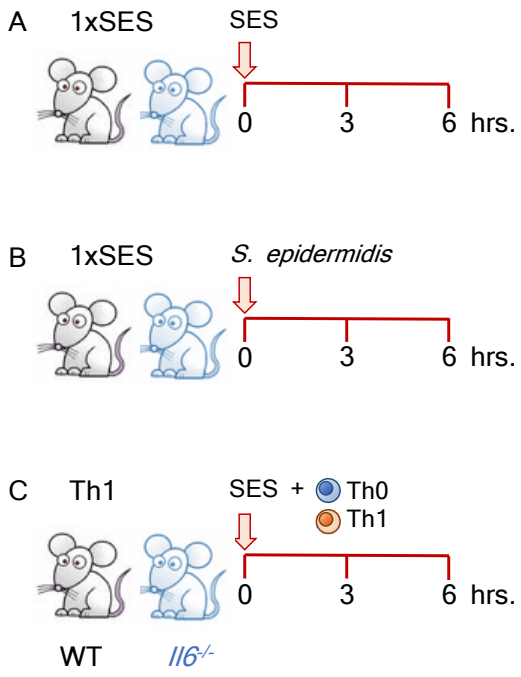

Figure 2.2. Murine models of peritoneal inflammation. A. Each vial of SES was reconstituted in 0.75 ml of sterile PBS, and wild type (WT) or IL-6 deficient (*Il6*$^{-/-}$) mice were intraperitoneally (i.p.) injected with 0.5 ml of resuspended SES. **B.** A defined dose of *S. epidermidis* (5x10^{8} cfu/mice) was injected (i.p.) into WT and *Il6*$^{-/-}$ mice. **C.** Naïve CD4^{+} T cells were polarised into Th1 cells using anti-CD3, anti-CD28 and SES-CM, as specified in *Section 2.4.2*. Th1 cells were adoptively transfer (i.p) into WT, *Il6*$^{-/-}$ and *Il6ra*$^{-/-}$ mice together with a single dose of SES. Control mice received an equivalent amount of sorted naïve CD4^{+} (Th0) T cells. At 3 and 6 h, peritoneal lavage and peritoneal tissue were collected for analysis.

2.4. *In vitro* experiments

2.4.1. Generation of monocytic cell-derived SES-induced conditioned medium (SES-CM)

Resident peritoneal mononuclear cells were recovered by peritoneal lavage (*Section 2.5.3*) from WT mice and cultured in completed RPMI 1640. Cells were seeded in a 24-well plate at a concentration of $1x10^6$ cells/well and allowed to adhere. Non-adherent mononuclear cells were removed, and cells were stimulated overnight with SES at 37°C, 5% CO_2. Each vial of lyophilised SES was reconstituted in 1 ml of complete RPMI 1640. Cells were stimulated in a final volume of 1 ml containing 50% (v:v) reconstituted SES. SES-CM was rendered cell free by centrifugation (500xg, 5 min).

2.4.2. SES-CM differentiation of $CD4^+$ T cells

FACS-sorted WT naïve $CD4^+CD25^-CD44^{lo}CD62L^{hi}$ cells (Table 2.2) were cultured in 96-well plates at a concentration of $1x10^5$ cells/well in completed RPMI 1640 and activated with anti-CD3 (plate-bound, 1 µg/ml, 45-2C11) and anti-CD28 (soluble, 5 µg/ml, 37.51) co-stimulation in the presence of SES-CM (1:1) for 4 days at 37°C and 5% CO_2 [33]. After 4 days, T cells were re-stimulated with 50 ng/ml PMA and 500 ng/ml ionomycin in the presence of 3 µM of monensin for 3 h and stained with fluorescently-labelled antibodies for CD4 and IFN-γ (Table 2.2). The proportion of IFN-γ^+ Th1 cells was assessed by flow cytometry (*Section 2.5.8*).

2.4.3. *In vitro* neutrophil effector function assay

Neutrophils derived from the circulation of WT and *Il6*$^{-/-}$ mice were used to assess the anti-bacterial properties of these cells from the blood. Whole blood was collected by cardiac puncture (*Section 2.5.1*), diluted 1:10 and washed 3 times in ice cold PBS. Cells were resuspended in serum-free RPMI 1640 containing 5 µM of APF and incubated for 30 min at 37°C.

APF-loaded cells were then split into 100 µl aliquots and cultured with the same volume of pre-warmed, opsonized CT-FR-stained *S. epidermidis* at 37°C (*Sections 2.2.3 & 2.2.4*). Cells were incubated for pre-determined intervals (0-30 min) before transfer to an iced water bath. Treated cells were maintained on ice for the subsequent steps.

Neutrophils were labelled with a fluorochrome-conjugated anti-Ly6G antibody (*Section 2.5.8*). After staining, cells were washed 3 times in Red Blood Cell lysis (Life Technologies), and resuspended in 200 µl of Flow buffer (PBS supplemented with 0.5% (w:v) BSA, 5mM EDTA and 7.5 mM sodium azide) for flow cytometry analysis (*Section 2.5.8*).

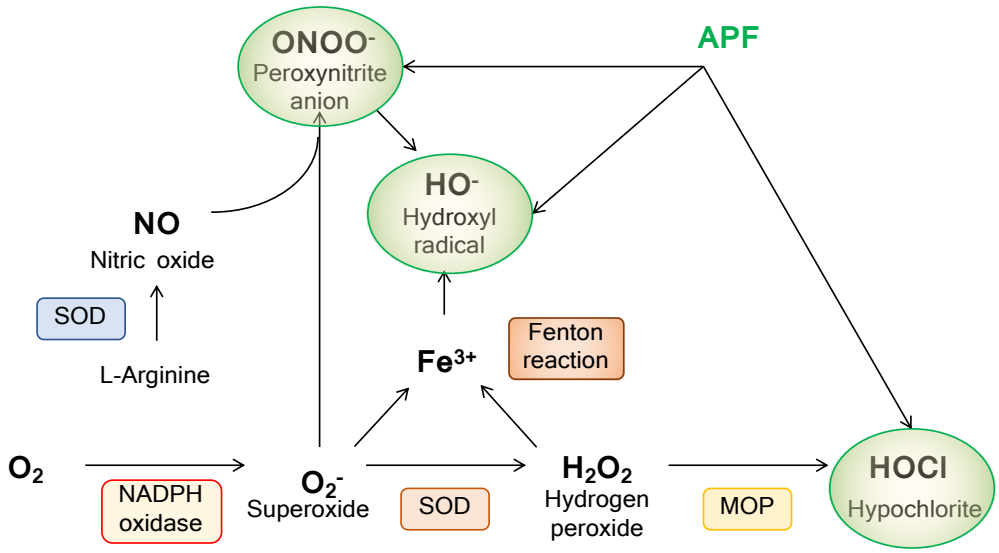

Figure 2.3. Aminophenyl fluoresceine (APF) was used to monitor respiratory burst in neutrophils. This fluorescent probe can detect peroxynitrite anions, hydroxyl radical and hypochlorite (outlined in green).

2.5. Sample collection and processing

2.5.1. Collection of whole blood

Total blood from WT and *Il6*$^{-/-}$ was collected by cardiac puncture (1 ml syringe, 25G needle; both from BD) as to minimise platelet activation. Blood was immediately transferred to a BD™ Vacutainer™ Plastic K2EDTA tube (BD) containing EDTA as anticoagulant. Tubes were gently inverted 180º and back 8 to 10 times to ensure mixing with the wall-coated EDTA and placed on ice until use.

2.5.2. Collection of blood serum

Total blood was collected (*Section 2.5.1*) and transferred to a sterile tube before incubation for 30 min at room temperature to allow blood coagulation. Samples were rendered cell free by centrifugation at 2000xg for 10 min and the serum carefully transferred to a new tube.

2.5.3. Peritoneal lavage

To harvest resident peritoneal mononuclear cells, the peritoneal cavity was lavage with 5 ml of complete RPMI 1640 (21G needle, BD) (see *Section 2.3.2* & *Section 2.4.2*). For the immunodetection of inflammatory mediators, the peritoneal cavity was lavaged with 2 ml of sterile PBS (21G needle). Lavaged samples were rendered cell-free (2000xg, 5 min, 4ºC) and stored at -80ºC. For *in vivo* neutrophil phagocytosis assays, the cavity was lavaged with 2 ml of RPMI 1640 (21G needle) containing 5 μM of APF as described in *Section 2.3.5*.

2.5.4. Peritoneal membrane collection

Parietal peritoneal membrane was collected using standard aseptic techniques. Two sections of the peritoneal lining were harvested (Figure 2.4) and immediately snap frozen in liquid nitrogen. Tissues sections were stored at -80ºC for RNA extraction (*Section 2.5.5*) and additional validation purposes.

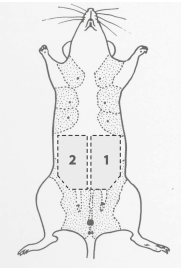

Figure 2.4. Representation of the mouse abdomen. The parietal peritoneal membrane was sampled in two halves. Half 1 was used to extract RNA. Half 2 was stored for further validation.

2.5.5. Total RNA extraction from peritoneal membrane

Total RNA was extracted using the RNeasy Mini Kit (QIAGEN). Here, the manufacturer's protocol for total RNA extraction was adapted for fibrous tissue. All steps were performed in a laminar flow hood. Peritoneal membranes (*Section 2.5.4*) were weighed and homogenised in 1 ml of RLT Buffer supplemented with β-Mercaptoethanol (1:100 v:v) per 80 mg of tissue using a D1000 Handheld Homogenizer (Benchmark Scientific). The suspension (600 µl) was diluted with 2 volumes of RNase-free water and treated with proteinase K (Invitrogen, 0.2 mg/ml final concentration) for 10 min at 55°C. Samples were centrifuged at 10,000xg for 5 min to remove debris, and the supernatant transferred to a new tube containing an equal volume of 70% (v:v) ethanol. Total RNA was extracted using a 15 min in-column DNase digestion protocol as outlined in the manufacturer's instructions (QIAGEN). RNA was eluted in 50 µl of RNase-free water, and its quantity, purity and integrity assessed using a NanoDrop 2000 Spectrophotometer (Thermo Scientific) and RNA Nano chip analysis on the Agilent 2100 Bioanalyser (Agilent).

2.5.6. Complimentary (c)DNA synthesis

Total RNA was reverse transcribed into c DNA using a random oligonucleotide primer method (Precision nanoScript 2 Reverse Transcription kit; Primer design). For all samples, cDNA was generated from 1 µg of total RNA (*Section 2.5.5*) as described in the manufacturers' instructions. Resulting cDNA was diluted 1:2 to obtain a final concentration of 25 ng/µl and stored at -20°C for up to 6 months.

2.5.7. Quantitative Polymerase Chain Reaction (qPCR)

Gene expression was quantified by qPCR using TaqMan Gene Expression Assay (Applied Biosystems) chemistry, and following manufacturers' instructions. The reaction was performed in a MicroAmp Optical 384-well Reaction Plate with Barcode (Applied Biosystems), using 5 µl of TaqMan Fast Advanced Master Mix, 0.5 µl of TaqMan Gene Expression Assay (consisting in the primers and probes; Table 2.1), 3.5 µl of nuclease-free water and 1 µl of cDNA (generated as outlined in *Section 2.5.6*), and using the Fast protocol in the QuantStudio 12K Flex Real-Time PCR system (Applied Biosystems).

Data was analysed using a comparative threshold cycle (Ct) method [201, 202]. This method equates the expression of the gene of interest as relative to an internal housekeeping control gene. Here, Ct values are defined as the PCR cycle number in which the signal of the reporter crosses an arbitrary placed threshold within the exponential phase of amplification. Ct is inversely related to the amount of amplicon or target gene present in the sample. Thus, a more abundant amplicon reaches the exponential phase of amplification sooner, resulting in a lower Ct value. Ct values for each gene of interest are then standardised against a comparative analysis of control housekeeping genes. In the present thesis, the gene *Tbp* was used as internal housekeeping control.

Table 2.1. List of primers used in this thesis

Gene	Specie	Assay ID	Dye	Amplicon Length
Tbp	Mouse	Mm00446971_m1	FAM-MGB	93
Socs3	Mouse	Mm00545913_s1	FAM-MGB	76
Irf1	Mouse	Mm01288580_m1	FAM-MGB	66
Isg15	Mouse	Mm01705338_s1	FAM-MGB	107
Il1b	Mouse	Mm00434228_m1	FAM-MGB	90

2.5.8. Flow cytometry

For antibody staining of cell surface markers, cells ($2x10^5$ cells) were resuspend in 50 µl of Blocking Buffer (Flow buffer containing 0.008% (v:v) Fc-Block; anti-CD16/CD32), and incubated for 10 min at 4°C. After blocking, 50 µl of fluorochrome-conjugated antibodies specific for cell surface proteins were added and incubated for 30 min at 4°C. See Table 2.2 for specific information on antibodies used in flow cytometry. Cells were washed twice in Flow buffer, resuspended in 200 µl Flow buffer and immediately acquired using a Beckman Coulter Cyan-ADP flow cytometer. For imaging flow cytometry, cells were resuspended in 100 µl of PBS and acquired using the ImageStream imaging flow cytometer (Amnis).

Table 2.2. List of antibodies used in this thesis

Antibody	Specie	Conjugated	Clone	Company
CD62L	anti-mouse	FITC	MEL-14	eBioscience
CD25	anti-mouse	PE	PL61.5	eBioscience
CD44	anti-human/mouse	APC	IM7	eBioscience
CD4	anti-mouse	PerCP-Cyanine5.5	RM4-5	eBioscience
IFN-γ	anti-mouse	FITC	XMG1.2	eBioscience
Ly6G	rat anti-mouse	v450	1A8	BD Bioscience
CD16/ CD32	rat anti-mouse	-	2.4G2	BD Bioscience

2.5.9. Enzyme-linked immunosorbent Assay (ELISA)

Inflammatory cytokines were quantified in peritoneal lavage, cell cultures supernatant and serum samples using commercially available ELISA. All ELISA protocols were based on the manufacturer's instructions. Table 2.3 summarizes the assays used and provides information relevant to the capture and detection antibodies, as well as the sensitivity range of the assay.

Table 2.3. List of ELISA kits used in this thesis

ELISA	Manufacturer	Cat #	Capture antibody	Standard	Detection antibody
IL-6	BD Bioscience	555240	1:250 dilution	1000-15.6 pg/ml	1:250 dilution
	R&D Systems	DY406	2.0 µg/ml	1000-15.6 pg/ml	150 ng/ml
IL-6R	R&D Systems	DY1830	3.0 µg/ml	3000-46.9 pg/ml	400 ng/ml
gp130	R&D Systems	DY468	2.0 µg/ml	8000-125 pg/mL	100 ng/ml
IFN-γ	R&D Systems	DY485	4 µg/ml	2000-31.3 pg/ml	400 ng/ml
IL-12	BD Bioscience	555165	1:120 dilution	1000-15.6 pg/ml	1:60 dilution

2.6. Statistical analysis

The resource equation was used to determine the most appropriate statistical group size for *in vivo* experiments where no previous data was available for power analysis.

Resource equation: **E=N-T-B**

Where; **E** =10-20, **N**=total number of animals, **T**=Number of treatments and **B**=Block degrees of freedom in the Analysis of variants (ANOVA).

When preliminary data was available, power calculation (0.95 power) was performed using G power software. While individual experiments were conducted with small group numbers, comparisons between independent experiments and historical data showed a high degree of consistency. In addition, experimental mouse numbers were often restricted by the availability of mice, and where possible the study design was adapted to accommodate the principles of the 3Rs in animal research [203].

Statistical analysis was performed using Graph Pad Prism version 6. One-way analysis of variance (ANOVA) with Bonferroni correction was used to determine significant difference between the means of three or more independent groups. Time course experiments consisted of two variables (time and treatment) and therefore were analysed by two-way ANOVA, with Bonferroni post-tests to compare treatments between individual time points and conditions. Correlation between two variables was assessed by linear regression. $p < 0.05$ were considered significant, and all data points plotted as mean ± SEM as outlined in the individual figure legends.

Specific mathematical modelling and statistical analysis for clustering is detailed in Chapter 3 and 4 (*Sections 3.2.11* & *4.2.2*).

Chapter 3. RNA-sequencing of the inflamed peritoneal membrane

3.1. Introduction

DNA sequencing methods have revolutionised the way in which we study genomic and epigenetic information. Sequencing reactions were traditionally built around the 'first generation' automated Sanger method. Sanger sequencing dominated the industry for many years and contributed to the first annotated sequence of the human genome [204]. Recent advances have led to the development of next-generation sequencing (NGS) platforms that are cheaper, faster and more accurate [204]. The introduction of these methods enabled the study of genetics, gene regulation, epigenetics and large-scale population-based investigations.

Advances in the next generation sequencing of RNA (termed RNA-sequencing or RNA-seq) has displaced hybridization-based approaches (i.e. microarrays) for transcriptome analysis. These methods offer several advantages. Unlike microarrays, RNA-seq is not limited to detecting transcripts that correspond to already known genome sequences [205, 206]. In addition, RNA-seq now allows studies of coding and non-coding RNAs, and investigations of differential mRNA splicing and small RNA variants [205, 206]. Thus, RNA-seq provides a holistic and unbiased interpretation of gene regulation.

In this Chapter, experiments describe the development of an RNA-seq platform and downstream bioinformatics pipeline for the study of inflammation-induced gene changes in the peritoneal membrane of SES challenged mice.

3.2. Materials and Methods

3.2.1. *In vivo* models of inflammation and samples

RNA-seq was established to profile the transcriptome of the peritoneal membrane during acute resolving inflammation. This approach allowed a computational analysis of STAT1 and STAT3 gene signatures in response to IL-6, and settings where IFN-γ secreting Th1 cells contribute to the local inflammation [33]. Acute inflammation was induced in WT and *Il6*$^{-/-}$ mice by the (i.p.) administration of a single dose of SES (*Section 2.3.2*). Parietal peritoneal tissue was extracted at 3 and 6 h post SES administration (*Section 2.5.4*). These coincide with the optimal timing of STAT1 and STAT3 activation in the peritoneal membrane of SES challenged mice [33]. Unchallenged WT and *Il6*$^{-/-}$ mice were used as controls. Recurrent peritoneal inflammation promotes peritoneal fibrosis through the expansion of IFN-γ secreting CD4^{+} Th1 cells [33]. To replicate this pro-fibrotic state, *ex vivo* expanded Th1 cells were adoptively transferred into mice together with SES (*Section 2.3.3*). In this regard, the adoptive transfer of *ex vivo* SES-polarised Th1 cells restores peritoneal fibrosis in *Il6*$^{-/-}$ mice that are normally protected from this form of pathology [33]. Peritoneal tissue was harvested at 3 and 6 h post treatment and compared to mice adoptively transferred with an equivalent number of naïve CD4^{+} T cells (Th0).

3.2.2. RNA sequencing

High-throughput RNA sequencing was performed using the Ion Proton™ Next-Generation Sequencing System (Life Technologies) that uses an ion semiconductor sequencing technology based on the detection of hydrogen ions released during DNA polymerization [207, 208]. In this technology, cDNA libraries are loaded into Ion Spheres™ Particles (ISP), which encapsulate the automated amplification of the DNA template. DNA is then sequenced using an ion semiconductor technology (Figure 3.1) [207, 208].

The pipeline for RNA sequencing is outlined in Figure 3.2. To minimize batch effects and avoid technical bias, samples were randomized within each

experiment (i.e. samples derived from SES alone treatment groups and those including Th1 cells) prior to library preparation.

3.2.3. Input RNA and integrity assessment

Total RNA extracted from the peritoneal membrane of WT and *Il6*$^{-/-}$ mice (*Section 2.5.5*) was used as input. Samples displaying an RNA Integrity Number (RIN) of >8 were selected for the construct of libraries for sequencing (Figure 3.2B). While high integrity and purity is critical for the success of RNA-based approaches (i.e. transcriptome analysis), samples with a similar RIN value ensure a consistent and comparable output for subsequent differential gene expression analysis [209]. RIN was calculated using the RNA Integrity Number Algorithm with the Agilent 2100 Bioanalyser system software (Agilent) [210]. This approach takes into account characteristics of different regions of the electropherogram (a visualised trace of the electrophoresis) recorded by the Agilent 2100 Bioanalyser to get a robust and reliable prediction of the RNA integrity.

For library preparation, 2-4 μg of total RNA was used as an input. This concentration of RNA was optimised to reduce the number of duplicate reads derived from the final library preparation (*Sections 3.2.9* & *3.3.4*).

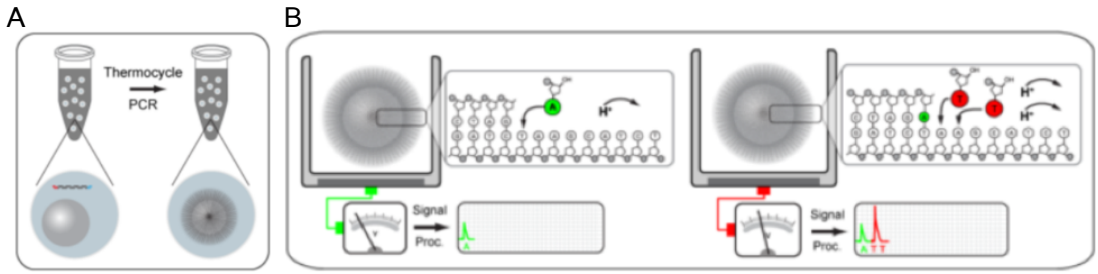

Figure 3.1. Overview of the Ion Proton System for NGS. A. Templates are attached to the Ion Spheres Particles (ISP), where they are amplified by PCR. **B.** ISPs are then loaded in the microchip's wells. The wells are loaded sequentially with dATP, dCTP, dGTP and dTTP. Upon inserted of one of these nucleotides into the elongating strand, a hydrogen is released, which is detected by an ion sensor.

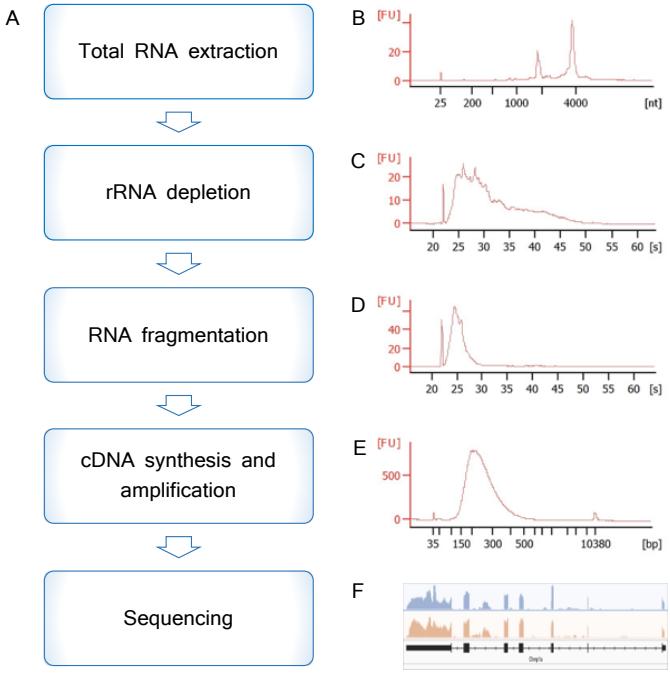

Figure 3.2. RNA sequencing workflow. A. Schematic overview of the RNA-seq pipeline. **B.** Total RNA was extracted from WT and *Il6*$^{-/-}$ mice. Only samples with RIN of >8 were used. **C.** Ribosomal RNA (rRNA) was depleted from 4 µg of total RNA input. **D.** rRNA-depleted total RNA was then fragmented. **E.** The fragmented, rRNA depleted RNA was converted into cDNA and amplified (using 10 cycles of PCR). Final libraries were diluted to a final concentration of 35 pM and barcoded for sequencing. **F.** Reads were mapped to the *Mus musculus* reference genome (mm10).

3.2.4. Ribosomal RNA depletion

The RiboMinus™ Eukaryote System v2 (ambion) was used to remove cytoplasmic (5S, 5.8S, 18S and 28S) and mitochondrial (12S and 16S) ribosomal (r)RNA from the extracted RNA sample. This system utilises oligonucleotide process designed against highly conserved regions of eukaryotic rRNA. Probes are bound to magnetic beads, and rRNA removed by negative selection using magnetic separation.

Residual rRNA contamination was assessed on an Agilent 2100 Bioanalyser. All samples showed <1% rRNA contamination following treatment (Figure 3.2C). To test the efficiency of the RNA-seq pipeline, an internal standard was added to the reaction mix using recommendations from the External RNA Controls Consortium (ERCC) – termed the ERCC RNA Spike-In Control Mixes (ambion) [211].

3.2.5. Fragmentation of rRNA-depleted RNA and library preparation

Libraries were constructed using the Ion Total RNA-Seq Kit v2 (Life Technologies). The kit provides reagents to fragment, purify and concentrate the rRNA-depleted RNA, and is able to reverse transcribe the RNA into cDNA. Reagents are also provided to amplify, purify and quantify the cDNA sample before sequencing. Each step of the library preparation is detailed below:

Fragmentation of the rRNA-depleted RNA – 10 µl of the rRNA-depleted RNA were used in this step. Samples were incubated at 37°C with RNase-III as outlined in the manufacturer's instructions. Samples containing <100 ng of RNA were incubated for 3 min, while samples of >100 ng of RNA were incubated for 10 min. To stop the reaction, 20 µl of ice-cold nuclease-free water was added and the tubes placed on ice. The fragmented RNA was purified using the Magnetic Bead Purification Module (Life Technologies). To assess the yield and size distribution of the fragmented RNA, a 1 µl aliquot was loaded onto an RNA Pico Kit chip (Agilent) and run on the Agilent 2100 Bioanalyser. This protocol generates a fragmentation profile with an average size of 100-200 nucleotides (Figure 3.2.D).

Reverse Transcription – Samples of total fragmented RNA (11 µl) were concentrated using the Centrivap Concentrator (Labconco) to a final volume of 3 µl. Complimentary RNA oligonucleotide adapters were hybridized (65°C for 10 min, 5 min at 30°C) and ligated (1 h at 30°C) to each sample (see manufacturer's instructions). Ligated samples were reverse transcribed into cDNA (70°C for 10 min, followed by 30 min at 42°C) and purified using the Magnetic Bead Purification Module. Purified cDNA was amplified as detailed in Table 3.1. To increase the quality of the cDNA libraries and reduce the introduction of duplicated sequences (*Sections 3.2.9* & *3.3.4*), the number of PCR amplification cycles was reduced from 16 to 10 using a total RNA input quantity of 4 µg. During amplification, all libraries were barcoded using the Ion Xpress RNA-seq Barcode 01-16 kit (Life Technologies) to multiplex the NGS reads within a single reaction. Samples were purified using the Magnetic Bead Purification Module. The quality and integrity of the DNA libraries was assessed on the Agilent 2100 Bioanalyser using the Agilent High Sensitivity DNA Kit (Agilent). Library preparations were evaluated for the percentage of DNA fragments that were <160 bp in size. Analysed showed that <20% of DNA fragments resided within this threshold (Figure 3.2E).

Library quantification and pooling – Generated libraries were quantified by PCR (qPCR) using the Ion TaqMan quantitation assay (Life Technologies). This is a direct quantification test that uses an *Escherichia coli* DH control library as a standard. Quantification was performed as *per* manufacturer's instruction using a standard curve ranging from 0.05-34.0 pM DNA. To obtain an accurate quantification, samples were assessed at three different dilutions. These were derived from the results obtained from the Bioanalyser (generally 1:1000, 1:10000, 1:20000). All Libraries were adjusted to an optimal concentration of 35-50 pM for downstream sequencing. To ensure an accurate dilution before sequencing, samples were again quantified by qPCR, and dilutions adjusted where necessary.

Libraries were loaded onto the Ion Proton™ Chip at a ratio of 2:1 using the Ion Chef™ Instrument as outlined in the manufacturer's instructions (Life Technologies). Final libraries concentrations were optimised to minimise aberrant IPS polyclonality and to maximise the chip load for sequencing (*Section 3.3.2*).

Table 3.1. Library amplification

Stage	Temperature	Time
Hold	94°C	2 min
Cycle (x2)	94°C	30 sec
	50°C	30 sec
	68°C	30 sec
Cycle (x10-16)	94°C	30 sec
	62°C	30 sec
	68°C	30 sec
Hold	68°C	5 min

3.2.6. RNA sequencing analysis run

The Ion Proton™ System for Next-Generation Sequencing uses the Torrent Suite™ Software to monitor each sequencing reaction. For example, it provides an RNA-seq plugin to analyse the cDNA reads resulting from the sequencing reaction. With this tool, reads are aligned to the reference genomes hg19 and mm10 using STAR [212] and Bowtie2 [213]. Although these applications can be used to provide a complete analysis (e.g., differential gene expression analysis, isoform expression), these platforms were only used to align the genes to the reference genome (Figure 3.3).

3.2.7. Sequencing quality control (QC)

Two quality control (QC) measures were included in each sequencing reaction. The Ion Proton™ System provided a documentation of ISP density (i.e. number of ISP loaded with cDNA template), percentage of usable reads (here, polyclonal ISPs are discarded), and the mean length of each read. Analysis using the fastQC software (Braham Institute) [214] provided an independent QC assessment and also identified any issues related to the quality of the starting library (e.g., percentage of GC content).

3.2.8. Reads mapping strategy and quality control of mapping

RNA-seq raw reads were mapped using the STAR and Bowtie2 aligners within the Torrent Suite™ Software RNA-seq plugin (Figure 3.3). Here, the STAR algorithm ensures the accurate mapping of reads spanning between two exons [212], while the Bowtie2 algorithm reports the fraction of total reads represented by rRNA [213]. The samtools statistical package 'stats' (http://www.htslib.org) in the GitHub platform was used to assess the quality of the mapped data (e.g., the number of mapped reads, number of duplicates, percentage of forward and reverse strands).

3.2.9. Assessment of duplicated reads

One of the issues associated with the analysis of RNA-sequencing data relates to whether the computational removal of duplicated sequencing reads (e.g., introduced through potential PCR bias) improves the accuracy of the downstream analysis [215-219]. Although the general consensus is to retain the duplicated reads for analysis, some key considerations must be taken into account [215]. For example, it is important to determine whether the number of duplicate reads assigned to a given gene biased the overall expression level for that gene within the dataset. To address this issue, all datasets were applied to the Bioconductor package dupRadar [219].

3.2.10. Differential gene expression analysis

The DESeq2 package from Bioconductor was used to identify significantly regulated genes based on changes in fold expression and associated statistical evaluation [220]. DESeq2 compares the differences in mapped reads for a given gene using shrinkage estimation for dispersion and fold change within each condition to improve stability and interpretability of the estimates [220].

3.2.11. Statistical analysis of changes in gene expression over time

All differentially regulated genes were grouped in clusters according to their level of expression over the 3-6 h time course. This analysis was performed in collaboration with Dr Barbara Szomolay (Systems Immunity University Research Institute, School of Medicine, Cardiff University), and provided an opportunity to study genes with similar patterns of expression in each experimental condition. Several methods were applied to determine the optimal number of clusters: silhouette [221], the visual 'elbow method' [222], and gap statistics [223]. Genes were then assigned to each defined cluster by K-means clustering [224]. This method partitions the data into a previously defined number of clusters in which each observation is assigned to an individual cluster based on the nearest mean.

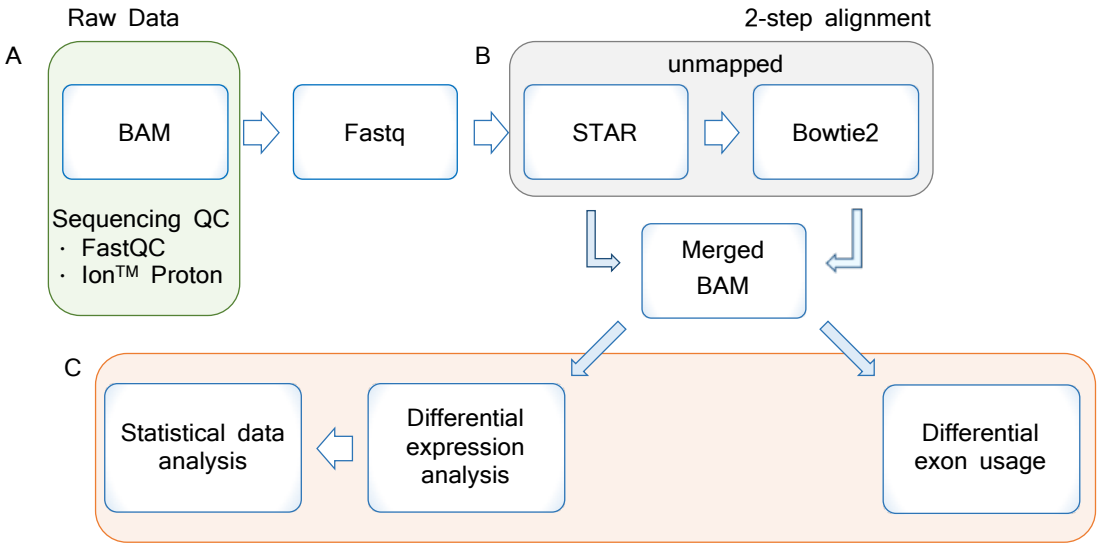

Figure 3.3. Schematic overview of the RNA-seq data analysis strategy. **A.** Raw reads were QC using the Ion Proton System Torrent Suite and FastQC. **B.** Reads were mapped using the STAR and Bowtie2 aligners. **C.** Differential gene expression together with statistical data analysis and differential exon usage analysis was performed on the merged files. Differential exon usage analysis will be detailed in Chapter 7.

3.3. Results

3.3.1. Defined Ion Chip loading ensures higher amount of usable reads

Next generation sequencing was performed using the Ion Proton System. Initial optimisation experiments assessed how the library input concentration influenced both the polyclonality and sequencing quality (Figure 3.4). This was evident at both a low (35 pM) and high (50 pM) library concentration. Diluting the samples to 40 and 35 pM reduced polyclonality whilst ensuring sufficient library template for sequencing. Thus, 35 pM of template were found to be the optimal library concentration for ISP loading (Figure 3.4).

3.3.2. Higher total RNA input and lower amplification cycles reduce sequence duplications

Inadvertent PCR amplification contributes substantially to sequencing biases associated with library generation and downstream RNA-seq analysis. Although difficult to control, several measurements were undertaken to minimise the introduction of bias. The Ion Total RNA-Seq Kit v2 recommends 1-5 µg of RNA as input and 16 cycles of PCR for library amplification in its protocol. Our first libraries were therefore generated using 2 µg of total RNA and 16 cycles of amplification (Figure 3.5A & B). However, the mapping statistics showed a substantial amount of duplication. While duplicated reads may not necessarily be indicative for PCR bias (as stated earlier), the amount of RNA starting material was increased and the amplification cycles reduced to determine whether the number of duplicates could be reduced. Thus, subsequent experiments used 4 µg of input RNA and 10 cycles of PCR amplification. This strategy slightly reduced the percentage of duplicated reads (Figure 3.5A & B).

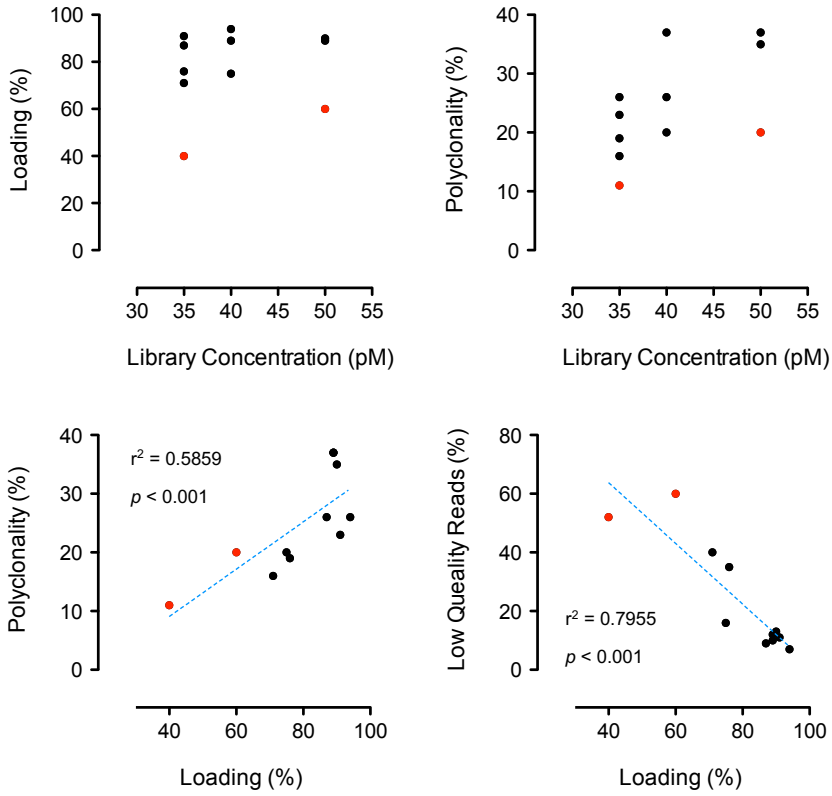

Figure 3.4. Optimisation of the RNA-sequencing loading run. SES experiment was used to optimise the sequencing run. Correlation between the amount of input cDNA loaded for sequencing (Library concentration), the chip loading, the ISP polyclonality and the amount of low quality reads. Each dot represents a sequencing run, with 2 samples per run. Red dots represent failed runs.

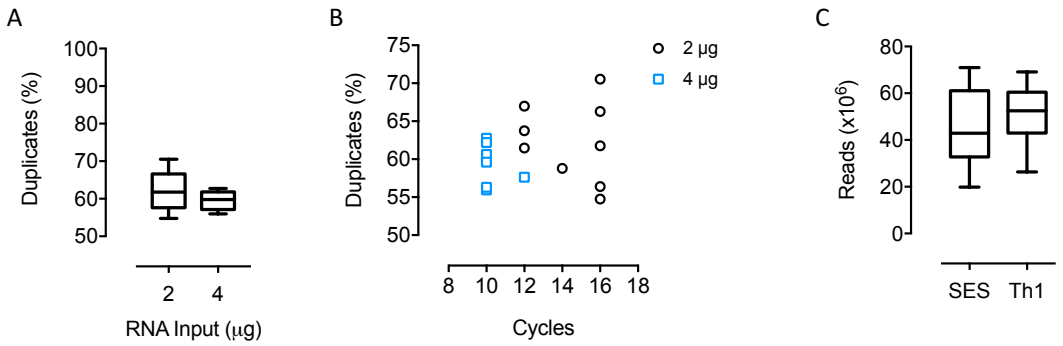

Figure 3.5. Mapping statistics. A. Number of duplicated reads per input within the SES experiment. **B.** Number of duplicates per total PCR cycles for each input in the SES experiment. **C.** Number of mapped reads per sample for both SES and Th1 experiments. For **A** and **C**, data is represented as box plots with extending bars to the lowest and highest values

3.3.3. Ion torrent provides sufficient depth of coverage and optimal mapping

The mapping of the raw NGS reads was performed using STAR and Bowtie2 aligners from the RNA-seq plugin within the Torrent Suite™ software (*Section 3.2.8*). As this mapping strategy is optimised for the Ion Proton™ Technology, it provided the highest percentage of mapped genes to the reference genome. The samtools statistical package 'stats' (*Section 3.2.8*) was used to assess the quality of the mapping. Following this strategy, more than 95% mapping was achieved in both experiments (Table 3.2). The distribution between forward and reverse strand was ~50% (Table 3.2). Only samples with more than $2.0x10^7$ mapped reads were used for subsequent analysis (Figure 3.5C).

Table 3.2. Mapping statistics

	Mapped reads (%)	Forward strand (%)	Reverse strand (%)
SES	95.86 ± 0.31	55.02 ± 0.90	44.98 ± 0.90
Th1	96.92 ± 0.19	54.83 ± 0.51	45.17 ± 0.51

3.3.4. Duplication does not affect the differential gene expression analysis

The Bioconductor package dupRadar was used to determine whether duplicated reads had an impact on the subsequent differential gene expression analysis. For a given sample, the number of duplicated reads within each gene was plotted against its fold change when compared its control (Figure 3.6).

High duplication did not correlate with an increased fold change (Figure 3.6). Thus, based on the data from Figure 3.5 and Figure 3.6, there was no evidence for the introduction of a PCR-derived bias within the datasets. Duplicated reads were therefore not excluded from the downstream analysis.

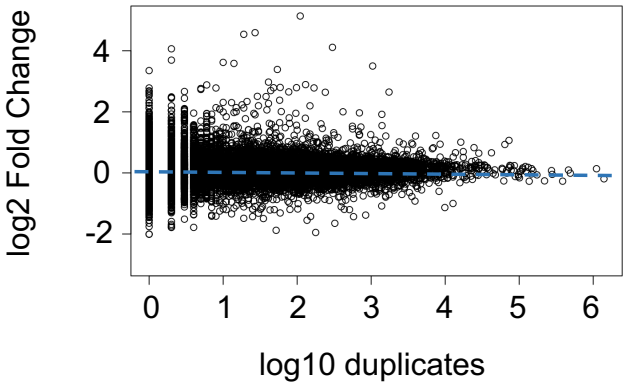

Figure 3.6. Duplicated reads do not bias differential gene expression. The number of duplicates for a given gene was compared to the relative fold change against untreated controls. Representative dot plot was generated by the package dupRadar.

3.3.5. Differential gene expression

Mapped reads were tested for differential gene expression using the DESeq2 package [220]. To establish the cut-off that will be used throughout the analysis, differences between mice receiving naïve $CD4^+$ T-cells (Th0) and SES or SES alone were compared at 3 h. The introduction of Th0 cells had minimal impact on gene expression and was used as a baseline threshold for the identification of genes selectively induced by inflammation. Using this approach, analysis considered all genes with a statistical variation of $p<0.01$, and an absolute fold change of >1.75. All pseudogenes or genes with a transcript support level of 5 (TSL5) were excluded from the analysis [225]. TSL is a method to assess whether a given transcript is supported by primary data (mRNA and Expressed Sequence Tag) from the Ensembl and UCSC projects [225]. Transcripts annotated with a TSL5 mean that no single mRNA transcript has been found to support the model structure, and therefore their annotation should be considered speculative [225].

For the SES experiment, baseline control data for each genotype were compared to gene changes seen at 3 and 6 h post SES treatment. In this regard, analysis of datasets from non-challenged WT and *Il6*$^{-/-}$ mice identified 64 differentially regulated genes. These differences included immune-related genes, such as *Ccl6*, *Ccl9*, *Il31ra*, *Nos3* or *Ly6D*. Subsequent analysis therefore took into account the basal expression of these genes when comparing across genotypes.

Evaluation of gene regulation across the time course of SES activation identified 377 (at 3 h) and 185 (at 6 h) differentially regulated genes in SES stimulated WT mice (Table 3.3). A comparable analysis of SES treated *Il6*$^{-/-}$ mice identified 267 and 213 genes at 3 and 6 h. The addition of Th1 cells dramatically enhanced the number of regulated genes under SES activation (Table 3.3). These equated to 782 and 1280 genes in WT mice at 3 and 6 h, and 1262 and 1195 at 3 and 6 h in *Il6*$^{-/-}$ mice.

3.3.6. There are three distinct patterns of genes expression over time in both conditions

Computational analysis of the RNA-seq data was used to cluster genes displaying similar temporal patterns of regulation (*Section 3.2.11*) [226]. Analysis was conducted in the genes significantly regulated in at least one of the experimental conditions when compared to respective controls. This equated to 677 genes for the SES experiment and 2307 genes for the Th1 experiment. For the SES experiment, the silhouette, gap statistics and elbow methods all suggested 3 as the optimal number of clusters for both WT and *Il6*$^{-/-}$ (Figure 3.7A). Analysis was also performed for the Th1 adoptive transfer experiment. Here, the three methods also identified 3 distinct patterns of gene regulation in SES stimulated WT and *Il6*$^{-/-}$ mice receiving Th1 cells (Figure 3.7B).

Once the optimal number of clusters was identified, significantly regulated genes were assigned to each cluster according their temporal pattern of expression over the 6 h time course by K-means clustering [224] (Figure 3.8). This clustering strategy will be used in subsequent sections of this thesis to explore functional associations within each pattern of temporal gene expression (see Chapters 4 & 5).

Table 3.3. Differentially expressed genes

		Time (h)	p<0.05	p<0.01	p<0.01, FC>1.75
SES	**WT**	3	706	452	377
		6	396	219	185
	***Il6*$^{-/-}$**	3	573	335	267
		6	657	290	213
Th1	**WT**	3	1937	1296	782
		6	3169	2108	1280
	***Il6*$^{-/-}$**	3	3595	2289	1262
		6	3612	2181	1195

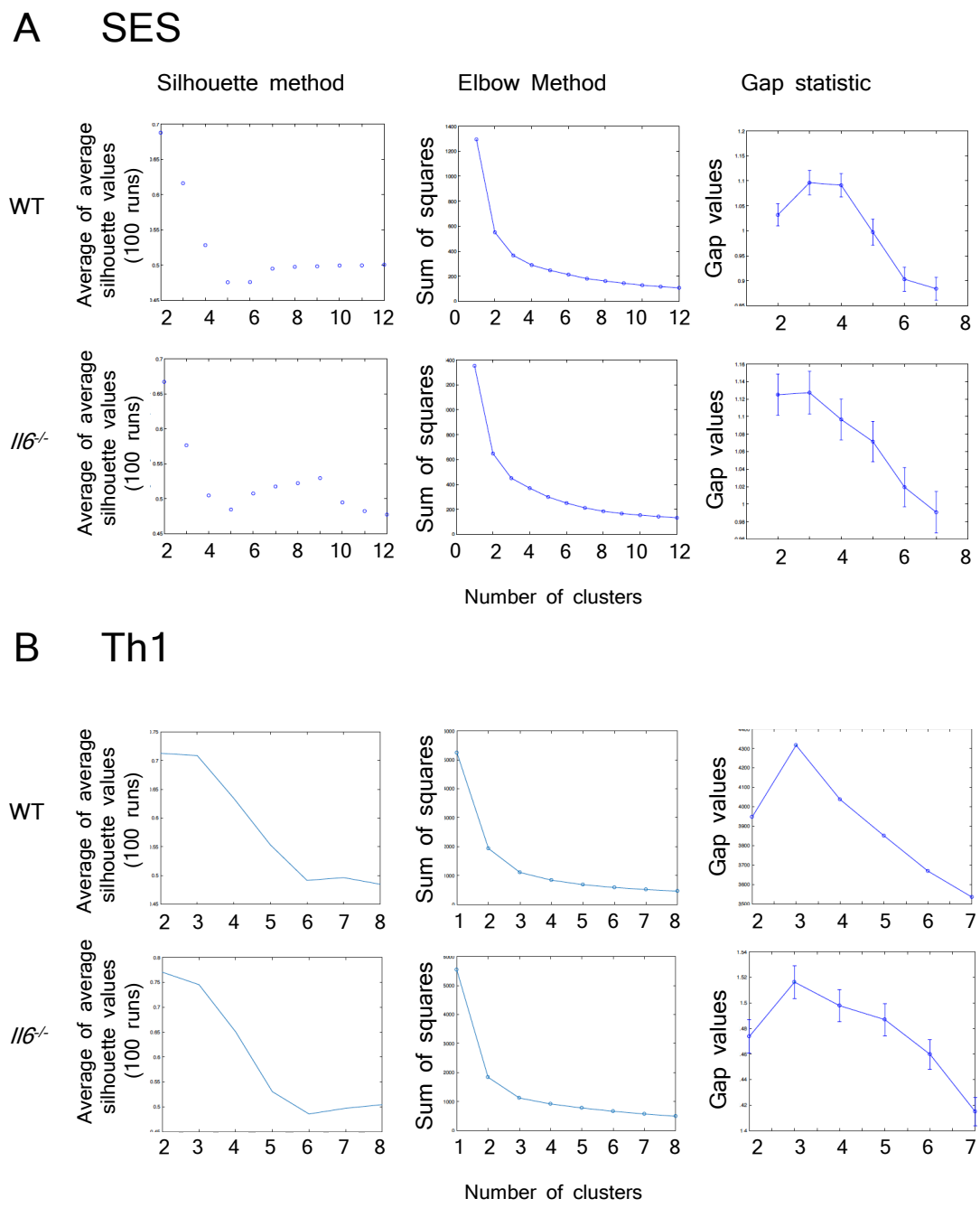

Figure 3.7. Identification of the optimal number of cluster for the RNA-seq datasets for WT and *Il6*$^{-/-}$. The silhouette, gap statistics and elbow methods were used to determine the optimal number of clusters to organise differentially regulated genes from SES treated (**A**) and SES together with Th1 adoptive transfer treated mice (**B**).

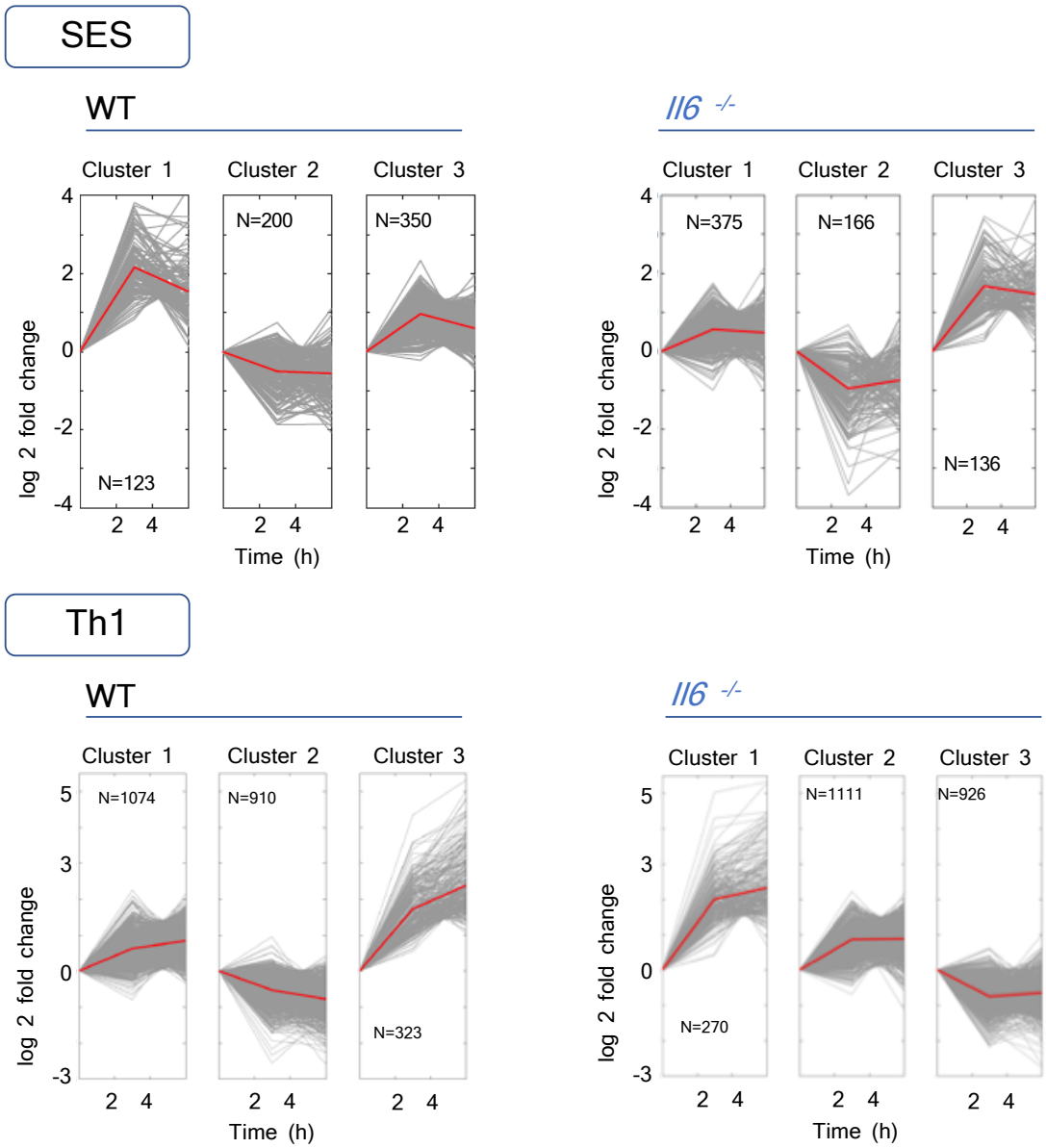

Figure 3.8. Cluster analysis. Genes were clustered according to their changes in expression over time using the K-means clustering algorithm.

3.4. Discussion

Studies outlined herein established RNA-seq methodologies and an analysis pipeline for evaluation of peritoneal lining tissue using the Ion Proton™ Next-Generation Sequencing System. The Ion Proton technology has the capacity to sequence fragments of a higher length than other platforms, and provides sufficient sequence coverage to map reads for transcript discovery [227]. During the first part of this Chapter, experiments evaluated the optimal input library concentration to minimise ISP polyclonality and maximise sequencing quality. This ensured a consistent and sufficient amount of useable sequencing reads throughout the experiments.

One important aspect of the sequencing QC determined whether it was appropriate to remove computationally duplicated sequencing reads. These can arise both from natural duplicates or PCR-duplicates – i.e. reads that originate from the same RNA molecule as a result of aberrant PCR amplification [215]. In line with previous studies in the literature [215-219], gene expression analysis showed that duplicates did not affect the overall gene expression fold change. Thus, replicates were not removed from the analysis.

Statistical data analysis was used to evaluate changes in gene expression over time. This analysis enabled the clustering of the differentially regulated genes according their pattern of expression over the course of inflammation. The importance of such approach resides in his potential to obtain an integrated understanding of the biological processes occurring in the peritoneal membrane during acute and chronic inflammation. In this regard, Eisen and co-workers have previously shown that genes that share a similar pattern of expression also share common roles in cellular processes [226]. Thus, the use of this analysis to organise our data provided holistic information of the dynamical changes in the transcriptome of the peritoneum during the inflammatory course.

Chapter 4. Transcriptomic analysis of the peritoneal membrane during acute resolving inflammation

4.1. Introduction

Inflammation in response to bacterial infection promotes anti-microbial immunity. Here, acute resolving inflammation ensures competent host defence and the restoration of tissue homeostasis [15]. However, a persistent or recurrent activation of inflammation can cause chronic inflammation and deleterious tissue damage. Therefore, the inflammatory response must be appropriately regulated [9, 15].

Cellular communication between leukocytes and local resident tissue cells controls the initiation, maintenance and resolution of the inflammatory episode [9]. This interaction promotes the transition from innate to adaptive immunity, and ensures the successful resolution of inflammation [228]. Several mediators including chemokines, cytokines, and bioactive lipids are involved in this crosstalk [26, 41, 229]. The inflammatory cytokine IL-6 is integral to this process and directs the transition from innate to adaptive immunity [9], and is essential for anti-microbial defence against viruses, bacteria and parasites [61-65]. In the context of peritonitis, studies in our laboratory have shown that *Il6*$^{-/-}$ mice are less able to contain bacterial infection, and display a heightened dissemination of infection into the bloodstream and wider tissues. Experiments described in this Chapter will identify the IL-6 regulated gene changes in the peritoneum that are associated with this outcome during acute resolving inflammation.

4.2. Materials and Methods

4.2.1. Data visualization

Heatmaps – The software GENE-E [230] or the online tool Morpheus [231] were used to identify differences in gene regulation. Heat map visualisations were presented as either the normalised read counts (FPKMs; *Fragments Per Kilobase of exon per Million fragments mapped per sample*) of those genes differentially expressed in at least one of the experimental conditions; or as the log2 transformation of the fold change (log2FC) when compared to respective controls. All datasets were hierarchically clustered using Spearman's rank correlation coefficient. Spearman's rank correlation is a non-parametric measure of correlation between the rank of two variables (in the present study, gene expression and condition), which does not assume linear association between those variables.

Venn diagrams – Venn diagrams were used to visualise the gene overlap between different conditions with the web tool Venn [232].

Volcano plots – To illustrate the distribution of genes either induced or suppressed, datasets were visualised by volcano plots. Data was expressed as a log2FC against the log10 adjusted *p* value using the R package ggplot2 [233].

4.2.2. Statistical data analysis

The identified clusters reported in Chapter 3 were tested to establish potential relationships between the inflammatory response observed in WT and *Il6*$^{-/-}$ mice. In collaboration with Dr. Barbara Szomolay, analysis considered the non-overlapping genes between groups to study the differences between the clusters in WT and *Il6*$^{-/-}$ mice using the two-sample two-dimensional Kolmogorov-Smirnov (Two-sample 2D K-S) test [234] and the multivariate Kruskal-Wallis (MVK) test [235]. Analysis assessed changes in gene expression at each time point and from across the entire time course (0-6 h) to establish statistical evaluation between WT and *Il6*$^{-/-}$ mice. In this regard, the MVK test is a non-parametric test that determines whether the medians of two groups are different. The non-

parametric two-sample 2D K-S test compares the distance between the empirical distribution functions of two conditions.

4.2.3. Data interpretation: Ingenuity pathway analysis

Molecular pathway analysis was conducted using Ingenuity Pathway Analysis (IPA; version 2.1) [236], which employs both bespoke in-house developed algorithms and manually curated databases (Ingenuity Knowledge Base) to identify associations with pathways, networks and genes of interest. "Comparison Analysis" identified gene changes based on the classification of '*Canonical Pathways*', '*Upstream Regulators*' and '*Downstream Effects*'.

Canonical Pathways identifies the most significantly regulated pathways affected by the genes of interest. It also predicts whether these pathways are activated or suppressed based on changes in the expression of genes.

The *Upstream Regulator Analysis* feature predicts the identity of upstream molecules, including receptors and transcription factors responsible for directing gene expression within the dataset.

Downstream Effects Analysis anticipates increases or decreases in downstream biological activities based on the direction of change of the genes in the dataset.

For IPA analysis, all 677 differentially expressed genes as identified in Chapter 3 (*Section 3.3.5* & *3.3.6*) were used. Genes from each cluster were uploaded separately using the statistical cut offs applied in Chapter 3 ($p < 0.01$; fold change>1.75). This allowed a comparison of those genes significantly altered between conditions.

4.3. Results

4.3.1. Experimental validation of acute resolving peritonitis

Acute resolving inflammation was induced following peritoneal stimulation with SES (*Section 2.3.2*). Changes in inflammation were quantified using ELISA and qPCR (Figure 4.1). Two aspects of IL-6 activity were evaluated – (1) components of the IL-6 receptor cassette, and (2) some IL-6 regulated STAT1 or STAT3 target genes. Interleukin-6 was only detected in the peritoneal lavage of WT mice at 3 h post SES administration. The levels of sIL-6R peaked at 3 h in both WT and *Il6*$^{-/-}$ mice, while sgp130 levels were reduced in *Il6*$^{-/-}$ mice at 6 h (Figure 4.1A). Quantitative PCR analysis of mRNA derived from the inflamed peritoneal lining evaluated several STAT1 and STAT3 target genes (Figure 4.1B). *Socs3* was strongly upregulated in WT mice 3 h after SES injection, while *Irf1* showed a slight increase in both genotypes. *Il1b* expression was used as control and was enhanced at 3 h in both genotypes as a result of the acute TLR activation (Figure 4.1B).

4.3.2. Transcriptomic analysis of SES activated peritoneal tissue

Spearman's rank correlation was used to establish similarities in the transcriptome profile of WT and *Il6*$^{-/-}$ mice after SES stimulation. This approach grouped the experimental samples away from the non-treated controls. Within the SES treatment samples, the *Il6*$^{-/-}$ SES 6 h dataset grouped furthest away from the others, suggesting that IL-6 plays an important role in regulating the transcriptional response following SES challenge at this latter time point (Figure 4.2). SES triggered changes in 377 and 185 genes in WT mice at 3 h and 6 h, respectively. In *Il6*$^{-/-}$ mice, 267 genes at 3 h and 213 genes at 6 h were altered (Figure 4.3). Most of these genes were unique to an individual condition or time point (Figure 4.3B). Most of the genes controlled by SES in WT mice were substantially induced. (Figure 4.3A). This was particularly evident at 3 h post SES challenge. Conversely, *Il6*$^{-/-}$ mice show a distinctive number of genes strongly down-regulated (Figure 4.3A).

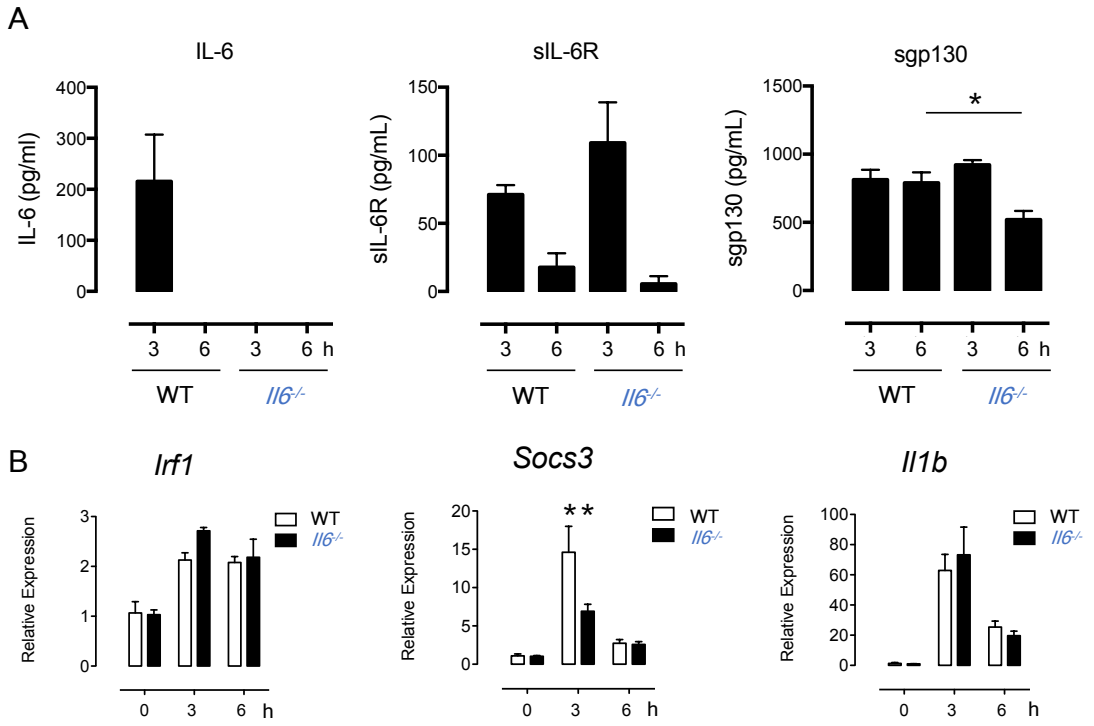

Figure 4.1. Experimental validation. Peritonitis was induced as detailed in *Section 2.3.2* **A**. The levels of IL-6, sIL-6R and sgp130 were evaluated by ELISA. **B.** The expression of STAT1 and STAT3 target genes *Socs3* and *Irf1* was evaluated by qPCR. *Il1b* expression was measured as a positive control for TLR-inflammasome activation. n= 4 mice per group. Statistical analysis was performed by two-way ANOVA with Bonferroni correction for multiple comparisons, *p<0.05; **p<0.01.

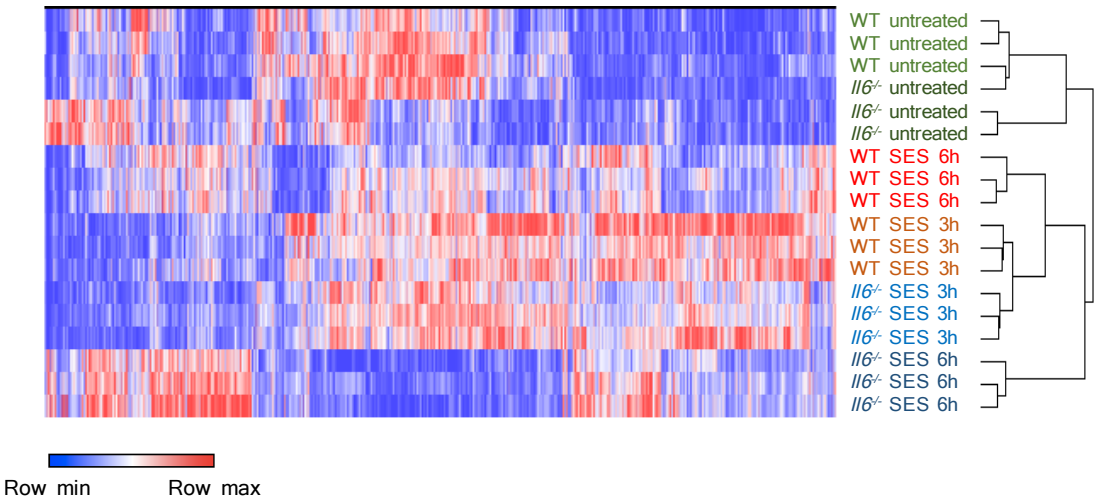

Figure 4.2. Impact of IL-6 in the transcriptome. Hierarchical cluster analysis (by Spearman's rank correlation) of WT and *Il6*$^{-/-}$ mice at 0 h (untreated), 3 h (SES 3 h) and 6 h (SES 6 h) based on the expression level of the 677 genes being differentially regulated in at least one of the experimental conditions. The expression level is represented as the normalised read counts (FPKM).

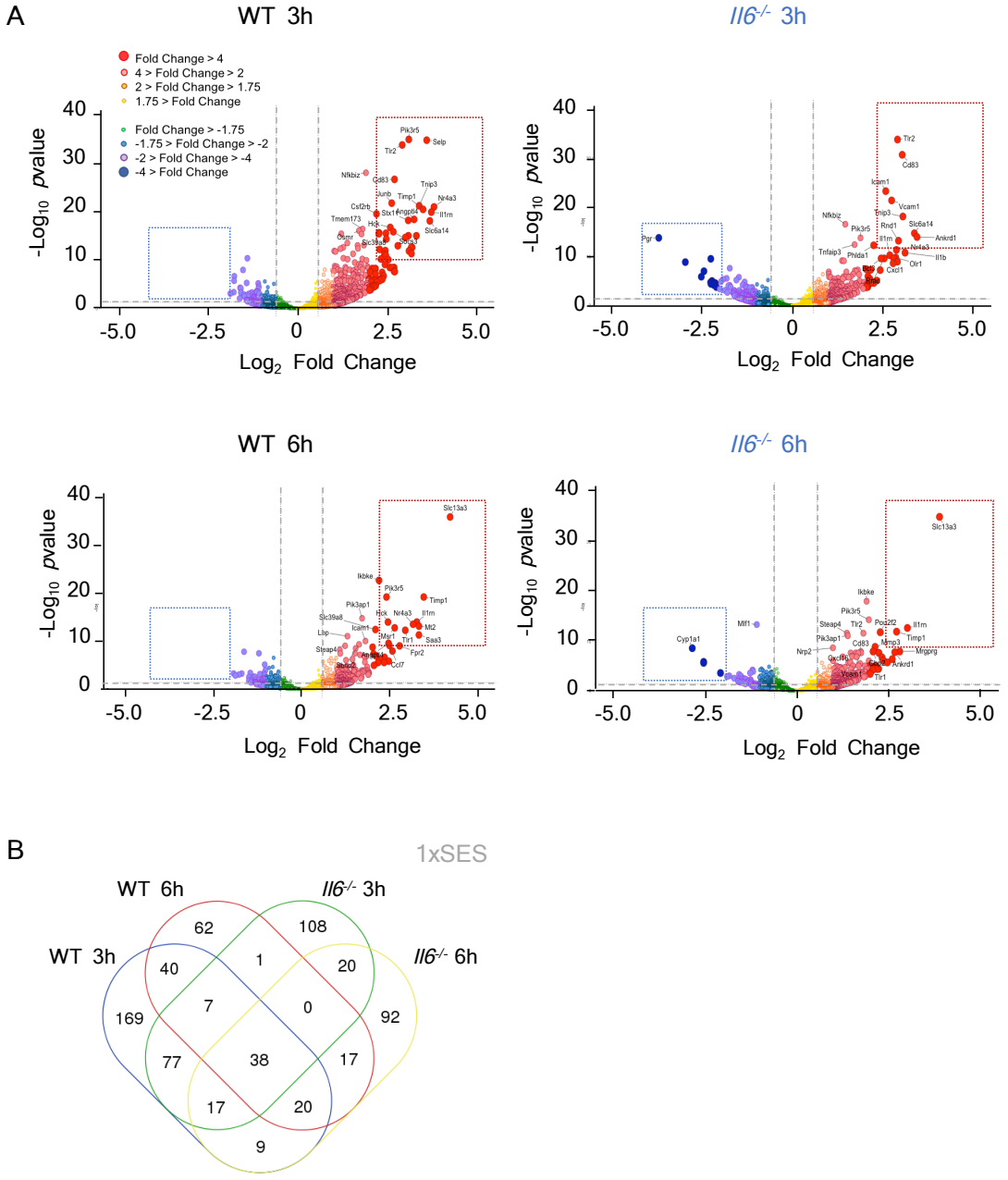

Figure 4.3. Volcano plot analysis of differentially expressed genes in WT and *Il6*$^{-/-}$ mice after SES stimulation. A. Data shows the differential expression of genes in WT and *Il6*$^{-/-}$ mice at 3 and 6 h after SES stimulation compared to corresponding untreated controls. **B.** Venn diagram demonstrates the number of genes that are commonly or uniquely expressed in each condition.

4.3.3. Both WT and *Il6*$^{-/-}$ mice show 3 distinct patterns of gene expression over time

Cluster analysis previously identified three distinct patterns of differential gene expression within our RNA-seq datasets from both WT and *Il6*$^{-/-}$mice following SES stimulation (Figure 3.8). To test whether these patterns of expression were statistically related, data from WT and *Il6*$^{-/-}$mice were compared using different statistical test (*Section 4.2.2*) (Table 4.1 and 4.2). Statistical analysis was performed over the 0-6 h time period using the Two-sample 2D K-S test and MVK test on the following data: (1) log2FC gene expression at 3 h and 6 h, and (2) rate of change of log2FC gene expression at 3 h and 6 h (termed "slope"). These methods identified close similarities between the patterns identified in WT and *Il6*$^{-/-}$ mice (Figure 4.4). For example, Cluster-1 from WT mice is closely related to Cluster-3 from *Il6*$^{-/-}$ mice (Tables 4.1 & 4.2). These groups therefore share similar patterns of gene expression or gene "Behaviours" – termed "Behaviour 1" (B1), "Behaviour 2" (B2) and "Behaviour 3" (B3) (Figure 4.4).

Studies evaluated the identity of the genes assigned to each behaviour. Even though both WT and *Il6*$^{-/-}$ mice share three distinct patterns of gene expression, 24% of the genes do not overlap between genotypes (Figure 4.4B). Individually, the Jaccard index [237] between pairwise Behaviours is < 0.63 (Figure 4.4C). The Jaccard index is a statistic used to compare the similarity between two sample sets. When both sets are identical, the Jaccard index equals one 1. In our datasets, a Jaccard index of 1 would indicate that, for example, Cluster-3 from WT mice comprises the same genes that Cluster-1 from *Il6*$^{-/-}$ mice. However, this is not the case, suggesting that IL-6 has an important impact in the control of peritoneal membrane gene expression in response to SES challenge.

Table 4.1. Two-sample two-dimensional Kolmogorov-Smirnov test

		WT			
		Cluster 1	**Cluster 2**	**Cluster 3**	
Il6$^{-/-}$	**Cluster 1**	2.39E-41	1.38E-42	**0.0018**	slope
		1.16E-40	8.62E-49	**0.0005**	log2FC at 3 and 6 h
	Cluster 2	1.25E-49	**0.0001**	1.18E-61	slope
		5.23E-46	**0.0002**	1.09E-62	log2FC at 3 and 6 h
	Cluster 3	**0.0194**	1.12E-52	1.44E-15	slope
		0.0253	1.33E-50	3.46E-21	log2FC at 3 and 6 h

Clusters from WT and *Il6*$^{-/-}$ regulated genes were tested for similarly using the two-sample two-dimensional Kolmogorov-Smirnov. The *p* value associated to each comparison is shown (significance level of 0.1%). Data outlined in blue highlight clusters with the closest similarities. Slope = rate of change of log2FC gene expression at 3 and 6 h.

Table 4.2. Multivariate Kruskal-Wallis test

		WT			
		Cluster 1	**Cluster 2**	**Cluster 3**	
Il6$^{-/-}$	**Cluster 1**	222.87	318.17	**24.37**	log2FC at 3 and 6 h
	Cluster 2	230.66	**20.74**	317.73	log2FC at 3 and 6 h
	Cluster 3	**12.91**	265.33	158.68	log2FC at 3 and 6 h

Clusters from WT and *Il6*$^{-/-}$ regulated genes were tested for similarly using the Multivariate Kruskal-Wallis. The variance associated to each comparison is shown. The critical value of chi^2 statistics is 13.8155 at significance level of 0.1%. Data outlined in blue highlight clusters with the closest similarities.

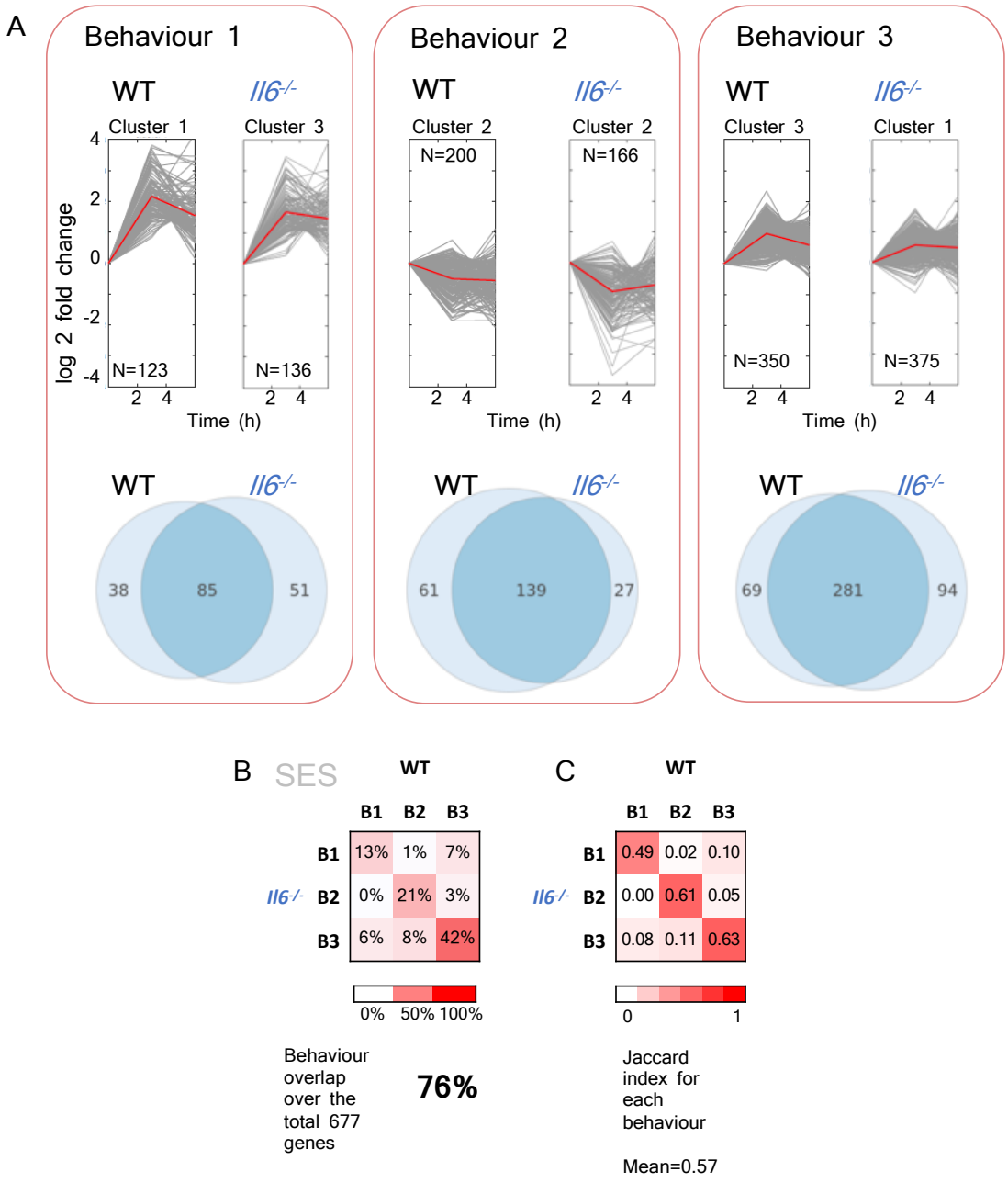

Figure 4.4. Cluster analysis and overlap between the differentially expressed genes in WT and *Il6*$^{-/-}$ mice after SES stimulation. A. Genes were plotted according to their expression over time (0-3-6 h). Red lines represent the mean expression within each group (centroid). Cluster analysis shows three patterns of expression (termed "Behaviours") similar in WT and *Il6*$^{-/-}$ mice. The Venn diagrams show the gene overlap in terms of absolute number between common Behaviours. **B & C.** Representation of the percentage of overlap between each Behaviour over the total 677 differentially expressed genes (**B**), and the Jaccard similarity coefficient between Behaviours (**C**).

4.3.4. Control of STAT1 and STAT3 over the transcriptome

The importance of STAT1 and STAT3 activity in the control of gene expression after SES challenge was evaluated using "Upstream Regulator Analysis" in IPA (Figure 4.5). Only genes within B1 and B3 predicted a significant activation of STAT1 and STAT3 as upstream regulators in IPA (z-score>2). Here, STAT3 is a strong gene regulator in WT in both B1 and B3, while STAT1 is predicted to be active mainly in B1 of *Il6*$^{-/-}$ mice (Figure 4.5A & 4.5C). Studies next focused on the genes associated to both transcription factors in WT and *Il6*$^{-/-}$ mice. The total number of genes regulated by STAT1 and STAT3 (as predicted by IPA) is presented for both B1 and B3 (Figure 4.5B & 4.5D). In B1, a vast proportion of genes were commonly regulated by STAT1 or STAT3 in both WT and *Il6*$^{-/-}$ mice (Figure 4.5B). On the other hand, most of the genes controlled by STAT1 or STAT3 in B3 were unique to WT mice (Figure 4.5D). SES is an activator of TLR2 [56, 238], and its predicted activation in IPA was used as control. Here, TLR2 is predicted to be active at the early stages of inflammation in WT and *Il6*$^{-/-}$ mice in B1.

Using the same criteria, analysis next considered the top canonical pathways activated in the membrane as a result of SES challenge. Again, only B1 and B3 predicted canonical pathways with a z-score > 2 (Figure 4.5E). Here, pathways including acute phase response signalling, TREM1 signalling and iNOS signalling were selectively enriched in datasets from WT mice as compared to *Il6*$^{-/-}$ mice.

4.3.5. Impact of acute inflammation in the biological functions within the stromal compartment

To gain further insight into the biological functions associated with each gene Behaviour, IPA was used to perform "Downstream Effects Analysis" (Figure 4.6). This provided insight into the downstream biological activities associated with the identified genes of interest.

The top functional categories defined for B1 and B3 are shown in Figure 4.6A & 4.6C. The functions associated with B1 corresponded to those related to immune cell trafficking and movement, haematological processes, cell-to-cell signalling and the regulation of inflammation. These include genes induced at 3 or

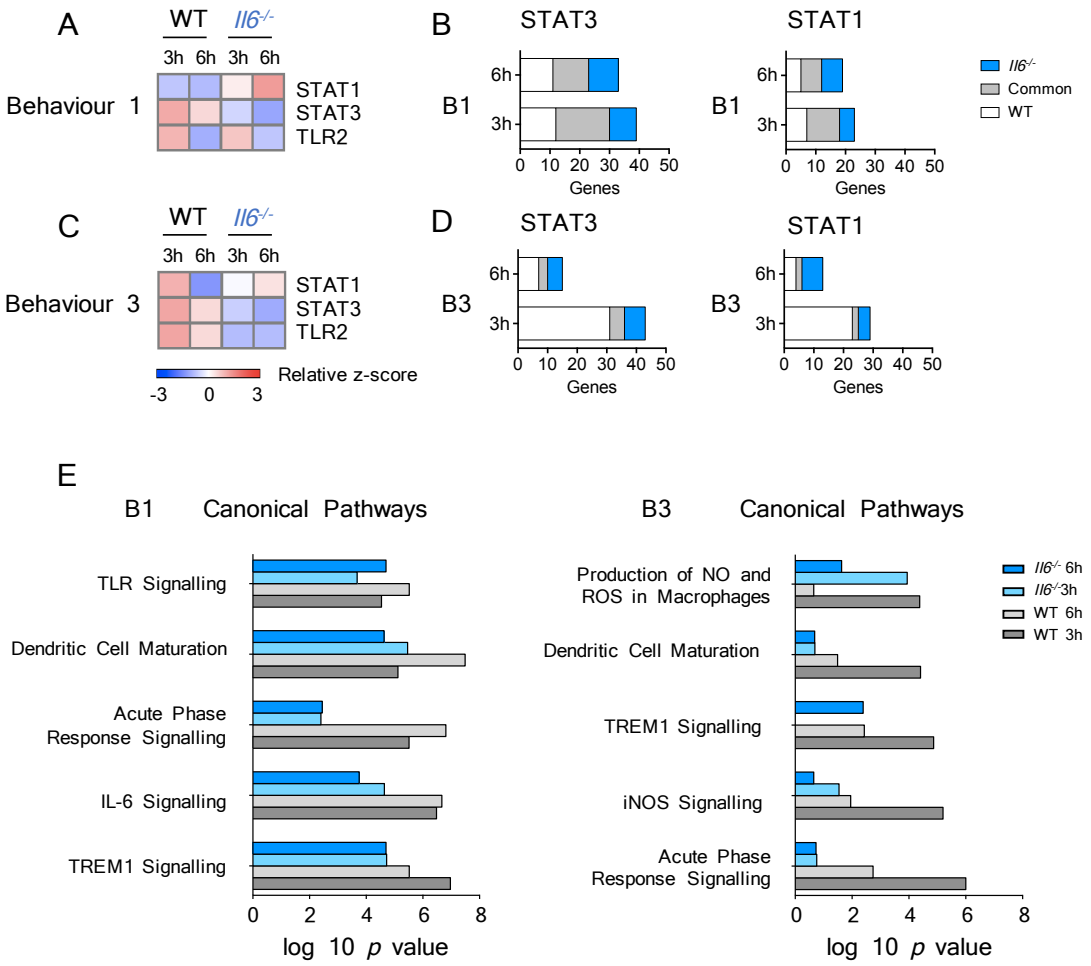

Figure 4.5. Upstream regulator and canonical pathway analysis by IPA. **A & C.** STAT1, STAT3 and TLR2 activation was predicted in IPA for Behaviour 1 (**A**) and 3 (**C**), and their relative z-score plotted in a heat map. **B & D.** Common and unique genes to WT and *Il6*$^{-/-}$ datasets that are predicted to be under STAT1 and STAT3 control in B1 (**B**) and B3 (**D**). **E.** Top 5 canonical pathways (z-score > 2) in B1 and B3.

6 h as a consequence of peritoneal SES challenge. For example, genes linked with B1 contributed to changes in phagocyte migration and chemotaxis. In WT mice, these included definitions relevant to the activation of phagocytes and leukocytes, cellular adhesion and angiogenesis (Figure 4.6B).

On the other hand, genes in B3 accounted for more homeostatic functions – cell development and survival, tissue morphology and haematological system development and function (Figure 4.6C & 4.6D). Interestingly, some function related to cell movement are upregulated in WT mice when compared to IL-6 deficient counterparts. This may account for those genes involved in trafficking that are dependent on IL-6.

4.3.6. Genes associated to competent host defence

Unpublished observations in our laboratory suggest that mice lacking *Il6* are unable to successfully control infections. Bioinformatics analysis of the described RNA-seq data is in close agreement with these findings.

Under B1, *Il6*$^{-/-}$ mice showed impaired immune signatures relevant to the activation of leukocytes, degranulation of cells and the production of reactive oxygen species when compared to WT (Figure 4.6). An exhaustive transcriptome analysis was therefore performed using these genes. Among the 56 genes involved in the activation of leukocytes, 9 of them were predicted to be under STAT3 regulation in WT mice (*Cx3cl1, Cdkn1a, Il4r, Ccl12, Lbp, Ccr5, C5ar1, Saa1* and *Fcgr1a*) (Figure 4.7A). The expression of these genes was significantly suppressed in *Il6*$^{-/-}$ mice (Figure 4.7B). This difference in expression between WT and *Il6*$^{-/-}$ mice was especially notable for *Il4ra*, *Lbp* and *Saa1*.

Cellular adhesion plays a vital role in leukocyte recruitment and priming [175, 239]. Twenty genes involved in phagocyte adhesion were shown to be differentially expressed between WT and *Il6*$^{-/-}$ mice as a result of SES stimulation (Figure 4.8A). These included the adhesion molecules E-selectin, P-selectin, Intercellular Adhesion Molecule-1 (ICAM-1), and Vascular Cell Adhesion Molecule-1 (VCAM1) (*Sele*, *Selp*, *Icam1* and *Vcam1*, respectively). For example, *Selp* shows a very transient and strong increase in WT mice at 3 h (Figure 4.8B),

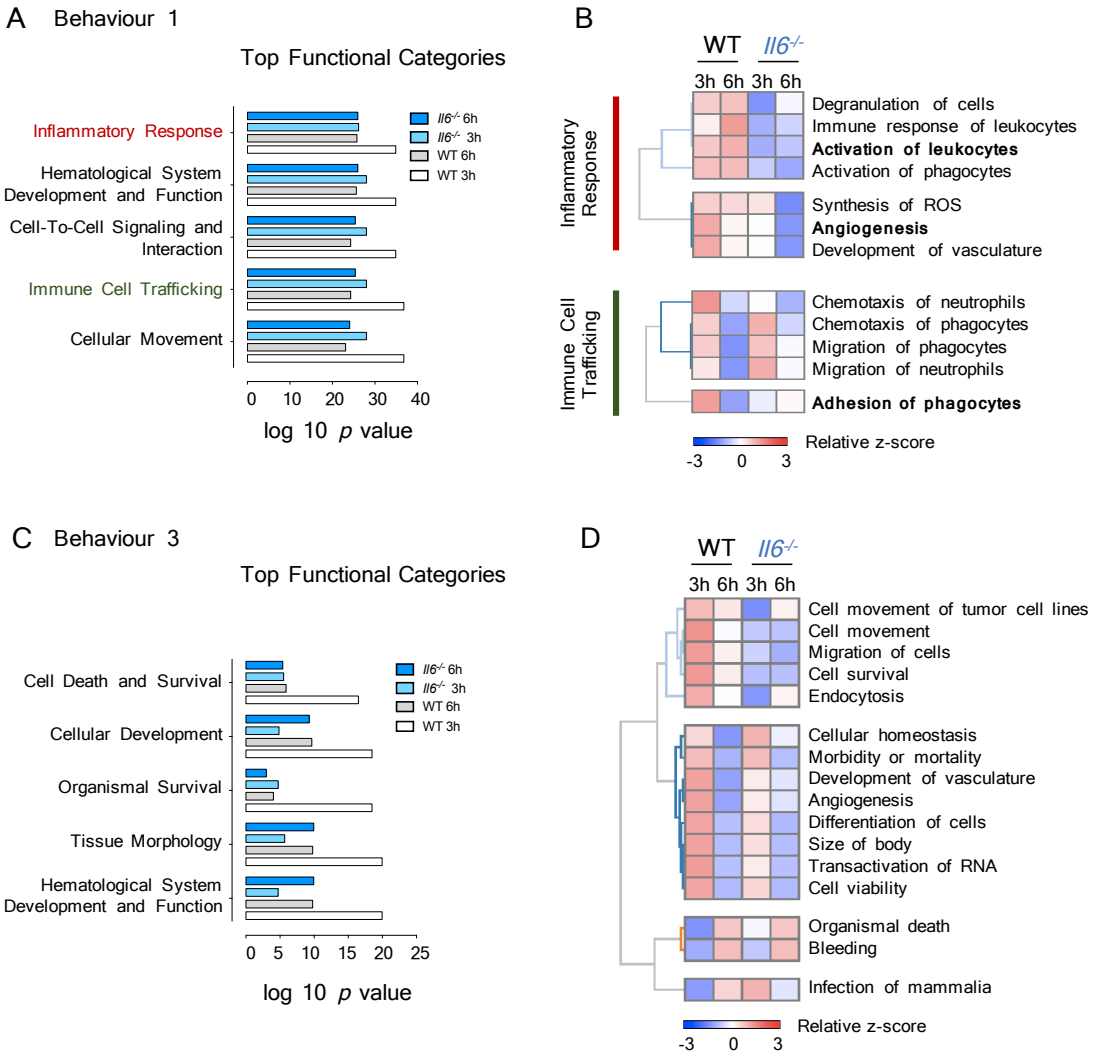

Figure 4.6. Biological function analysis. A & C. Top functional categories enriched in B1 (**A**) and B3 (**C**). **B & D.** The most significant functions (z-score > 3.5) associated to the genes in B1 (**B**) and B3 (**D**).

and it was identified as one of the most prominently regulated genes in WT mice at 3 h (Figure 4.2). Conversely, *Vcam1* is strongly upregulated at 3 h, especially in *Il6*$^{-/-}$ mice.

Functions related to chemotaxis and cell migration were also observed in B3 (Figure 4.8C). Here, leukocyte and phagocyte migration functions were substantially enhanced in WT mice. They included genes involved in cellular adhesion (*Cd44*, *Vcan*), ECM remodelling (*Ddr2*, *Mmp9*, *Col4a1*) and cytoskeletal rearrangement (*Vav1*, *S1pr1, Pdpn*) (Figure 4.8D). Interestingly, the gene encoding for the Atypical Chemokine Receptor 1 (*Ackr1*, also known as Duffy Antigen Receptor for Chemokines, DARC) was also upregulated in WT mice (Figure 4.8D). IPA predicted that ten of these genes were controlled by STAT3 (*Myd88, Serpine1, Vcan, Cd40, S1pr1, Hif1a, Mmp9, Fas, Plaur* and *Tnf*).

Taken together, these findings support the idea that stromal signals modulate a successful host response and that this response is defective in the *Il6*$^{-/-}$ mice.

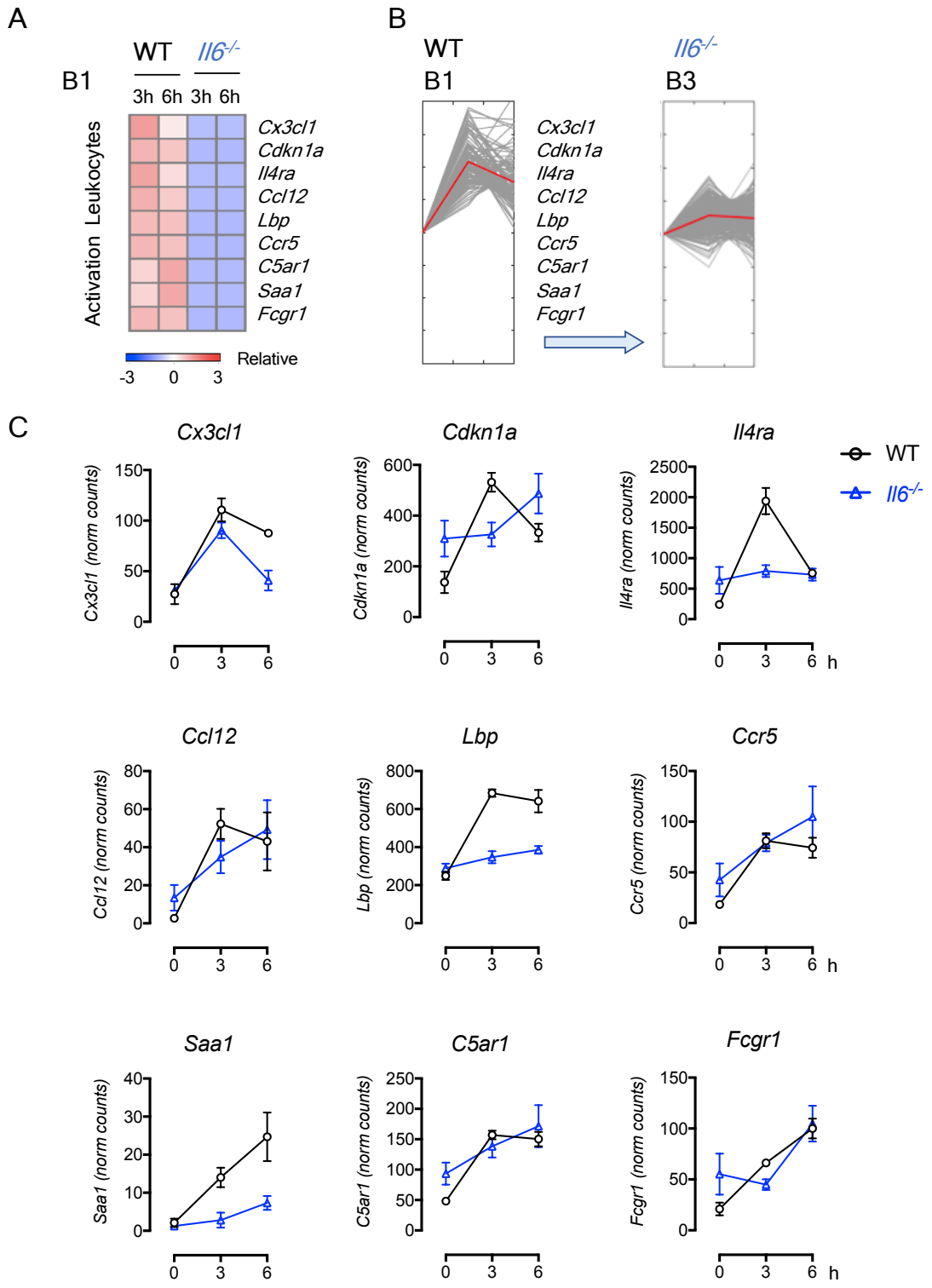

Figure 4.7. STAT3 control over host defence. **A.** Genes extracted from activation of leukocytes that are under the control of STAT3 in WT mice. Genes are plotted using the log2 fold change transformation. **B.** These genes show a behaviour that changes from B1 in WT to B3 in *Il6*$^{-/-}$ mice. **C.** Normalised read counts of the selected genes.

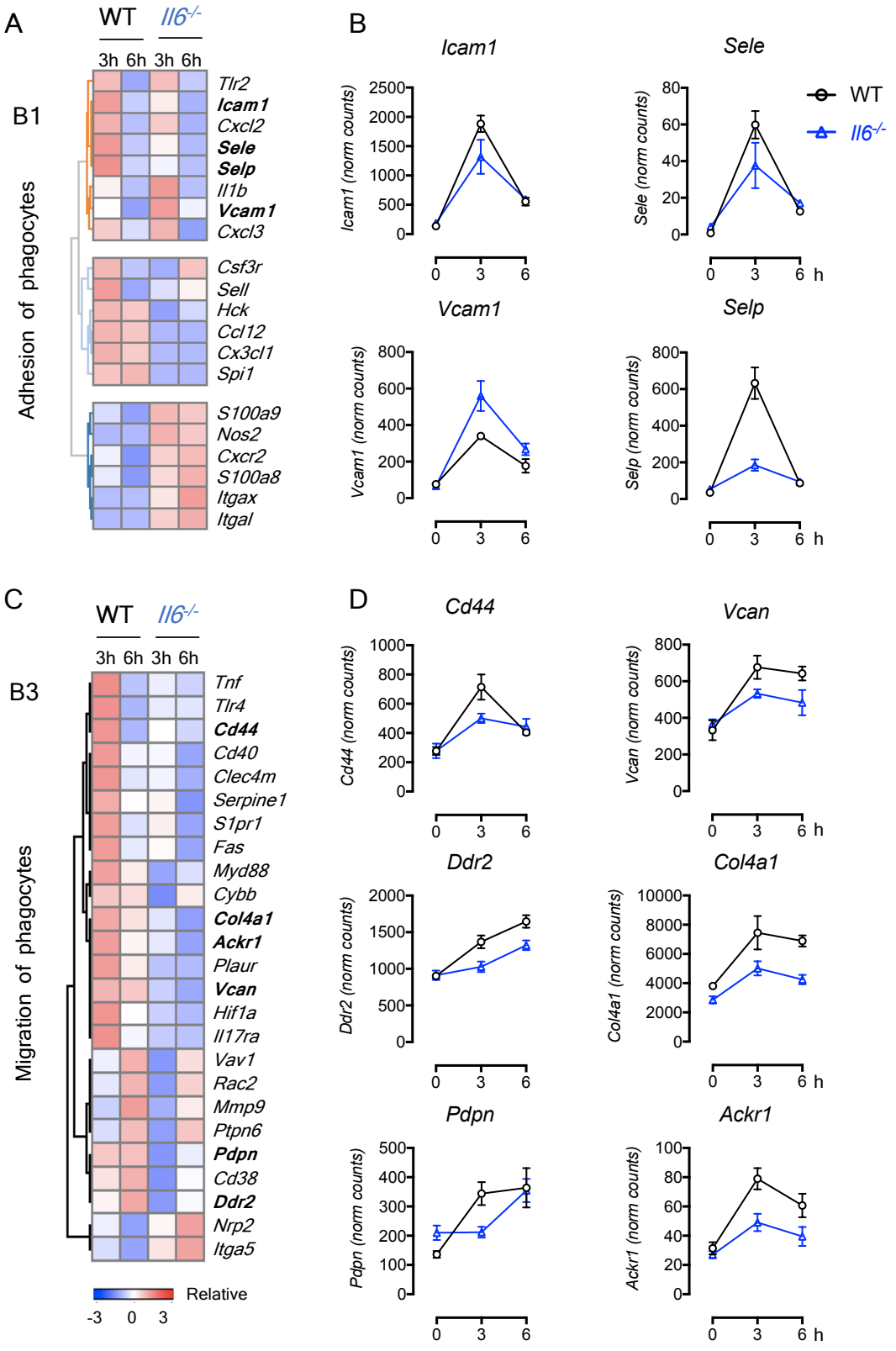

Figure 4.8. Impact of phagocyte migration and adhesion in the immune response against infection. A & C. Heat map showing the expression (log2FC) of genes in B1 involved in the function adhesion of phagocytes (**A**) and in B3 involved in migration of phagocytes (**C**). **B & D.** Normalised counts from RNA-seq of selected genes.

4.3.7. Impact of SES in tissue damage and homeostasis

Genes under B3 were involved in tissue morphology and cellular homeostasis (Figure 4.6C and D). Previous studies in our laboratory demonstrated that the onset of fibrosis was due to an altered turnover of the ECM by proteases [33]. Therefore, the influence of these proteases during acute inflammation was investigated. Several matrix metalloproteinases (MMPs) and their inhibitors (TIPMs) were differentially expressed in response to SES. These included *Mmp3*, *Mmp8*, *Mmp9*, *Mmp13* and *Timp1* (Figure 4.9A). Importantly, *Timp1* expression was rapidly induced in WT at 3 h post SES challenge and maintained through the 6 h time point (Figure 4.9D).

Collagens play an important role in the homeostasis of the ECM and are key components of the peritoneal membrane. Five collagen genes were differentially expressed in our dataset (*Col27a1*, *Col3a1*, *Col4a1*, *Col5a2* and *Col4a2*) (Figure 4.9B). *Col3a1* and *Col5a2*, which correspond to fibrillary collagens [240], were specifically upregulated in WT mice over the time course (Figure 4.9D).

Among the genes most highly upregulated in our dataset are those encoding for solute carriers (SLCs). These proteins are essential for the transport of sugars, amino acids, nucleotides, inorganic ions and drugs across biological membranes [241]. Given the use of the peritoneal membrane as a semipermeable barrier for the exchange of fluids in peritoneal dialysis, the expression of solute carriers in our dataset was investigated (Figure 4.9.C). Here, 16 genes encoding for the SLCs were differentially regulated in at least one of the conditions, and included *Slc10a6, Slc12a2, Slc25a34, Slc26a10, Slc26a3, Slc38a2* and *Slc39a14.*

Finally, the regulation of ion transport (e.g., iron, zinc) by the host is an important anti-microbial activity [242]. Several molecules implicated in iron sequestration and metabolism were differentially regulated in WT and *Il6*$^{-/-}$ mice after SES administration (*Hp*, *Lcn2*, *Hif1a* and *Txnip*) (Figure 4.10).

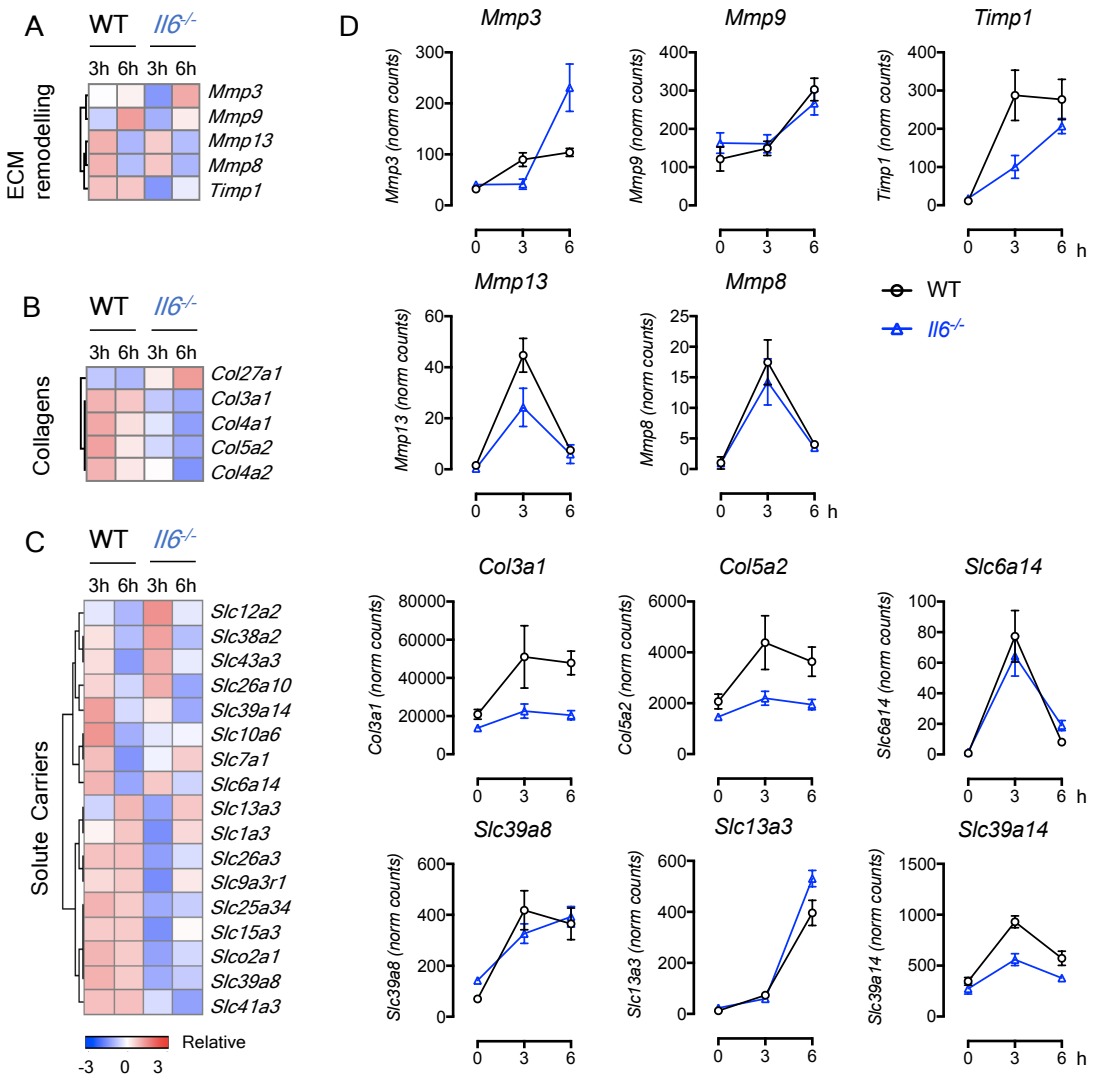

Figure 4.9. Tissue remodelling and morphology markers. A, B & C. Heat map showing the MMPs and TIMPs (**A**), collagens (**B**) and solute carrier (**C**) genes differentially express under SES stimulation in WT and *Il6*$^{-/-}$ mice. Genes are plotted using the log2 fold change transformation. **D.** Normalised counts from RNA-seq of selected genes.

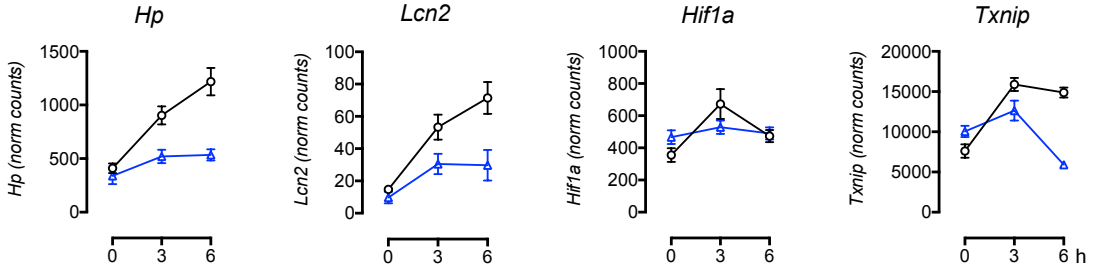

Figure 4.10. Importance of iron sequestration and redox status to host defence. Normalised counts for several genes involved in iron transport (*Hp*) and sequestration (*Lcn2*); and redox status (*Hif1a*) and (*Txnip*).

4.4. Discussion

There is extensive literature relating to the role of IL-6 in host defence against infections [61-64]. As a truly pleiotropic cytokine, IL-6 regulates multiple aspects relevant to the control of tissue homeostasis, the immune response to infection, and the appropriate regulation of inflammation [9, 41]. Previous studies in our laboratory have emphasized the anti-microbial properties of this cytokine in controlling bacterial peritonitis. Specifically, *Il6*$^{-/-}$ mice are unable to successfully clear the infection, and show increased bacterial dissemination as compared to WT controls.

This Chapter provides a holistic overview of the changes occurring in the peritoneal membrane after an episode of acute resolving inflammation. First, a detailed transcriptome analysis of the peritoneum over a 6 h time course is presented for both SES challenged WT and *Il6*$^{-/-}$ mice. RNA-seq identified three distinct patterns of gene expression that are shared by both genotypes. However, approximately a quarter of the differentially expressed genes do not share common overlaps between WT and *Il6*$^{-/-}$ mice, which emphasises the major role of IL-6 in controlling the stromal inflammatory responses to SES.

Studies focussed on the impact of STAT1 and STAT3 in regulating gene expression within the peritoneal membrane. While IL-6 activation of STAT3 contributes to host defence during acute inflammation [21, 95, 243], STAT1 activity after recurrent episodes of peritonitis is linked to fibrosis [33]. The results outlined in this Chapter are in line with these observations. Here, IPA analysis predicted a strong activation of STAT3 in WT mice after acute resolving SES-induced peritonitis.

Computational analysis showed that STAT3 activation was associated to the upregulation of immune-related canonical pathways and downstream biological effects. For example, TREM1 signalling is proposed to be an important pathway involved in the protective immunity against bacterial infection, and relationships between IL-6, TLRs and TREM1 have been previously suggested [244-246]. In addition, several key genes were identified to be differentially regulated as a result of IL-6 signalling. These included some soluble antimicrobial peptides such as *Lbp*;

molecules implicated in complement activation (*C5ar1*), leukocyte migration (*Ackr1*) and adhesion (*Selp*, *Icam1*); and EMC remodelling (*Timp1*, *Col3a1* and *Col5a1*). Interestingly, the increase in collagen production may be important to prevent bacterial dissemination during the early stages of the infection [32].

The peritoneum is a serous, semi-permeable membrane that forms the lining of the abdominal cavity. It is used as a dialysis membrane for the removal of metabolites, uremic toxins, salts and water from end-stage renal failure patients [155]. In this regard, SLCs may be important in peritoneal dialysis as they facilitate the transport of sugars, amino acids, nucleotides, inorganic ions and drugs through biological membranes [241]. Our datasets show that the expression of specific SLCs is enhanced during inflammation. For example, the family 39 (*Slc39*) transporter which are responsible for iron transport [241]. In this regard, iron is often used as an essential cofactor in the generation of anti-microbial immunity [242, 247], and the control of iron availability by the host also constitutes an important mechanism of anti-microbial defence. For example, neutrophil lipocalin (*Lcn2*) interferes with iron acquisition by binding to bacterial ferric siderophores [248], and mice deficient in *Lcn2* display impaired bacterial clearance during lung infection [249]. Similarly, haptoglobin (*Hp*) can bind haemoglobin released from damaged erythrocytes, and thereby limits the bioavailability of free iron for uptake by microbes [247]. Finally, the inflammatory expression of hypoxia-inducible factor-1α (*Hif1a*) in the tissue microenvironment has been shown to improve the bactericidal capacities of neutrophils [250]. Thus, the upregulation of genes that regulate iron availability (e.g., *Lcn2, Hif1a* and *Hp*) in WT but not *Il6*$^{-/-}$ mice emphasise the importance of this metal in host defence and may account for additional support in the overall anti-microbial response.

Taken together, the data suggest that the stromal compartment modulates the innate immune response in a coordinate way: not only ensures the correct infiltration and activation of innate cells, but also potentially provides and antimicrobial environment and structural support to prevent bacterial growth and dissemination from the site of infection.

Chapter 5. Adaptation of the transcriptional profile of the peritoneal membrane by Th1 cells

5.1. Introduction

IL-6 controls both innate and adaptive immune responses essential for competent anti-microbial host defence [9, 228]. For example, IL-6 regulates $CD4^+$ T cell proliferation, differentiation and survival [9, 251], and is implicated in the development of $CD4^+$ T cell memory recall [252, 253].

Our laboratory has previously described the IL-6-mediated expansion of $CD4^+$ effector T-cells in response to recurrent episodes of peritoneal inflammation [33]. Repeated inflammation led to the generation and maintenance of peritoneal IFN-γ-secreting Th1 cells. These Th1 cells were identified as pro-fibrotic. In this regard, IFN-γ induced STAT1 signalling in the peritoneal membrane was shown to distort the physiological turnover of extracellular matrix to drive peritoneal fibrosis [33]. This process is completely IL-6 dependent. It is however unclear what impact the presence of pro-fibrotic $CD4^+$ T-cells may have on the host defence against bacteria.

To address this question, *ex vivo* expanded Th1 cells were adoptively transferred to mice receiving SES challenge. Experiments considered the following:

a. The impact of pro-fibrotic Th1 cells on the transcriptomic profile of the peritoneal membrane during inflammation.

b. How an alteration in the balance between STAT1 and STAT3 signalling may influence the control of anti-microbial host defence versus inflammation induced tissue damage.

5.2. Material and Methods

5.2.1. Adoptive transfer of *ex vivo* SES-CM polarised Th1 cells

Th1 cells were generated from naïve $CD4^+$ T-cells by anti-CD3 and anti-CD28 co-stimulation in the presence of conditioned media from SES treated peritoneal resident cells (see *Section 2.4.2*). SES-polarised Th1 cells were adoptively transfer into WT and *Il6*$^{-/-}$ mice together with SES as described in *Sections 2.3.4*. Mice receiving a comparable amount of sorted naïve $CD4^+$ T-cells (Th0) were used as controls.

5.2.2. Data visualization and interpretation

The reader is referred to methods outlined in Chapter 4 (*Section 4.2*).

5.3. Results

5.3.1. Impact of naïve CD4$^+$ T-cell transfer on the transcriptomic profile of the inflamed peritoneum

To mimic the pro-fibrotic environment conducive to the development of peritoneal fibrosis, WT and *Il6*$^{-/-}$ mice were adoptively transfer with *ex vivo* expanded Th1 cells co-administered with SES. Control mice received an equivalent number of sorted naïve CD4 T-cells (Th0) together with SES (*Section 2.2.4*). At 3 and 6 h time points, peritoneal lavage and peritoneal stromal tissue were harvested for cytokine quantification and transcriptomic analysis, respectively.

Transfer of Th1 cells promoted an increase in peritoneal IFN-γ and the activation of STAT1 within the peritoneal stromal tissue obtained from SES treated WT, *Il6*$^{-/-}$ and *Il6ra*$^{-/-}$ mice [33] (Figure 5.1). No change in IFN-γ activity was observed following the transfer of control Th0 cells. The presence of IFN-γ in the peritoneal cavity boosted the expression of IL-6 in WT mice after SES challenge (Figure 5.1C). STAT1 and STAT3 activity within the peritoneal membrane was confirmed using qPCR analysis for target genes controlled by these transcription factors (Figure 5.1D).

Studies next tested the impact of Th0 cells on the transcriptome of WT and *Il6*$^{-/-}$ mice receiving SES (Figure 5.1E). Here, responses in mice receiving Th0 cells and SES were directly compared to mice receiving SES alone (Chapter 3). All differentially regulated genes were subjected to a hierarchical clustering using Spearman's rank correlation, and presented as a heat map (Figure 5.1E). These data revealed that the presence of Th0 cells had a minimal impact on the transcriptional output seen during SES-induced inflammation. To allow us to identify gene changes attributed to the action of adoptively transferred Th1 cells, all datasets derived from these mice were corrected to mice receiving control Th0 cells.

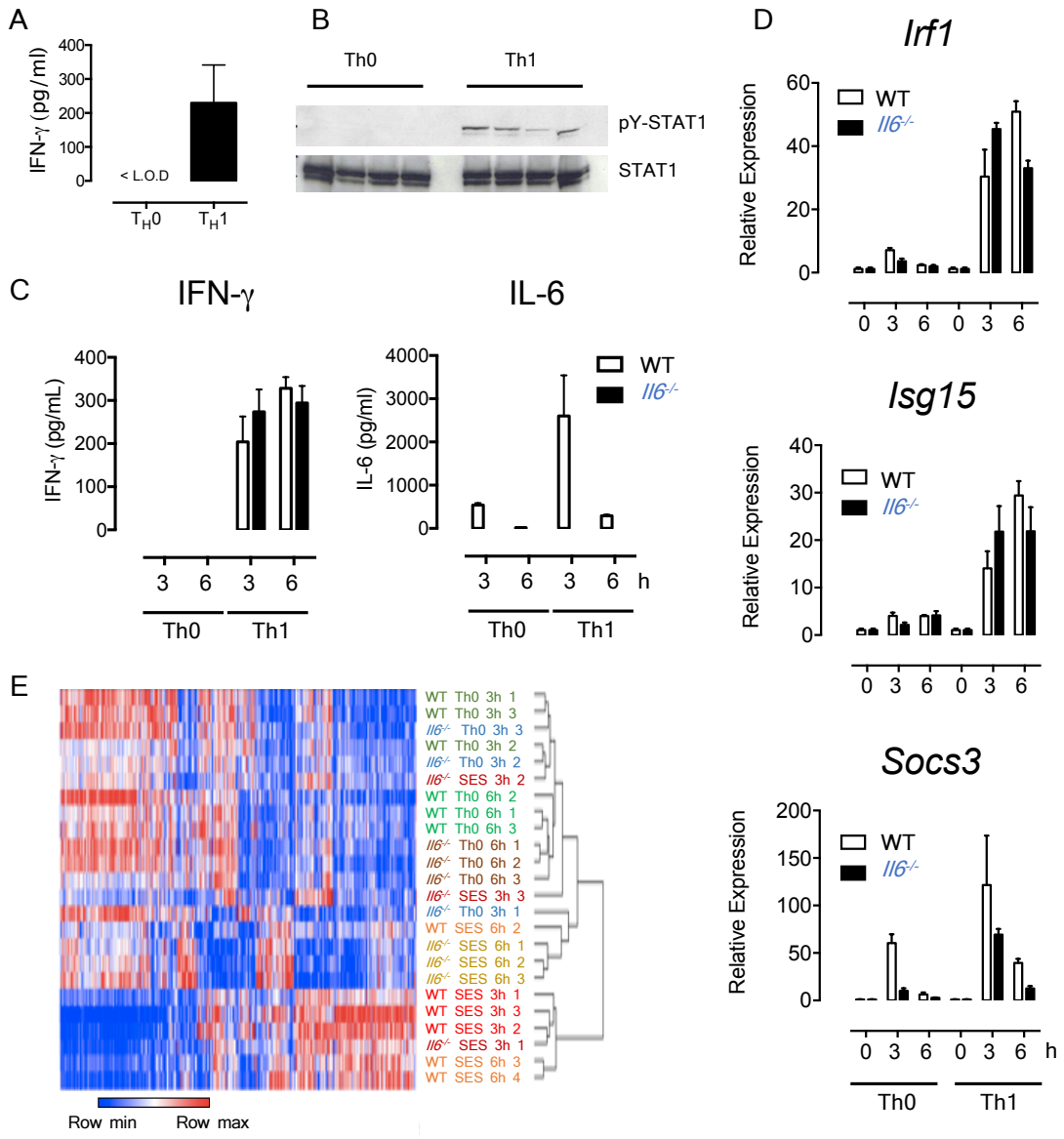

Figure 5.1. Analysis of Th1 and Th0 signalling in the peritoneum. A. The levels of IFN-γ in the lavage of *Il6ra*$^{-/-}$ mice 3 h after the transfer of sorted naïve (Th0) or SES-polarised Th1 cells together with SES were assessed by ELISA. **B.** Western blot of pY-STAT1 in the peritoneal membrane of *Il6ra*$^{-/-}$ mice 3 h after the transfer of Th0 or Th1 cells together with SES (**A** and **B** have been obtained from ref 33). **C.** The levels of IFN-γ and IL-6 were measured in WT and *Il6*$^{-/-}$ mice after the transfer of Th0 or Th1 cells together with SES by ELISA. **D.** qPCR of target genes for STAT1 (*Irf1*, *Isg15*) and STAT3 (*Socs3*). **E.** The genes differentially expressed between WT and *Il6*$^{-/-}$ mice receiving either a single dose of SES or SES together with Th0 cells were plotted as a heat map. The expression level is represented as normalised read counts per gene (FPKM). Samples were hierarchically clustered using Spearman's rank correlation.

5.3.2. Transcriptomic analysis of the peritoneal membrane following Th1 adoptive transfer

Transcriptomic analysis of the peritoneal membrane after adoptive Th1 cell transfer identified 2307 genes as differentially expressed in at least one of the experimental conditions when compared to Th0 controls. Hierarchical cluster analysis grouped all experimental (Th1) samples together, and these were distinct from the controls (Th0) (Figure 5.2).

Among the 2307 genes identified, 782 were differentially expressed at 3 h in WT mice, and 1262 in *Il6*$^{-/-}$ mice following transfer of Th1 cells. At 6 h, 1280 and 1195 genes were changed in WT and *Il6*$^{-/-}$ mice, respectively (Figure 5.3). A total of 407 genes were commonly regulated in all conditions (Figure 5.3B). The adoptive transfer of Th1 cells strongly induced a large number of genes in both genotypes (with an absolute fold change > 4) (Figure 5.3A).

5.3.3. Th1 cells control 3 distinct patterns of gene regulation

Using the statistical approaches outlined in *Section 3.2.11*, three distinct patterns of Th1-mediated gene expression were identified within the peritoneal stromal tissue from SES stimulated WT and *Il6*$^{-/-}$ mice (Figure 3.8). These patterns were comparable in both genotypes. Two-sample 2D K-S test and the MVK test (described in Chapter 4; *Section 4.2.2* & *4.3.3*) identified similarities between gene clusters (Table 5.1 & 5.2; Figure 5.4). Clusters 1, 2, & 3 from WT mice corresponding with Clusters 2, 3 & 1 from *Il6*$^{-/-}$ mice, respectively. Consistent with the nomenclature outlined in Chapter 4, these gene "Behaviours" were termed – "Behaviour 4" (B4), "Behaviour 5" (B5) and "Behaviour 6" (B6) (Figure 5.4).

To investigate the degree of overlap between these Behaviours, the percentage of commonly regulated genes over the total 2307 genes was calculated (Figure 5.4B & 5.4C). Overall, 89% of all the differentially expressed genes shared a common Behaviour between WT and *Il6*$^{-/-}$ mice (Figure 5.4B). Here, the Jaccard index calculated an individual overlap of 0.63 for B4; 0.88 for B5; and 0.8 for B6 (Figure 5.4C).

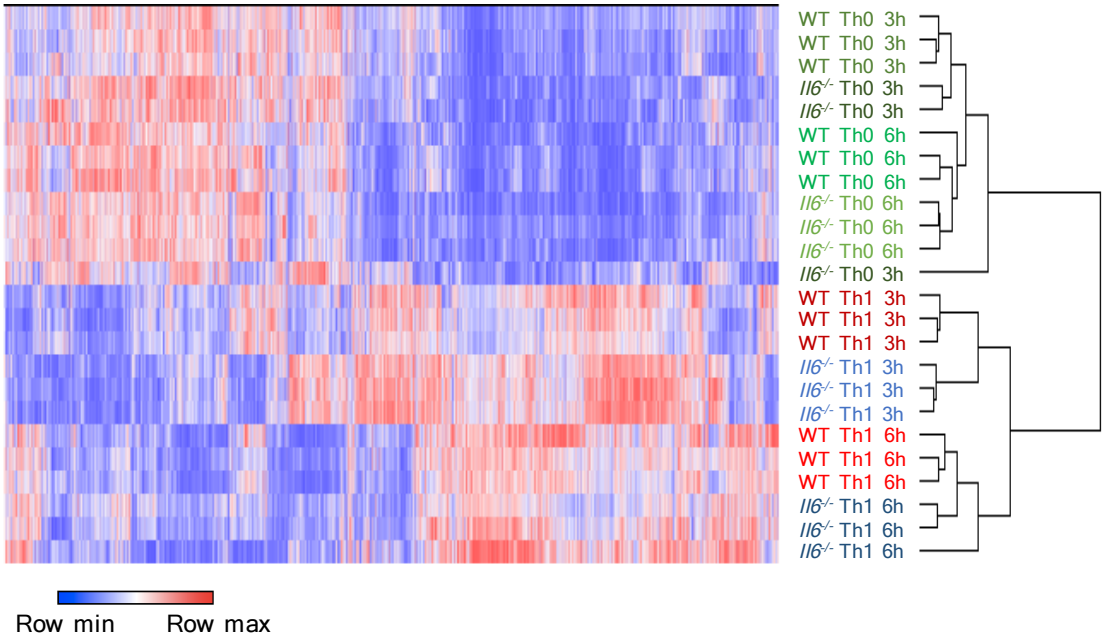

Figure 5.2. Hierarchical cluster analysis of WT and *Il6*$^{-/-}$ mice at 3 and 6 h after receiving SES together with T-cell adoptive transfer. WT and *Il6*$^{-/-}$ mice were administered (i.p.) with a dose of SES together with either sorted naïve T-cells (Th0) or *ex vivo* polarised Th1 cells. The heat map represents the expression level of the 2307 genes being differentially regulated in at least one of the experimental conditions (Th1) when compared to their correspondent control (Th0). The expression level is represented as normalised counts per gene (FPKM). Samples were hierarchically clustered using Spearman's rank correlation.

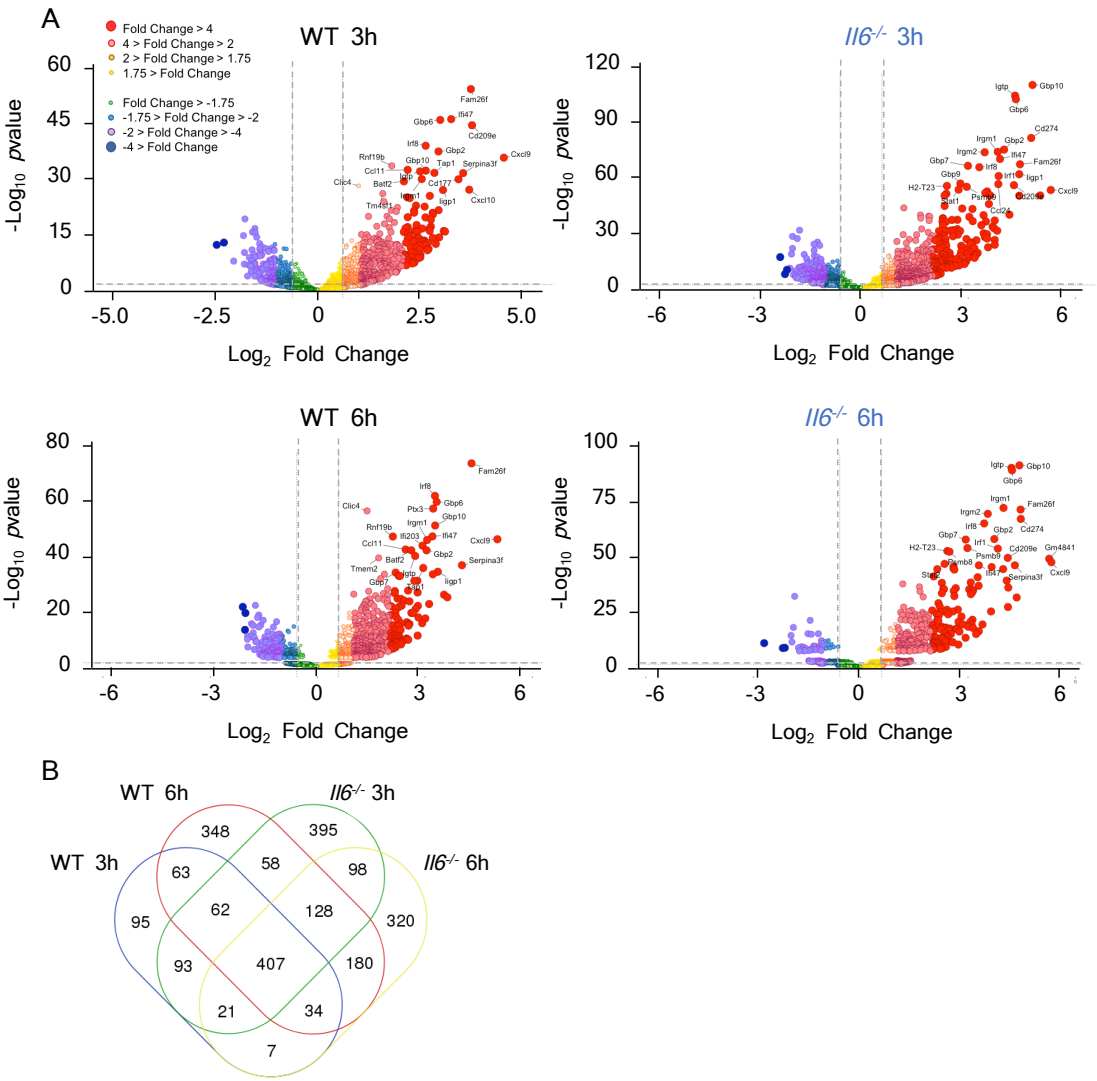

Figure 5.3. Volcano plot analysis of differentially expressed genes in WT and *Il6*$^{-/-}$ mice after the transfer of Th1 cells together with SES. A. Data shows the differential expression of genes in WT and *Il6*$^{-/-}$ mice at 3 and 6 h after Th1 adoptive transfer with SES when compared to corresponding Th0 controls. **B.** Venn diagram demonstrates the number of genes that are commonly or uniquely regulated in each condition.

Table 5.1. Two-sample two-dimensional Kolmogorov-Smirnov test

		WT			
		Cluster 1	**Cluster 2**	**Cluster 3**	
Il6$^{-/-}$	**Cluster 1**	1.81E-97	1.38E-130	**1.36E-03**	slopes
		1.07E-107	2.44E-131	**1.53E-03**	log2FC at 3 and 6 h
	Cluster 2	**2.09E-05**	1.84E-257	5.75E-74	slopes
		2.80E-05	1.20E-272	7.68E-105	log2FC at 3 and 6 h
	Cluster 3	1.12E-244	**5.28E-05**	1.56E-150	slopes
		6.80E-255	**1.22E-04**	2.05E-149	log2FC at 3 and 6 h

Clusters from WT and *Il6*$^{-/-}$ regulated genes were tested for similarly using the two-sample two-dimensional Kolmogorov-Smirnov. The *p* value associated to each comparison is shown (significance level of 0.1%). Data outlined in blue highlight clusters with the closest similarities. Slope = rate of change of log2FC gene expression at 3 and 6 h

Table 5.2. Multivariate Kruskal-Wallis test

		WT			
		Cluster 1	**Cluster 2**	**Cluster 3**	
Il6$^{-/-}$	**Cluster 1**	678.47	740.72	**7.38**	log2FC at 3 and 6 h
	Cluster 2	**28.28**	1575.02	674.67	log2FC at 3 and 6 h
	Cluster 3	1529.88	**19.39**	910.01	log2FC at 3 and 6 h

Clusters from WT and *Il6*$^{-/-}$ regulated genes were tested for similarly using the Multivariate Kruskal-Wallis. The variance associated to each comparison is shown. The critical value of chi^2 statistics is 13.8155 at significance level of 0.1%. Data outlined in blue highlight clusters with the closest similarities.

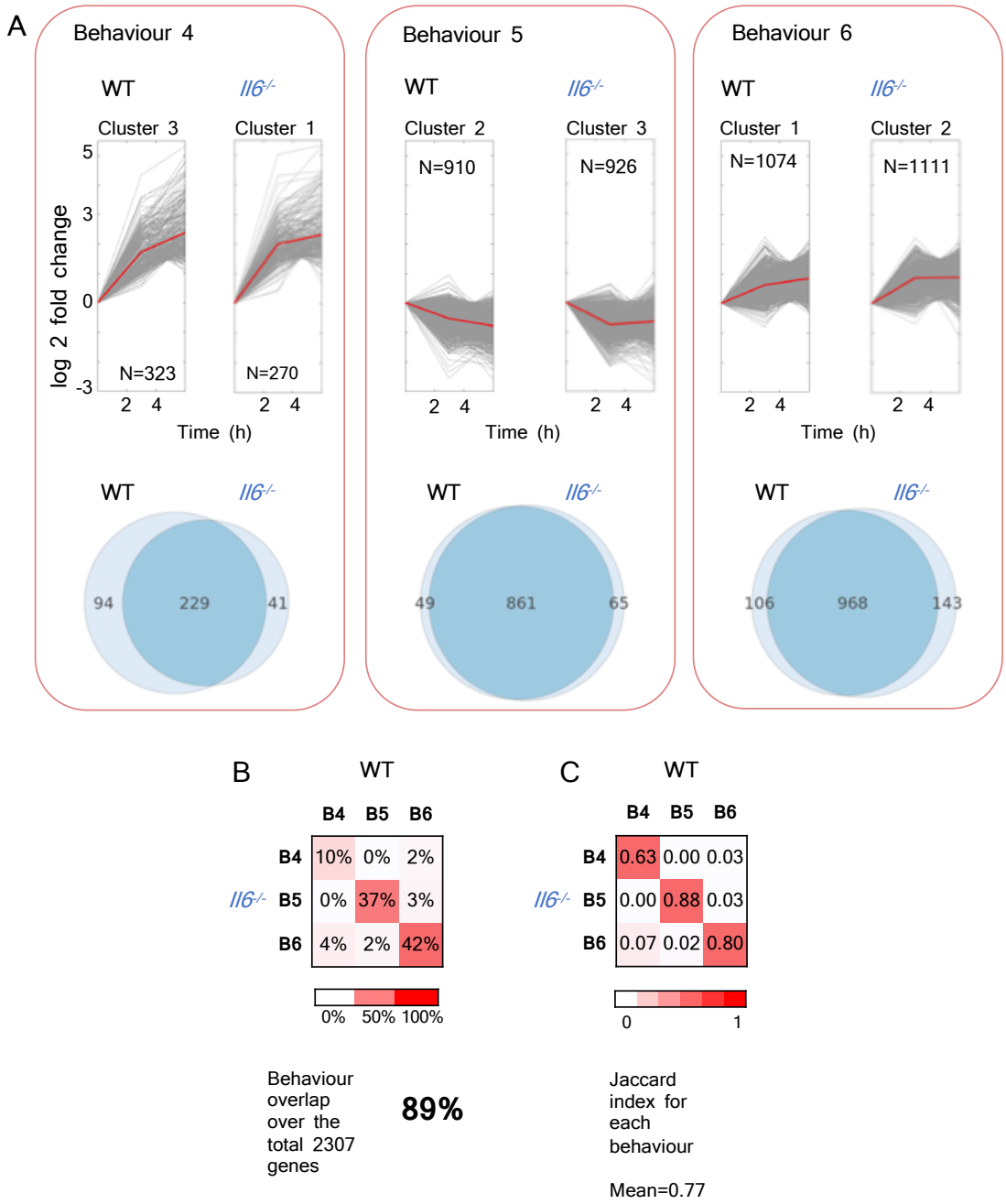

Figure 5.4. Cluster analysis and overlap between the differentially expressed genes in WT and *Il6*$^{-/-}$ mice after Th1 adoptive transfer. A. Genes were plotted according to their expression over time (0-3-6 h). Red lines represent the mean expression within each group (centroid). Cluster analysis showed three patterns of expression (termed "Behaviours") common in WT and *Il6*$^{-/-}$ deficient mice. The Venn diagrams show the gene overlap in terms of absolute number between common Behaviours. **B & C.** Representation of the percentage of overlap between each Behaviour over the total 2307 differentially expressed genes (**B**), and the Jaccard similarity coefficient between Behaviours (**C**).

5.3.4. Control of STAT1 and STAT3 in the stromal responses to Th1 adoptive transfer

The transfer of Th1 cells promotes an alteration in the relative activation of STAT1 and STAT3 within the peritoneal membrane of SES challenged mice. To consider the impact of these changes, "Upstream Regulators Analysis" was performed in IPA (Figure 5.5). Only B4 and B6 were predicted to have an activation of STAT1 and STAT3 above 2 (z-score > 2) (Figure 5.5A & C). Here, STAT3 was regulated in WT mice under B4, and in *Il6*$^{-/-}$ under B6. On the other hand, STAT1 activity was enhanced in *Il6*$^{-/-}$ mice in B4 and in both genotypes under B6. This was specific to the 6 h time point.

Next, studies evaluated the genes predicted as linked to STAT1 and STAT3 activity in both B4 and B6 (Figure 5.5B & D). Here, most of the genes associated with STAT1 and STAT3 were common to both WT and *Il6*$^{-/-}$ mice. While this was particularly evident in B4, genes common to both genotypes were also abundant in B6. Top "Canonical Pathway Analysis" of the genes within B4 and B6 showed that Th1 adoptive transfer enhanced pathways linked with interferon signalling (Figure 5.5E). These were observed in both genotypes.

5.3.5. Th1 control of the biological functions

IPA explored the downstream biological functions associated with the genes assigned to each pattern of gene regulation. The top functional categories defined for B4, B5 and B6 are shown in Figure 5.6. Computational analysis included signatures associated to cellular movement and immune cell trafficking, tissue morphology, cellular function and inflammatory response. Interestingly, these functions were enriched in a similar fashion for both WT and *Il6*$^{-/-}$ animals. These findings demonstrate that the effect of Th1 cell transfer on to the transcriptomic profile of the peritoneum is independent of IL-6.

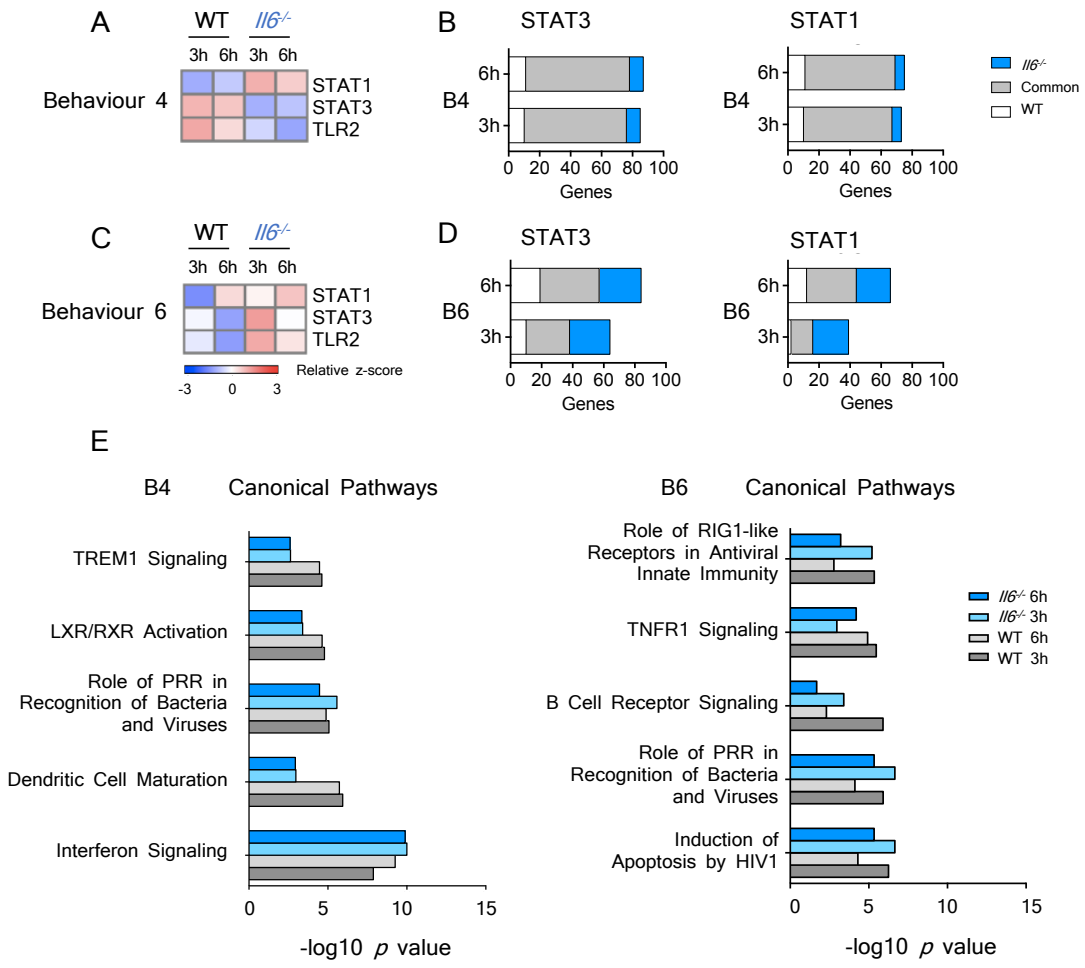

Figure 5.5. Pathway analysis. A & C. STAT1, STAT3 and TLR2 activation was predicted in IPA for B4 (**A**) and B6 (**C**), and their relative z-score plotted in a heat map. **B & D**. Common and unique genes to WT and *Il6*$^{-/-}$ datasets that are predicted to be under STAT1 and STAT3 control in B4 (**B**) and B6 (**D**). **E.** Top 5 canonical pathways (z-score > 2) in B4 and B6.

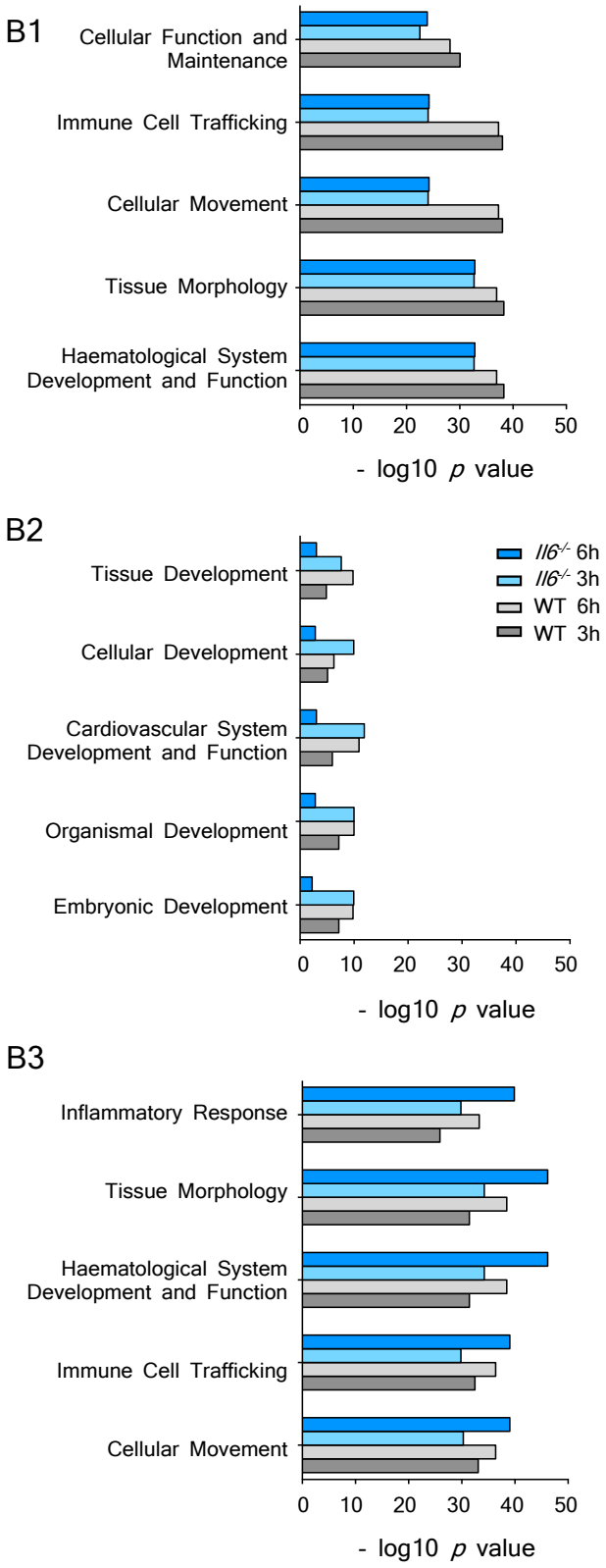

Figure 5.6. Top functional categories in each Behaviour. Genes within each Behaviour were uploaded to IPA and analysed for downstream biological effects.

5.3.6. Host defence-associated functions impaired in *Il6*$^{-/-}$ are rescued by Th1 adoptive transfer

As outlined in *Section 4.3.5*, biological functions associated with host defence were found to be impaired in *Il6*$^{-/-}$ mice receiving SES alone (Chapter 4). In contrast, IPA analysis predicted that the inflammatory response to SES was comparable between WT and *Il6*$^{-/-}$ mice after Th1 transfer (Figure 5.6).

Subsequent analysis therefore explored the impact of Th1 cells on the control of host defence in the peritoneal cavity (Figure 5.7). "Comparison Analysis" of the biological functions regulated during single SES stimulation or SES stimulation together with Th1 adoptive transfer was performed using IPA (Figure 5.7A). Functions impaired in *Il6*$^{-/-}$ mice during acute inflammation were restored following Th1 cell transfer, including signatures relevant to activation and immune response of leukocytes and phagocytes. This was especially evident at the 6 h time point (Figure 5.7A). Interestingly, 136 genes out of the 343 that were uniquely regulated in WT mice after SES stimulation were significantly regulated after the addition of Th1 cells in both genotypes. What is more, several of these corresponded to genes associated in Chapter 4 with host defence, including *Lcn2*, *Saa1*, *Ccr5*, *Selp*, *Hp* and *Vcan*, among others.

"Comparison Analysis" between both experiments was also used to determine the contribution of STAT1 and STAT3 in the transcriptome profile of the inflamed peritoneum for both WT and *Il6*$^{-/-}$ mice. Bioinformatic analysis focused on the genes that were differentially regulated across all conditions. The relative and absolute activation of STAT1 and STAT3, as predicted by IPA "Upstream Regulators Analysis", is presented in Figures 5.7C & D. STAT3 was uniquely activated in WT mice after single SES challenge. In the presence of Th1 cells, STAT1 signalling events were markedly increased and appeared to dampen the involvement from STAT3. This increase in STAT1 was observed in both WT and *Il6*$^{-/-}$ mice. This computational approach likely reflects the enhanced stromal tissue response to IFN-γ signalling seen in mice receiving CD4 Th1 cells. Here, the impact of Th1 cells on STAT3 is interesting (Figure 5.7C). These data may reflect a statistical over representation of STAT1 signatures and pathways within the datasets, but may also support a negative regulation of STAT3 activity by STAT1.

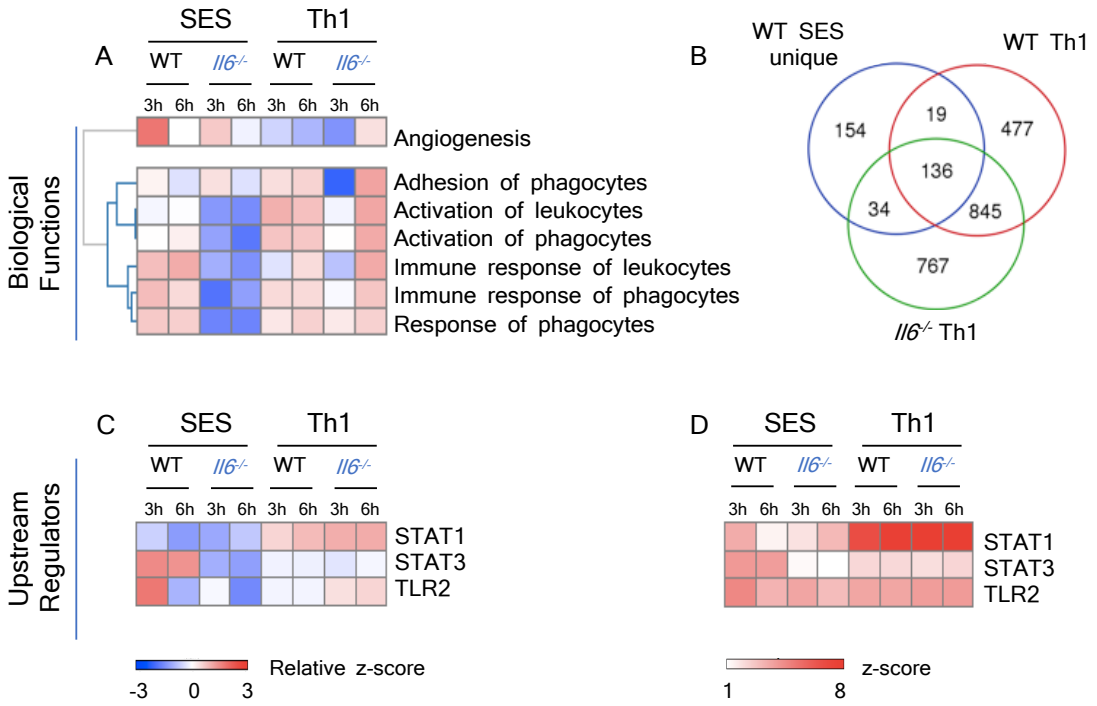

Figure 5.7. Biological functions associated to host defence. All differentially expressed genes in WT and *Il6*$^{-/-}$ mice during either acute SES-driven inflammation or inflammation induced with SES together with Th1 transfer were uploaded to IPA, and tested for "Comparison Analysis". **A.** Selected biological functions under the category Immune Response are presented in a heat map showing relative z-score. **B.** Overlap between the genes uniquely regulated in WT mice during SES and genes controlled by Th1 and SES in WT and *Il6*$^{-/-}$ mice. **C & D.** Upstream regulator analysis (z-score relative to each row, **B**; or absolute, **C**).

5.3.7. Impact of STAT1 signalling in tissue remodelling and damage

Our previous work has shown that enhanced peritoneal STAT1 signalling disrupts the homeostatic turnover of extracellular matrix by tissue proteases [33]. While this outcome is observed as a result of recurrent episodes of acute resolving peritonitis, studies now investigated whether the single adoptive transfer of Th1 cells is also associated to pro-fibrotic marks in the inflamed peritoneum. RNAseq datasets were therefore interrogated to explore changes in the expression of matrix proteases and their inhibitors (Figure 5.8). Here, the inflammatory regulation of 6 ADAMTS (A Disintegrin And Metalloproteinase with Thrombospondin motifs), 4 ADAMs (A Disintegrin And Metalloproteinase), 7 MMPs and 2 TIMPs was altered in response to Th1 cell transfer. A further 10 collagen-encoding genes were also differentially regulated by the introduction of Th1 cells (Figure 5.9). Surprisingly, all of these genes except one (*Col6a5*) were differentially downregulated as a result of IFN-γ signalling in the peritoneal membrane. Collagen fibrils are crosslinked by enzymes lysyl oxidases (LOX) to ensure a stable ECM [254-256]. Three lysyl oxidases were also differentially regulated in this dataset (Figure 5.9). Interestingly, *Loxl4* expression was inhibited in *Il6*$^{-/-}$ mice after SES challenge; and rescued as a result of Th1 transfer. Finally, hyaluronic acid (HA) is another large component of the ECM [240, 257]. HA is synthetized in the plasma membrane by the enzymes Hyaluronic Acid Synthases (HAS) [258], and simultaneously secreted to the extracellular space [259]. *Has1* and *Has2* were differentially regulated within the datasets derived from WT and *Il6*$^{-/-}$ mice (Figure 5.9). Collectively, these data suggest that Th1-mediated cell signalling in the peritoneal membrane distorts the homeostatic regulation of the ECM following inflammation.

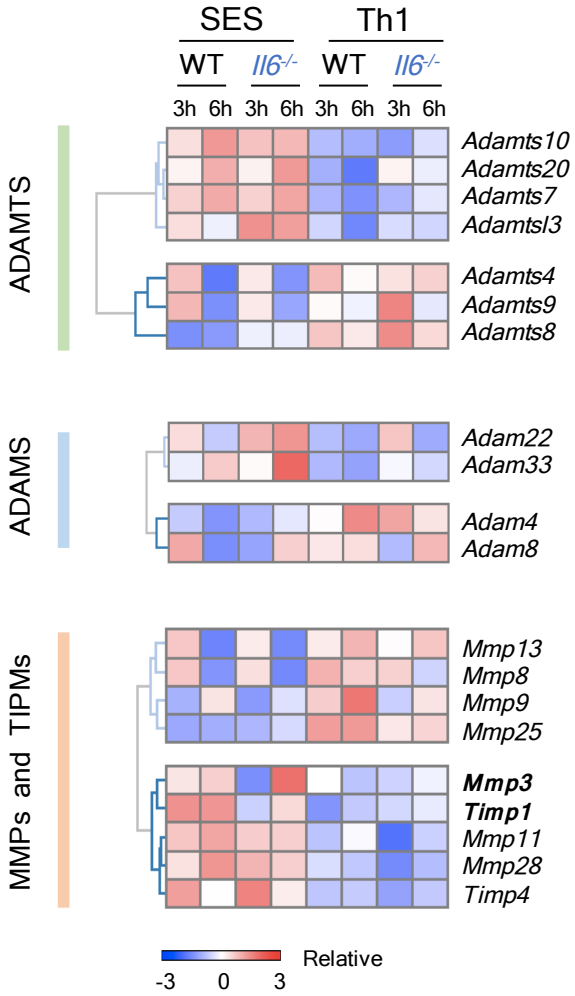

Figure 5.8. Genes related to ECM remodelling. Heat map showing the MMPs and TIMPs, ADAMs and ADAMTs genes differentially express under Th1 transfer in WT and *Il6*$^{-/-}$ mice. Genes are plotted using the log2 fold change transformation.

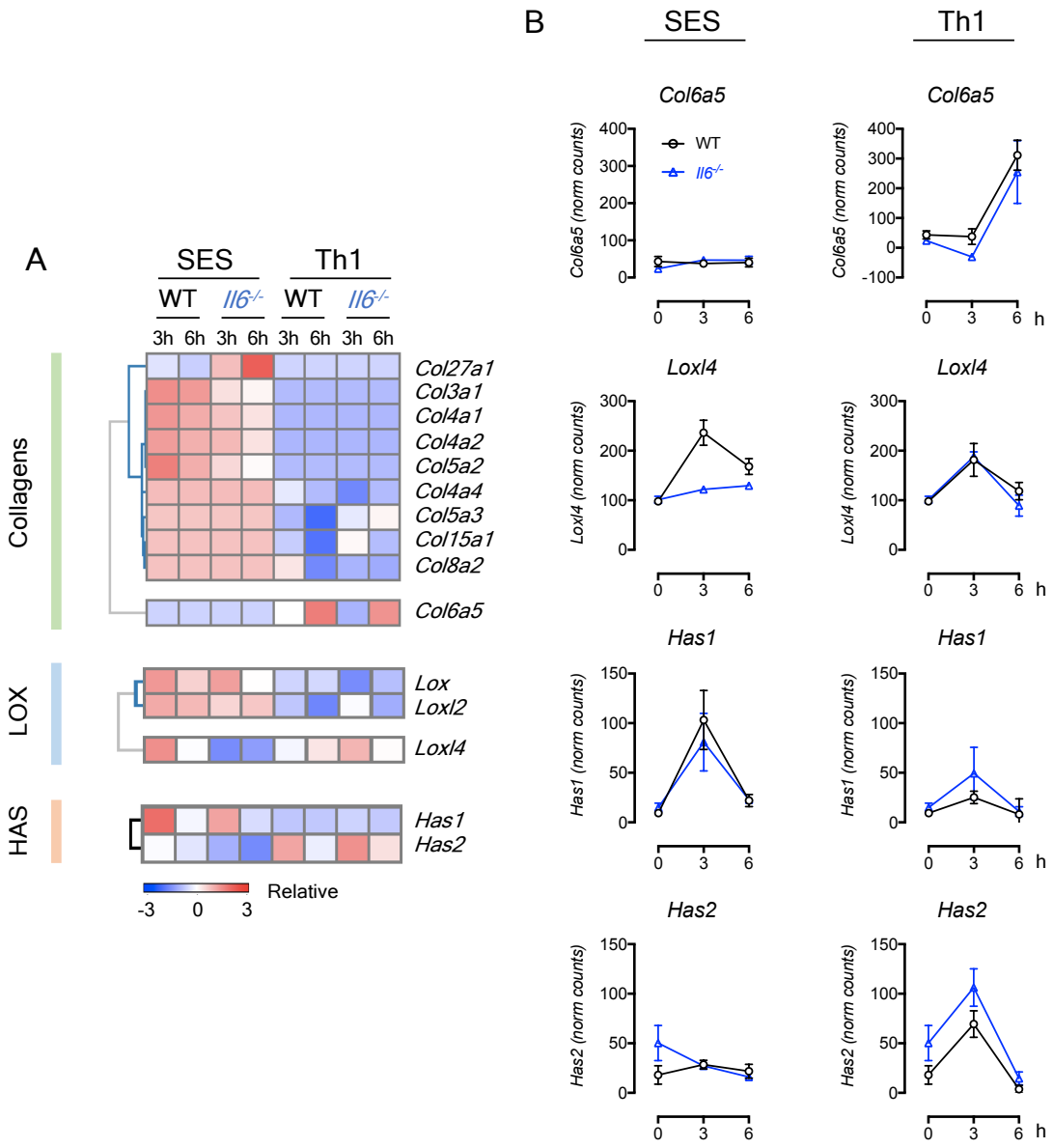

Figure 5.9. Genes related to ECM composition and structure. A. Heat map showing the differential expression in terms of log2 fold change in the SES and Th1 transfer experiment. **B.** Normalised read counts of selected genes. For Th1 experiment, the normalised counts under Th1 condition were compared (subtracted) to the mean of the Th0 controls.

5.4. Discussion

Studies in the Jones laboratory have linked the recruitment and local expansion of Th1 cells to the development of peritoneal fibrosis as consequence of recurrent inflammatory activation. Here, fibrosis is strictly IL-6 dependent [33]. At the same time, mice lacking IL-6 also show a defective immune response against infection. However, the impact of Th1 cells on the local anti-microbial response is unknown. This chapter aimed to understand the holistic changes occurring in the peritoneal membrane following Th1 cell expansion and recruitment.

The ability of IL-6 to signal via STAT3 and to a lesser extend via STAT1 is well documented [48]. IL-6 activation of STAT3 contributes to host defence during acute inflammation by various mechanisms [21, 95, 243]. IFN-γ signals via STAT1 [117], and the importance of IFN-γ-secreting Th1 cells in antimicrobial immunity has been broadly recognised [260-262]. Both cytokines have been shown to collectively influence neutrophil recruitment and apoptosis during acute inflammation [25]. Our findings are in close agreement with these studies, and the presence of IFN-γ significantly enhanced the peritoneal levels of IL-6.

A major finding in this Chapter was the evidence that the adoptive transfer of Th1 cells into *Il6*$^{-/-}$ mice restored the regulation of genes important for competent anti-microbial defence. Specifically, genes associated with neutrophil activation and iron sequestration that were defective in *Il6*$^{-/-}$ mice challenged with SES that did not receive Th1 cells. Importantly, this restoration was linked with a switch from a predominant STAT3 to a STAT1 signature in the peritoneal membrane. While these findings were derived from a computational analysis of the datasets, further studies are required to illustrate the functional significance of this potential signalling interplay. These findings also emphasise the congruence between IFN-γ and IL-6 acting *via* its soluble receptor in orchestrating innate immune responses [25, 263, 264]. Such interactions may also influence mechanisms essential for the homeostatic regulation of the extracellular matrix [257]. Here, Th1 cells affected changes in the expression of tissue proteases and their inhibitors, structural proteins and enzymes required for maintaining the integrity of the peritoneal lining [135, 257, 265, 266]. Such processes are relevant

to the development of tissue fibrosis. For example, *Has2* expression in humans is regulated by pro-inflammatory cytokines such as TNF-α, IFN-γ and IL-1β [267]. This enzyme catalyses the production of hyaluronic acid (HA), which contributes to angiogenesis [268] and immune regulation [269].

During acute resolving peritonitis, IL-6 signalling differentially regulated the expression of several collagen genes. The presence of Th1 cells significantly reduced the expression of these genes. However, Th1 cells dramatically altered the expression of collagen type VI (*Col6a5*) in both WT and *Il6*$^{-/-}$ mice. Interestingly, collagen type VI is increased during fibrogenesis in adipose tissue and liver [270-273], and its degradation by MMPs is considered an early indicator of liver fibrosis [272, 273]. In this regard, the alpha 2 chain of type VI collagen sequestrates pro-MMPs and inhibits their conversion to the active form [274], stressing the importance of this gene in ECM remodelling.

While these changes in gene expression following adoptive Th1 cell transfer suggest an altered control of ECM turnover, it is still unclear whether a single challenge of SES together with Th1 cells is sufficient to drive fibrosis. In this particular model, the recruitment of Th1 cells only occurs after the four challenges with SES [33]. Future studies will investigate whether Th1/IFN-γ-driven STAT1 activation in the membrane is sufficient to trigger peritoneal fibrosis, or whether recurrent episodes of inflammation are a prerequisite to prime the stroma for the onset of fibrosis.

Chapter 6. Tracking neutrophil effector functions in inflammation

6.1. Introduction

Interleukin-6 is essential for host defence against different pathogens [61-65]. Unpublished data for our laboratory (provided by Coles, Colmont, Hammond, Topley & Jones) demonstrate that *Il6*$^{-/-}$ mice have a reduced capacity to resolve peritoneal *S. epidermidis* infection. This was illustrated by a reduction in bacterial clearance from the site of infection and an increased dissemination to the bloodstream (Figure 6.1).

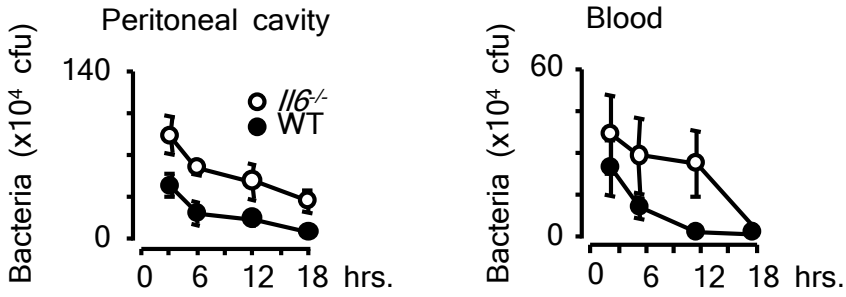

Figure 6.1. *Il6*$^{-/-}$ mice display reduced bacterial clearance and increased bacterial dissemination compared to WT mice. Peritonitis was induced in WT and *Il6*$^{-/-}$ by a single i.p injection of fluorescently labelled *Staphylococcus epidermidis* (5 x 10^8 CFU; *Section 2.3.3*). The peritoneal cavity was lavaged with 2ml PBS and blood extracted by cardiac puncture at defined time points. Bacterial count was quantified by serial agar viable plate analysis of samples following leukocyte pellet lysis. Value represent mean ± SEM n=6. Statistical analysis performed by t-test, * $p<0.05$.

Neutrophils are the first inflammatory cells to arrive at sites of bacterial infection. Although IL-6 does not affect the rate of neutrophil infiltration, IL-6 signalling influences the chemokine-directed trafficking [9, 20, 275] and apoptotic clearance of these cells [25, 275]. For example, studies in *Il6*$^{-/-}$ mice show that the profile of neutrophil recruitment is both heightened and more sustained in response to bacterial agonists (e.g., LPS, SES) [74, 276]. Moreover, neutrophils are important regulators of IL-6 bioactivity, and rapidly shed the IL-6R in response to various stimuli to allow IL-6 trans-signalling in inflamed tissues [20, 277]. This

process is critical to both the termination of neutrophil influx and the containment of bacterial infection. In this regard, reconstitution of IL-6 trans-signalling in *Il6*$^{-/-}$ mice improves bacterial clearance [102]. The mechanisms underpinning this response are currently unknown. Importantly, IL-6 does not appear to directly activate neutrophil responses [200, 278, 279]. Given that transcriptomic analysis of the peritoneal membrane following SES challenge identified alterations in anti-microbial activities as a consequence of IL-6 deficiency, and that IL-6 trans-signalling suppresses the expression of neutrophil-activating chemokines (e.g., CXCL1, CXCL8) by stromal tissue, it was hypothesised that IL-6 trans-signalling may also control the expression of factors that influence neutrophil effector functions.

Studies outlined in this Chapter will examine how IL-6 signalling influences the effector characteristics of the infiltrating neutrophils during acute bacterial infection.

6.2. Materials and Methods

6.2.1. *In vivo* neutrophil effector function assay

To assess the activation and effector characteristics of infiltrating neutrophils, WT and *Il6*$^{-/-}$ mice were administered (i.p.) with Cell Trace Far Red (CT-FR; 8 µM) labelled *S. epidermidis* (5x10^{8} cfu/mice in 0.5 ml of sterile PBS) (see *Section 2.2.3* & *Section 2.3.3*). At designated time points, the peritoneal cavity was lavaged with 2 ml of RPMI 1640 containing 5 µM of aminophenyl fluorescein (APF; see *Section 2.3.5*). Neutrophil phagocytosis and respiratory burst activity were examined by flow cytometry and imaging flow cytometry (*Section 2.5.8*).

6.2.2. *Ex vivo* neutrophil effector function assay

Whole blood was collected by cardiac puncture (*Section 2.5.1*). Samples were diluted 1:10 and washed 3 times in ice cold PBS. Cells were resuspended in serum-free RPMI 1640 containing 5 µM of APF and incubated for 30 min at 37°C. APF-loaded cells were split into 100 µl aliquots and cultured at 37°C with an equal volume of pre-warmed, opsonized CT-FR-labelled *S. epidermidis* (*Section 2.2.3* & *Section 2.2.4)*. Cells were incubated for a set of pre-determined time (0-30 min) before transfer to an iced water bath. Treated cells were maintained on ice for all subsequent steps prior to analysis by means of flow cytometry (*Section 2.5.8*).

6.2.3. Imaging flow cytometry analysis of neutrophil effector function

Neutrophils were treated as specified in *Sections 6.2.1* & *6.2.2*. After surface marker staining for Ly6G (Table 2.2), cells were resuspended in 100 µl of sterile PBS, and events (>8000 events per sample) were acquired at a low imaging rate and 60X amplification using the Amnis ImageStream®X Mark II Imaging Flow Cytometer (Amnis). The imaging rate is the number of cells acquired per second. Image amplification of 60X and a low rate of imaging ensured a high resolution and sensitivity during cell acquisition.

Acquired events were gated according to Area and Aspect Ratio Intensity in Channel 1 to discriminate single cells using the ImageStream software IDEAS (Amnis). Single cells were then plotted against Gradient RMS (Root Mean Square of the rate of change of the image intensity profile – defines events on focus) in Channel 1 to select cells inside the plane of focus. Neutrophils were gated according to Ly6G staining, visualised in Channel 7. Here, Channel 7 was chosen to minimise emission spectra overlap with APF (Channel 2) and CT-FR-labelled *S. epidermidis* (Channel 11).

Phagocytic activity was expressed as a *Phagocytic Index*, which reflects the number of bacteria ingested per a $Ly6G^+$ neutrophil during the incubation period. To evaluate the phagocytic index of neutrophils undergoing phagocytosis, the Application "Spot Counting" in IDEAS was used. Spots were counted in Channel 11 based on the distribution of CT-FR bacterial staining. The efficiency of phagocytic uptake was quantified by examining cells displaying either a low (1-2 counts) or high number (3 counts or more) of ingested bacteria.

6.3. Results

6.3.1. Neutrophil gating

Flow cytometry or imaging flow cytometry were used to monitor the activity of both circulating and infiltrating neutrophils (Figure 6.1). Neutrophils were identified by conventional flow cytometry according to Ly6G antibody staining and *Side Scatter* (*SSC*) analysis following by doublet discrimination by *Forward Scatter* (*FSC*) *Linear* and *Forward Scatter Area* analysis. Debris was discriminated using *SSC* Area and *FSC* Area (Figure 6.2A). Neutrophils accounted for ~14% of the total circulating leukocytes, while neutrophils recruited to the peritoneal cavity reflected ~50% of the inflammatory infiltrate at 3 h post bacterial infection. An equivalent neutrophil gating strategy is shown using imaging flow cytometry (Figure 6.2B).

6.3.2. Optimisation of neutrophil effector function

The application of fluorescently labelled bacteria in combination with the peroxidase substrate APF provides an opportunity to simultaneously evaluate the phagocytic uptake of bacteria and respiratory burst activity in neutrophils.

To identify the optimal labelling protocol for tracking *S. epidermidis* in our *in vivo* and *ex vivo* model systems, bacteria were incubated with varying concentrations of CT-FR (see *Section 2.2.3*). For *ex vivo* studies, 1 µM provided the best dye concentration to distinguish CT-FR positive and negative populations (Figure 6.3A). This concentration was however raised to 8 µM for all *in vivo* studies (Figure 6.3B).

Studies next determined the optimal concentration of APF for detection of reactive oxygen species (e.g., OH^-, NO_3^- and ClO^-) by activated neutrophils. Based on the manufacturer's instructions (APF, Life Technologies) 5 µM of APF was deemed sufficient for both the *ex vivo* and *in vivo* experimental systems (Figure 6.3 C & D, respectively). Importantly, 8 µM CT-FR and 5 µM APF could be used in

combination to simultaneously track both neutrophil phagocytosis and respiratory burst activity using imaging flow cytometry (Figure 6.3E).

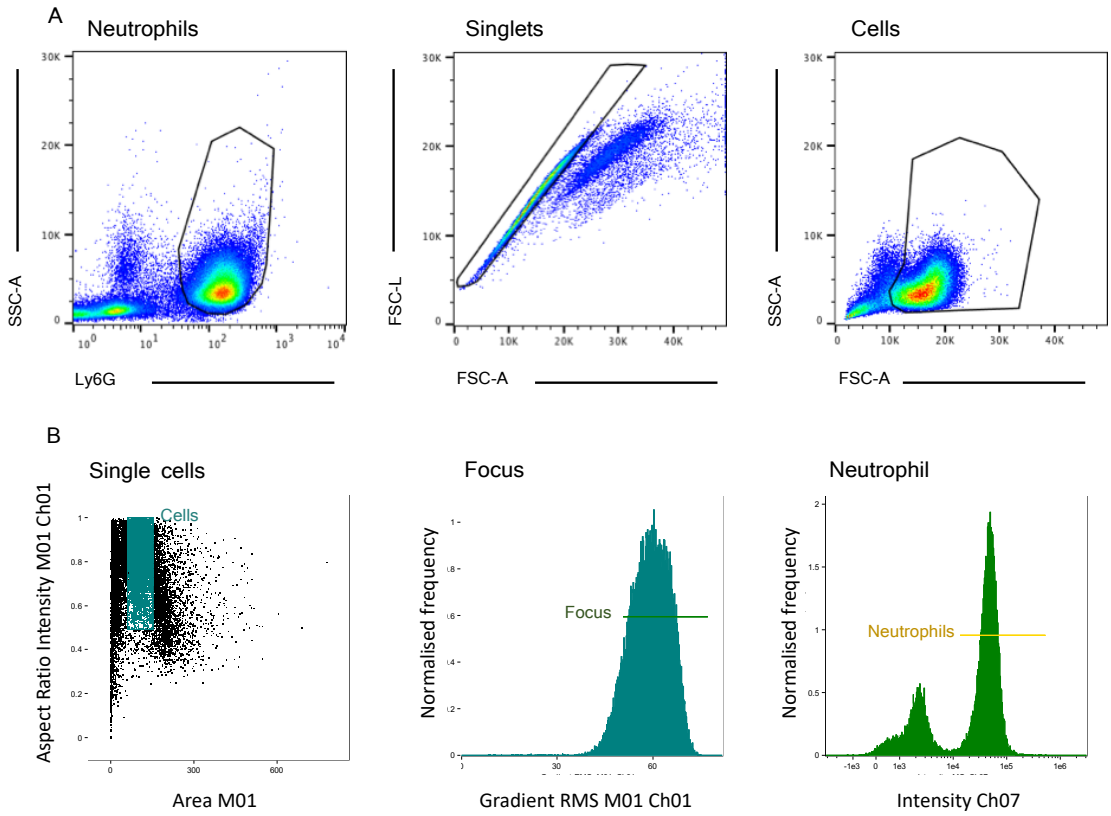

Figure 6.2. Gating strategy for neutrophil identification using flow cytometry (A) and ImageStream (B). A. Whole blood or peritoneal infiltrating leukocytes were collected by cardiac puncture or peritoneal lavage, and the neutrophil population assessed by flow cytometry using SSC, FSC and Ly6G membrane expression (**A**) or imaging flow cytometry using Area, Aspect Ratio Intensity and Gradient RMS in Channel 1 and fluorescence intensity in Channel 7 (**B**).

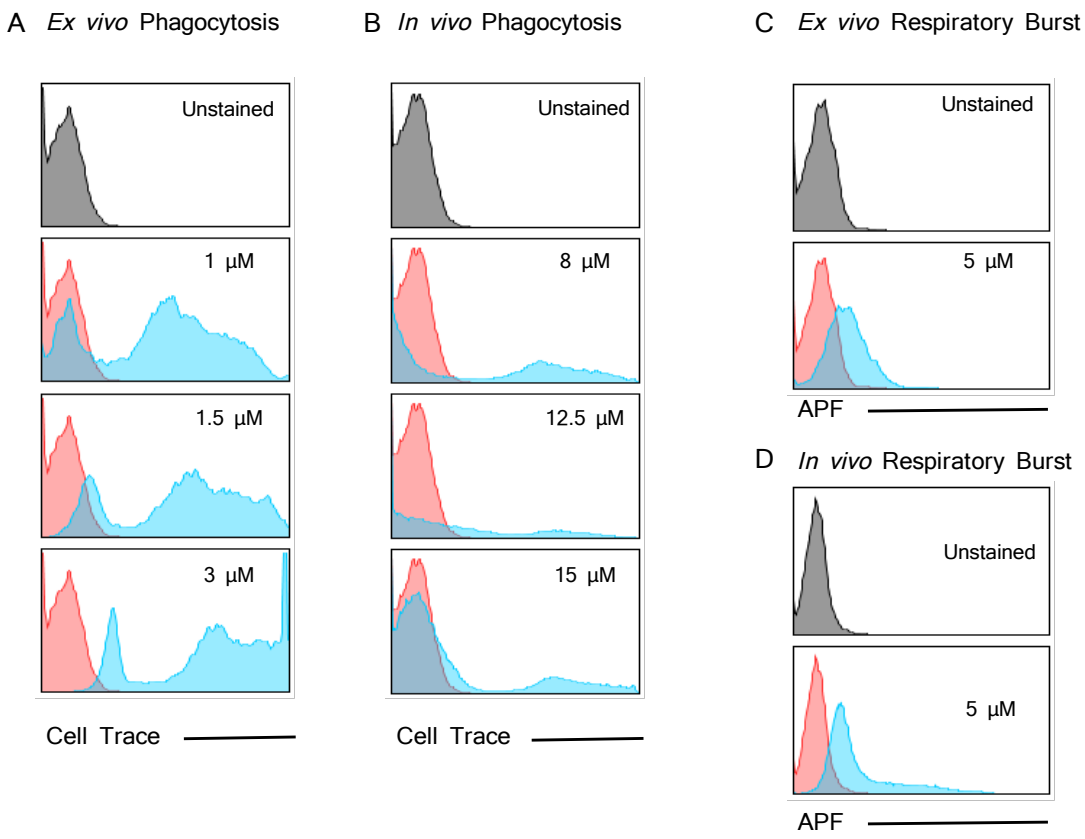
A Ex vivo Phagocytosis
Unstained
1 µM
1.5 µM
3 µM
Cell Trace
B In vivo Phagocytosis
Unstained
8 µM
12.5 µM
15 µM
Cell Trace
C Ex vivo Respiratory Burst
Unstained
5 µM
APF
D In vivo Respiratory Burst
Unstained
5 µM
APF

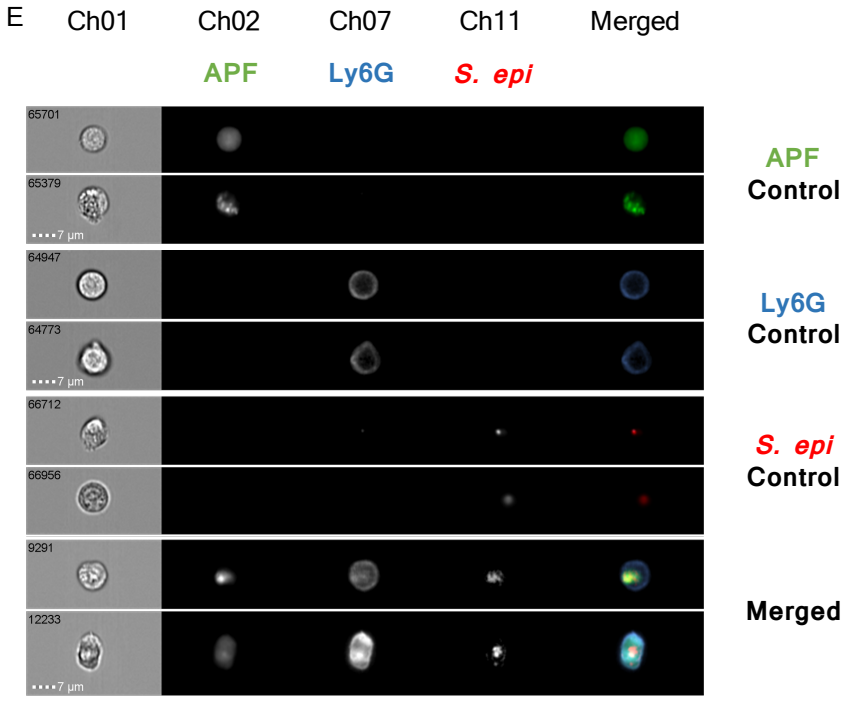
E
Ch01
Ch02
Ch07
Ch11
Merged
APF
Ly6G
S. epi
APF Control
Ly6G Control
S. epi Control
Merged

Figure 6.3. Optimisation of *S. epidermidis* Cell Trace Far Red Staining and APF load. A & C. Whole blood was collected by cardiac puncture and incubated with increased dye concentrations of CT-FR labelled *S. epidermidis* (**A**) or 5 µM of APF (**C**) for 30 min at 37°C prior to flow cytometry. **B, D & E.** Peritoneal inflammation was established with 0.5 ml of *S. epidermidis* labelled with increasing concentrations of CT-FR dye (**B**) and infiltrating neutrophils collected by peritoneal lavage with 2 ml of RPMI 1640 containing 5 µM of APF before analysis by flow cytometry analysis (**B & D**) or ImageStream (**E**).

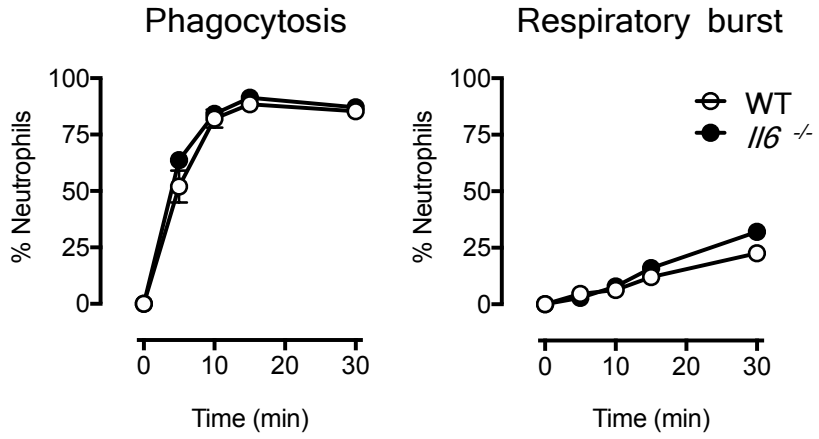

Figure 6.4. *Ex vivo* neutrophil effector function. Whole blood circulating neutrophils from WT and *Il6*$^{-/-}$ mice were incubated with 5 µM of APF (30 min, 37°C) prior to stimulation with opsonized, fluorescently-labelled *S. epidermidis* over a 30 min time course at 37°C. Flow cytometry allowed detection of neutrophils undergoing phagocytosis and respiratory burst. Graphs represent mean ± SEM of n = 2 mice per group.

6.3.3. Circulating neutrophils display a similar effector function in WT and *Il6*$^{-/-}$ mice

Using the parameters defined in *Section 6.3.2*, studies compared the effector characteristics of circulating neutrophils from WT and *Il6*$^{-/-}$ mice (Figure 6.4). Consistent with previous studies from the Jones laboratory [200], circulating neutrophils from WT and *Il6*$^{-/-}$ mice elicited comparable responses when evaluating phagocytosis and respiratory burst.

6.3.4. Infiltrating neutrophils elicit distinct effector function

Studies next compared the effector characteristics of infiltrating neutrophils from WT and *Il6*$^{-/-}$ mice during acute bacterial peritonitis. Mice were challenged (i.p) with fluorescent-labelled *S. epidermidis* ($5x10^8$ cfu/mice; see *Section 2.3.3*). An independent group of *Il6*$^{-/-}$ mice received a dose of *S. epidermidis* together with the IL-6-sIL-6R chimeric fusion protein HDS (50 ng/ml). Six hours after bacterial challenge, mice were sacrificed and the peritoneal cavity lavaged with 2 ml of RPMI 1640 containing 5 μM of APF. Phagocytosis and respiratory burst activity was monitored as described before (Figure 6.5). Infiltrating neutrophils from *Il6*$^{-/-}$ mice showed a defective neutrophil effector response when compared to WT control mice (Figure 6.5A). This defect was partially rescued through reconstitution of IL-6 trans signalling with HDS, and *Il6*$^{-/-}$ mice receiving both bacteria and HDS displayed a similar phagocytic response to WT (Figure 6.5A).

ImageStream also compared the morphology of infiltrating neutrophils from both genotypes and was used to quantify the number of bacteria actively engulfed by these cells (Figure 6.5B-D). Studies considered those neutrophils displaying a high phagocytic capacity. Neutrophils from *Il6*$^{-/-}$ mice displayed a reduced uptake of bacteria as compared to WT mice (Figure 6.5C & Figure 6.5D). Notably, this defect in bacterial uptake was restored by administration of HDS (Figure 6.5C & D).

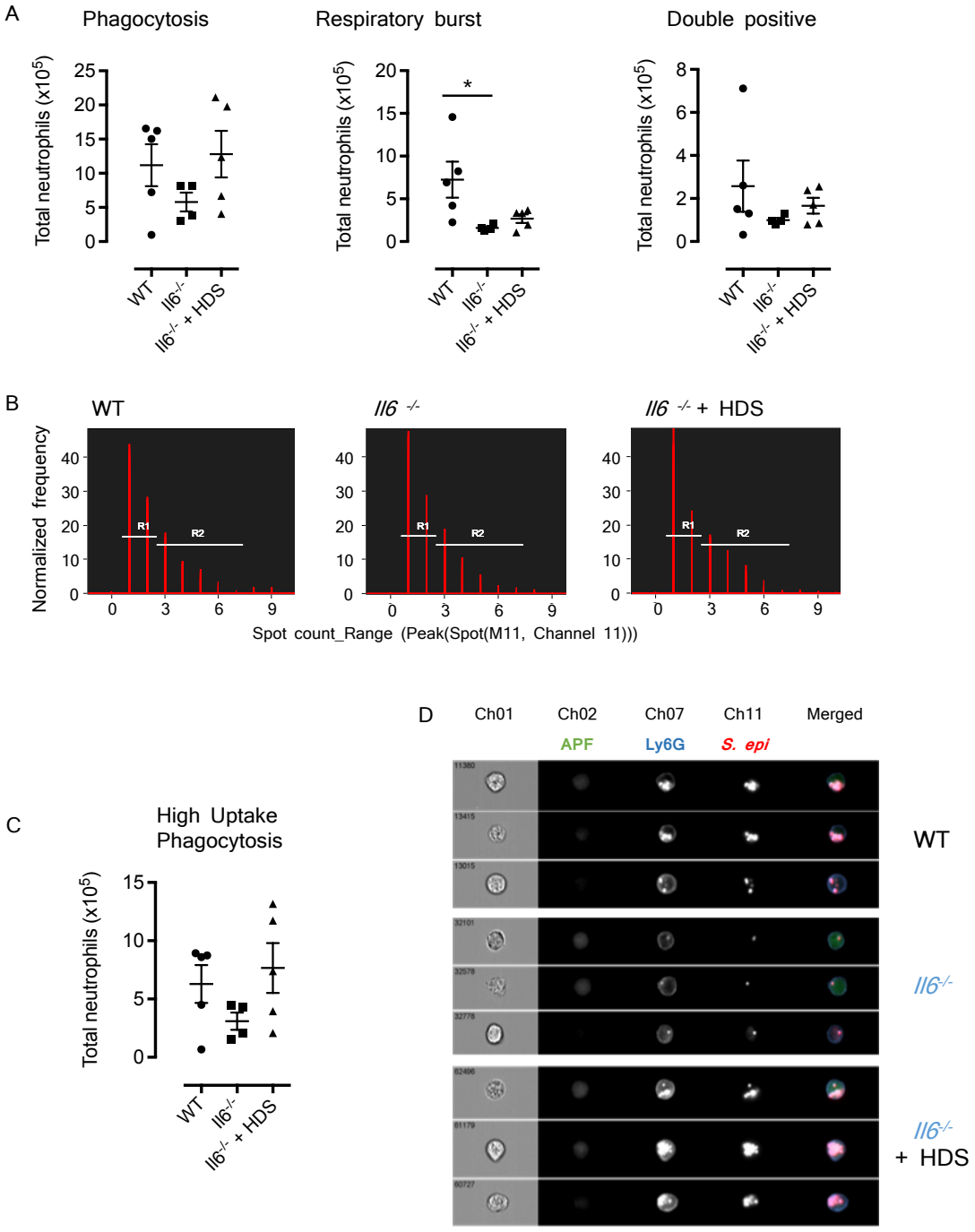

Figure 6.5. ***In vivo*** **neutrophil effector function.** WT and *Il6*$^{-/-}$ mice were challenged with fluorescently-labelled *S. epidermidis* (8 µM) and the lavage obtained with 2 ml of APF (5 µM) at 6 h after infection. **A.** Total number of neutrophils positive for phagocytosis, respiratory burst or both. **B.** Spot count assessment of the infiltrating neutrophils using ImageStream IDEAS software, where R1 and R2 refers to neutrophils with low and high bacterial uptake, respectively. **C.** Neutrophils with high bacterial uptake. **D.** Representative images in ImageStream. Statistical analysis was performed by one-way ANOVA with Bonferroni correction considering WT group as reference (**A** & **C**), *p<0.05.

6.3.5. Relationships between CD62L and IL-6R shedding and neutrophil effector function

The data presented in Figure 6.4 suggest that IL-6 activity regulates the functional characteristics or responsiveness of infiltrating neutrophils. To examine this in more detail studies monitored CD62L shedding as an index of neutrophil function following extravasation into the peritoneal cavity [20, 95, 280, 281]. Neutrophils were isolated at 3 and 6 h post infection of WT and *Il6*$^{-/-}$ mice (Figure 6.6). Circulating neutrophils were used as control (Figure 6.6). Neutrophils from both WT and *Il6*$^{-/-}$ mice showed a similar reduction in CD62L expression following entry into the peritoneal cavity (Figure 6.6). Thus, the reduced anti-microbial neutrophil functions seen under IL-6 deficiency appear to reflect an impaired neutrophil response to the local inflammatory environment rather than an intrinsic defect in their functional characteristics or response to chemotactic trafficking.

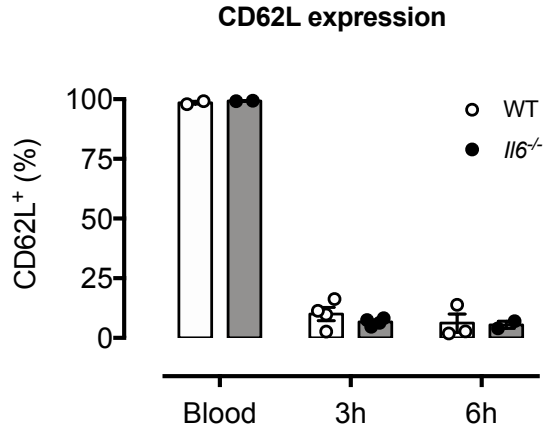

Figure 6.6. CD62L shedding. WT and *Il6*$^{-/-}$ mice were challenge with SES. After 3 and 6 h, infiltrating neutrophils were recovered by peritoneal lavage and the levels of CD62L assessed by flow cytometry. Circulating neutrophils were used as a positive control for CD62L expression.

6.4. Discussion

Studies investigated the effector characteristics of neutrophils in WT and *Il6*$^{-/-}$ mice during acute resolving bacterial peritonitis. Infiltrating neutrophils from *Il6*$^{-/-}$ mice showed a defective anti-microbial response at the site of infection, as illustrated by a reduction in bacterial phagocytosis and respiratory burst. Conversely, *ex vivo* stimulation of neutrophils from whole blood with *S. epidermidis* showed a similar effector activity of these cells between both genotypes. These data suggest that the local microenvironment contributes to the control of bacterial infection by neutrophils.

Previous studies illustrate that IL-6 does not directly activate neutrophil effector characteristics [278, 279]. Indeed, infiltrating neutrophils rapidly shed IL-6R from their surface following entry into inflamed tissues [200]. This sIL-6R release moderates IL-6 responsiveness and promotes IL-6 trans-signalling within the stromal compartment. We propose that this mechanism may orchestrate the release of other regulatory factors that help shape neutrophil activation. In line with this idea, previous studies in our laboratory have shown that the induction of bacterial peritonitis in *Il6*$^{-/-}$ mice receiving HDS resulted in improved bacterial clearance and reduced dissemination to the bloodstream. In the present study, reconstitution of IL-6 trans-signalling in *Il6*$^{-/-}$ mice with HDS was accompanied by a restoration of neutrophil phagocytosis. However, HDS administration did not restore respiratory burst. Circulating neutrophils are typically quiescent, which minimizes the release of ROS and proteolytic granules that would otherwise induce tissue damage [174]. Neutrophils therefore require prior activation or priming to be fully effective at the site of infection. This is usually a multistep process that is initiated during their extravasation from the blood to the inflamed tissue [174]. Data presented herein suggest that the cytokine control of phagocytosis and respiratory burst may require different signals. Previous studies are in close agreement with these findings. For example, Dewald and co-workers have reported that two independent signalling pathways are necessary for neutrophil activation and the subsequent respiratory burst response [282]. This is akin to the signalling differences observed in response to neutrophil-activating chemokines. For example, neutrophil degranulation and chemotaxis in response to IL-8/CXCL8

and GROα/CXCL1 are mediated by the chemokine receptors CXCR1 and CXCR2. In contrast, the activation of respiratory burst and associated phospholipase D activity is exclusive to CXCR1 [176]. Taken together, these studies support the idea that phagocytosis and respiratory burst responses are primed by two independent mechanisms. While phagocytosis is directly mediated by IL-6 trans-signalling, it is proposed that additional signals, (e.g., PGD_2 signalling) are needed to fully promote respiratory burst [200]. Interestingly, these priming mechanisms are independent to CD62L or IL-6R shedding, which is a hallmark of actively recruited neutrophils [20, 95, 280, 281].

Neutrophil phagocytosis and respiratory burst were monitored by flow cytometry and imaging flow cytometry. Respiratory burst was examined using APF. While APF provides a specific measurement of the reactive oxygen species OH^-, NO_3^- and ClO^-, it does not account for the production of other radicals such as H_2O_2 or NO. Therefore, these limitations should be taken into consideration. In this regard, the use of better fluorescent dyes or novel nanoprobes could be used to improve specificity and sensitivity for ROS detection [283].

The advantages of imaging flow cytometry over conventional flow cytometry consist in integrating two components: the spatial resolution provided by fluorescence microscopy with the quantitative analysis of flow cytometry [284]. In this case, imaging flow cytometry allowed evaluation of the co-localisation of the bacterial uptake and the subsequent respiratory burst within the phagosome. Imaging flow cytometry also allowed for the quantification of internalised particles. Here, the enhanced phagocytosis detected in WT neutrophils and *Il6*$^{-/-}$ neutrophils receiving HDS was the consequence of a substantial increase in bacterial uptake. It is proposed that the elevated phagocytic index facilitates bacterial clearance at the site of infection, preventing their dissemination to the circulation and therefore ensuring a successful host defence [102].

Chapter 7. *Il6st* gene splicing generates a soluble gp130 in mice

7.1. Introduction

The signalling complex for IL-6 comprises two receptor subunits: the non-signalling α-receptor (CD126, IL-6Rα, encoded by the *Il6ra* gene) and the signal transducing β-receptor glycoprotein 130 kDa (CD130, gp130, encoded by *Il6st*) [48]. Interleukin-6 binds both a membrane-associated and soluble form of the IL-6R (sIL-6R). These interactions afford IL-6 with the capacity to signal through two distinct mechanisms, termed classical IL-6R signalling and IL-6 trans-signalling [41, 48]. Both mechanisms rely on the membrane bound signal-transducing gp130 to transmit the IL-6 signal in target cells. While gp130 is ubiquitously expressed, IL-6R is restricted to hepatocytes, leukocytes, megakaryocytes and some specialised stromal cells [41]. These cells respond directly to IL-6 through classical IL-6R signalling. Conversely, cells that express gp130 remain responsive to IL-6 once IL-6 is bound to sIL-6R. Interleukin-6 trans-signalling is tightly regulated and is blocked by soluble forms of gp130 (sgp130) [78, 80]. Indeed, an engineered Fc-dimerized variant of sgp130 (sgp130-Fc) provides protection in several inflammatory diseases and cancer [81-83]. This modality is currently in clinical development under the drug name olamkicept [112].

To date, four variant forms of sgp130 with apparent molecular weights of 50, 75, 90 and 110 kDa have been detected in humans [285-288]. Although their mechanism of generation is still under investigation, studies suggest they are derived from alternative processing of the *Il6st* transcript. Limited proteolysis of the membrane bound gp130 may also contribute to the generation of sgp130, but this process only accounts for a minimal proportion of sgp130 [78, 79]. While a murine equivalent of sgp130 has been identified [289], the mechanism of generation of this sgp130 has not been defined.

The murine *Il6st* has 10 different annotated transcripts predicted by the Ensembl project [290] (Figure 7.1). Of them, only 2 transcripts (*Il6st*-203 and *Il6st*-206) have been annotated with a Transcript Level of Support of 1 (TSL1) [225] – a method to assess whether a given transcript is supported by primary data (mRNA and Expressed Sequence Tag) from the Ensembl and UCSC projects [225]. All other transcripts have been annotated with a TSL of 5 (TSL5), which means that no single mRNA transcript has been found to support the model structure, and

therefore their annotation should be considered speculative [225]. Importantly, only the transcript *Il6st*-203 (derived by RefSeq) has been demonstrated to encode for the membrane-bound murine gp130.

The human and murine *Il6st* share 86% and 77% homology at the genetic and protein level, respectively. Given the degree of homology between both genes, and the presence of several forms of sgp130 in human, it is proposed that similar sgp130 variants should co-exist in mice. This Chapter aims to investigate potential forms of sgp130 in mice using the RNA-seq data described in Chapter 3. Specifically, studies aim to:

a. Identify a soluble form of gp130 in mice.
b. Annotate a new transcript encoding for a viable form of sgp130 in mice.
c. Purify and characterize a murine form of sgp130.

7.2. Materials and methods

7.2.1. Differential exon usage analysis and *de novo* transcript assembly

The Ion Torrent System provides an opportunity to investigate high-throughput sequencing data from relatively long sequencing reads. This includes the analysis of exon boundaries and predictions of alternative mRNA splicing variants. The Bioconductor package DEXSeq [291] was used to generate a statistical evaluation of differential exon usage within the RNA-seq datasets.

Reads mapping to the *Il6st* gene were used to construct *de novo* transcripts from these region using the computational software Cufflinks [292].

7.2.2. Affinity purification of sgp130

Soluble gp130 was purified from WT peritoneal lavage samples using the GlycoLink Micro Immobilization Kit affinity columns (Thermo Fisher Scientific) as described by manufacturer's instructions. Briefly, a hydrazide-linked resin was used to prepare affinity columns conjugated a with polyclonal goat anti-mouse gp130 antibody (500 µg/column; AF468; R&D Systems). Peritoneal lavage samples (300 µl) were loaded onto the affinity column and incubated overnight at 4°C with agitation. After incubation, columns were centrifuged at 10000xg for 1 min to collect the flow-through fraction. The loading step was repeated 2 times with fresh sample to a total of 3 rounds of overnight incubation. Proteins attached to the columns were eluted with 200 µl of eluting buffer (0.1M glycine, pH 2.5). Eluted samples were equilibrated with 10 µl of Tris-HCl (1M, pH 9.0) and stored at -80°C in the presence of protease inhibitors (Promega).

7.2.3. Protein SDS-PAGE electrophoresis and detection using silver staining

Proteins were detected by silver staining following electrophoretic separation by SDS-PAGE. Briefly, samples were diluted in 4x protein sample buffer under reducing conditions (40% w:v glycerol, 240 mM Tris-HCl pH 6.8, 8% w:v SDS, 0.04% v:v bromophenol blue, 5% v:v β-mercapto-ethanol) and incubated for 5 min at 95°C to denature proteins prior to SDS-PAGE. Denatured samples were loaded onto a precast 12% (w:v) polyacrylamide gel (Bio-Rad). Electrophoretic separation was performed at 100 V in electrophoresis running buffer containing 25 mM Tris, 192 mM Glycine, 0.1% SDS (w:v) (pH 8.3) using a Mini-PROTEAN Electrophoresis Cells System (Bio-Rad).

After separation, proteins were detected by silver staining using the ProteoSilver™ Silver Stain Kit (Sigma) as per manufacturer's instructions. All steps were conducted at room temperature on an orbital shaker with agitation of 60 rpm. Gels were fixed overnight in 100 ml 50% (v:v) ethanol and 10% (v:v) acetic acid diluted in deionised water. After fixation, gels were washed in 100 ml of 30% (v:v) ethanol and 200 ml of deionized water for 10 min each prior sensitization (10 min) with 100 ml of sensitizer solution. Sensitized gels were washed twice with 200 ml of deionised water (10 min each) and equilibrated with 100 ml of silver solution (10 min). Gels were then washed with 200 ml of deionised water for 1 min prior to development with 100 ml of developer solution. Due to the low yield of sgp130 purified, gels were developed for 8-10 min. After development, 5 ml of ProteoSilver stop solution were added to the gels for 5 min. Gels were visualized using the Fluor-S Multi-imager (Bio-Rad).

7.2.4. Western blotting

Proteins separated by SDS-PAGE (*Section 7.2.3*) were transferred onto polyvinylidene difluoride (PVDF) membranes (Bio-Rad) by semidry electro-blotting (60 V for 1 h 30 min). Transfer buffer contained 25 mM Tris, 192 mM glycine, 10% (v:v) methanol. Membranes were blocked in a solution of Tris-buffered saline (TBS; 10 mM Tris-HCl, pH 7.6 and 150 mM NaCl) supplemented with 0.1% (v:v) Tween 20 (termed TBST) and 5% (w:v) skimmed milk powder

for 1 h, prior to overnight incubation with polyclonal goat anti-mouse gp130 antibody (0.2 µg/ml; AF468; R&D Systems). This was followed by a 1 h incubation at room temperature with horseradish peroxidase-conjugated secondary antibody (polyclonal rabbit anti-goat; 1:2000 dilution; DAKO) in TBST with 5% BSA. Proteins were detected using the chemiluminescent kit SignalFire™ ECL Reagents (Cell Signalling Technology) with the Amersham Hyperfilm ECL (GE Healthcare LS).

7.3. Results

7.3.1. Differential exon usage identifies alternative splicing of *Il6st* gene

Experiments determined the expression of IL-6 receptor components in RNA-seq datasets from the peritoneal membrane of SES challenged mice. Data was derived from both mice treated with SES alone or in combination with adoptively transferred Th1 cells. Differential exon usage (DEXSeq package, Bioconductor, *Section 7.2.1*) identified a spliced variant of *Il6st* (encoding for gp130) in all datasets. Comparison of datasets from WT and *Il6*$^{-/-}$ mice showed the alternate *Il6st* transcript to be differentially expressed at 6 h post SES challenge (Figure 7.1). This difference was however lost following the adoptive transfer of Th1 cells. No differences in *Il6ra* (encoding the cognate IL-6Rα) were observed in any condition.

7.3.2. Prediction of alternative splicing of *Il6st* in the peritoneal membrane correlates with increased sgp130 in the peritoneal cavity

To investigate whether the splicing of *Il6st* in the peritoneum accounted for the presence of sgp130 in the peritoneal cavity, WT and *Il6*$^{-/-}$ mice were challenged (i.p.) with either SES alone or in combination with Th1 cells (*Sections 2.3.2* & *2.3.4*, respectively). Peritoneal lavage samples were collected at 3 and 6 h post injection. Soluble gp130 and sIL-6R were quantified using ELISA (R&D Systems, *Section 2.5.8*) (Figure 7.2). Peritoneal sgp130 was detected in both SES challenged WT and *Il6*$^{-/-}$ mice (Figure 7.2A). Consistent with the DEXSeq prediction shown in Figure 7.1, peritoneal sgp130 levels were significantly higher in WT mice at 6 h post SES challenge (Figure 7.2). Transfer of Th1 cells enhanced the detection of peritoneal sgp130 in SES challenged mice (Figure 7.2B). Interestingly, sgp130 levels correlated with the detection of peritoneal sIL-6R lavage samples (Figure 7.2C). Thus, this data illustrates a close association between the control of positive and negative regulators of IL-6 trans-signalling.

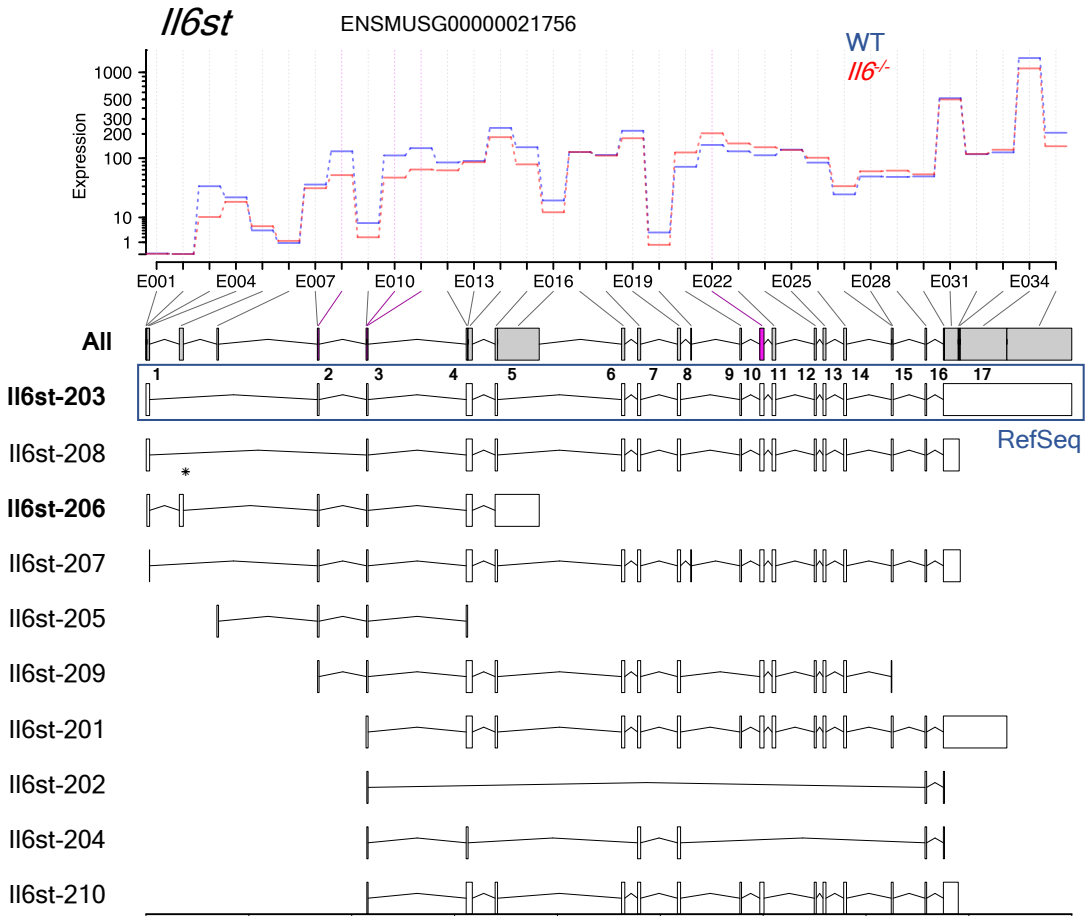

Figure 7.1. Differential exon usage analysis. Alternative splicing (DEXSeq package, Bioconductor, $p<0.01$) was assessed in RNA-seq data sets from the peritoneal membrane of WT and *Il6*$^{-/-}$ mice at 6 h post SES stimulation. Pink corresponds to predicted significant alternative exon usage.

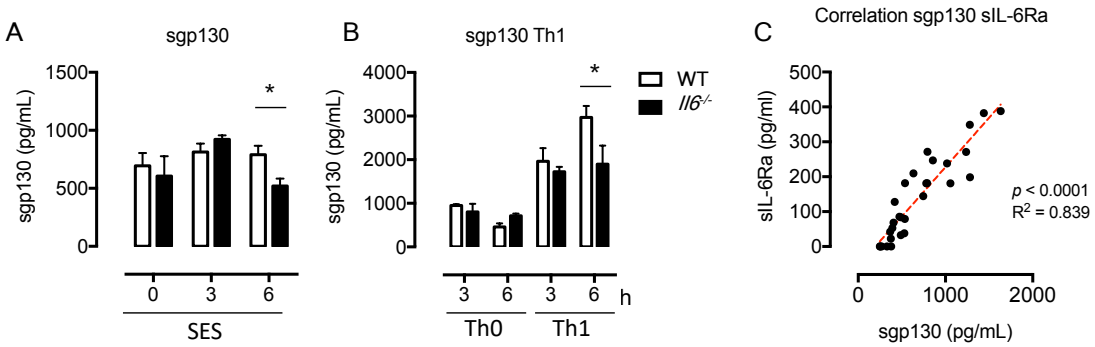

Figure 7.2. Detection of sgp130 in the peritoneal cavity. A & B. Levels of sgp30 in peritoneal lavage of mice receiving SES (**A**; n = 4 mice per group) or Th1+ SES (**B**; n = 3 mice per group). **C.** Correlation between the levels of sgp130 and sIL-6Rα in mice receiving SES alone. Statistical analysis was performed by two-way ANOVA with Bonferroni correction for multiple comparisons (**A** & **B**). *$p<0.05$

7.3.3. Identification of a novel transcript for sgp130

Studies next explored the annotated transcripts for *Il6st* based on the *Ensemble* annotation database [290] (Figure 7.3). The *Il6st* gene has 10 transcripts (outlined in Figure 7.1). However, only two of these have been identified with a TSL1 definition [225]. Transcripts annotated with a TSL5 were considered speculative, and therefore discarded from further analysis.

The transcript *Il6st*-203 encodes a protein of 917 amino acids that encodes the canonical membrane-bound gp130 (Figure 7.3). *Il6st*-203 remains the only murine gp130 transcript that has been functionally characterised *in vivo* [293]. The shorter *Il6st*-206 transcript encodes a protein of 164 amino acids (Figure 7.3B). Sequence analysis of the *Il6st*-206 variant suggested that the expression of this transcript would generate a protein lacking the type-I cytokine receptor-binding determinant – the WSXSW amino acid motif [294, 295]. Thus, if the *Il6st*-206 variant were expressed *in vivo* it would generate a functionally inactive form of sgp130.

To evaluate the expression of alternative transcripts for the *Il6st* gene, *de novo* transcript assembly was performed using Cufflinks [292]. Samples obtained from WT and *Il6*$^{-/-}$ mice at 6 h after SES challenge were used for this analysis. *De novo* transcript assembly identified a novel *Il6st* transcript that is predicted to contain two additional exons as compared to *Il6st*-206 (termed *Il6st*-SES; Figure 7.3A). This new form retains the correct reading frame of the reference sequence and predicts a stop codon just after the end of exon 7. Sequence analysis of the new transcript predicted a protein of 271 amino acids (Figure 7.3B). Although longer, this variant would also lack the WSXSW motif.

To establish whether other cell populations within the peritoneal cavity could generate sgp130, studies examined the contribution of tissue resident and infiltrating mononuclear cells. In collaboration with Professor Philip R. Taylor (Division of Infection & Immunity, The School of Medicine, Cardiff University), RNA-seq datasets were obtained for peritoneal resident macrophages isolated from zymosan treated mice (Figure 7.4). Cufflinks assembly identified a new transcript for the *Il6st* gene, which included exon 10 (Figure 7.4A). The identity of this transcript was also verified using the DEXSeq prediction (Figure 7.1).

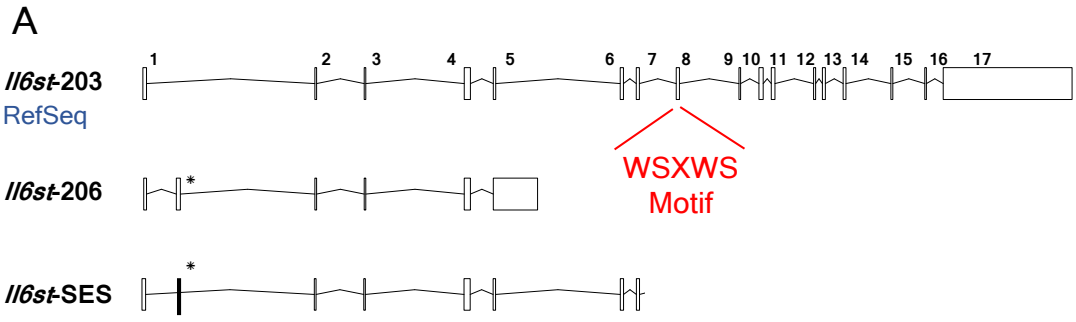

B

Il6st-203 - aa sequence (917aa)

MSAPRIWLAQALLFFLTTESIGQLLEPCGY
IYPEFPVVQRGSNFTAICVLKEACLQHYYV
NASYIVWKTNHAAVPREQVTVINRTTSSVT
FTDVVLPSVQLTCNILSFGQIEQNVYGVTM
LSGFPPDKPTNLTCIVNEGKNMLCQWDPGR
ETYLETNYTLKSEWATEKFPDCQSKHGTSC
MVSYMPTYYVNIEVWVEAENALGKVSSESI
NFDPVDKVKPTPPYNLSVTNSEELSSILKL
SWVSSGLGGLLDLKSDIQYRTKDASTWIQV
PLEDTMSPRTSFTVQDLKPFTEYVFRIRSI
KDSGKGY**WSDWS**EEASGTTYEDRPSRPPSF
WYKTNPSHGQEYRSVRLIWKALPLSEANGK
ILDYEVILTQSKSVSQTYTVTGTELTVNLT
NDRYVASLAARNKVGKSAAAVLTIPSPHVT
AAYSVVNLKAFPKDNLLWVEWTPPPKPVSK
YILEWCVLSENAPCVEDWQQEDATVNRTHL
RGRLLESKCYQITVTPVFATGPGGSESLKA
YLKQAAPARGPTVRTKKVGKNEAVLAWDQI
PVDDQNGFIRNYSISYRTSVGKEMVVHVDS
SHTEYTLSSLSSDTLYMVRMAAYTDEGGKD
GPEFTFTTPKFAQGEIE**AIVVPVCLAFLLT**
TLLGVLFCFNKRDLIKKHIWPNVPDPSKSH
IAQWSPHTPPRHNFNSKDQMYSDGNFTDVS
VVEIEANNKKPCPDDLKSVDLFKKEKVSTE
GHSSGIGGSSCMSSSRPSISSNEENESAQS
TASTVQYSTVVHSGYRHQVPSVQVFSRSES
TQPLLDSEERPEDLQLVDSVDGGDEILPRQ
PYFKQNCSQPEACPEISHFERSNQVLSGNE
EDFVRLKQQQVSDHISQPYGSEQRRLFQEG
STADALGTGADGQMERFESVGMETTIDEEI
PKSYLPQTVRQGGYMPQ

Il6st-206 - aa sequence (164)

MSAPRIWLAQALLFFLTTESIGQLLEPCGY
IYPEFPVVQRGSNFTAICVLKEACLQHYYV
NASYIVWKTNHAAVPREQVTVINRTTSSVT
FTDVVLPSVQLTCNILSFGQIEQNVYGVTM
LSGFPPDKPTNLTCIVNEGKNMLCQWDPGR
ETYLETNYTLKSE**W**

Il6st-SES - aa sequence (271)

MSAPRIWLAQALLFFLTTESIGQLLEPCGY
IYPEFPVVQRGSNFTAICVLKEACLQHYYV
NASYIVWKTNHAAVPREQVTVINRTTSSVT
FTDVVLPSVQLTCNILSFGQIEQNVYGVTM
LSGFPPDKPTNLTCIVNEGKNMLCQWDPGR
ETYLETNYTLKSEWATEKFPDCQSKHGTSC
MVSYMPTYYVNIEVWVEAENALGKVSSESI
NFDPVDKVKPTPPYNLSVTNSEELSSILKL
SWVSSGLGGLLDLKSDIQYRTKDAST**WIQV**
N

Figure 7.3. Sequence analysis of *Il6st* transcripts. A. Schematic representation of the transcripts *Il6st*-203 (membrane bound gp130, RefSeq), *Il6st*-206, and computationally predicted novel transcript (termed *Il6st*-SES). **B.** Amino acid sequence for the transcripts *Il6st*-203, *Il6st*-206 and *Il6st*-SES.

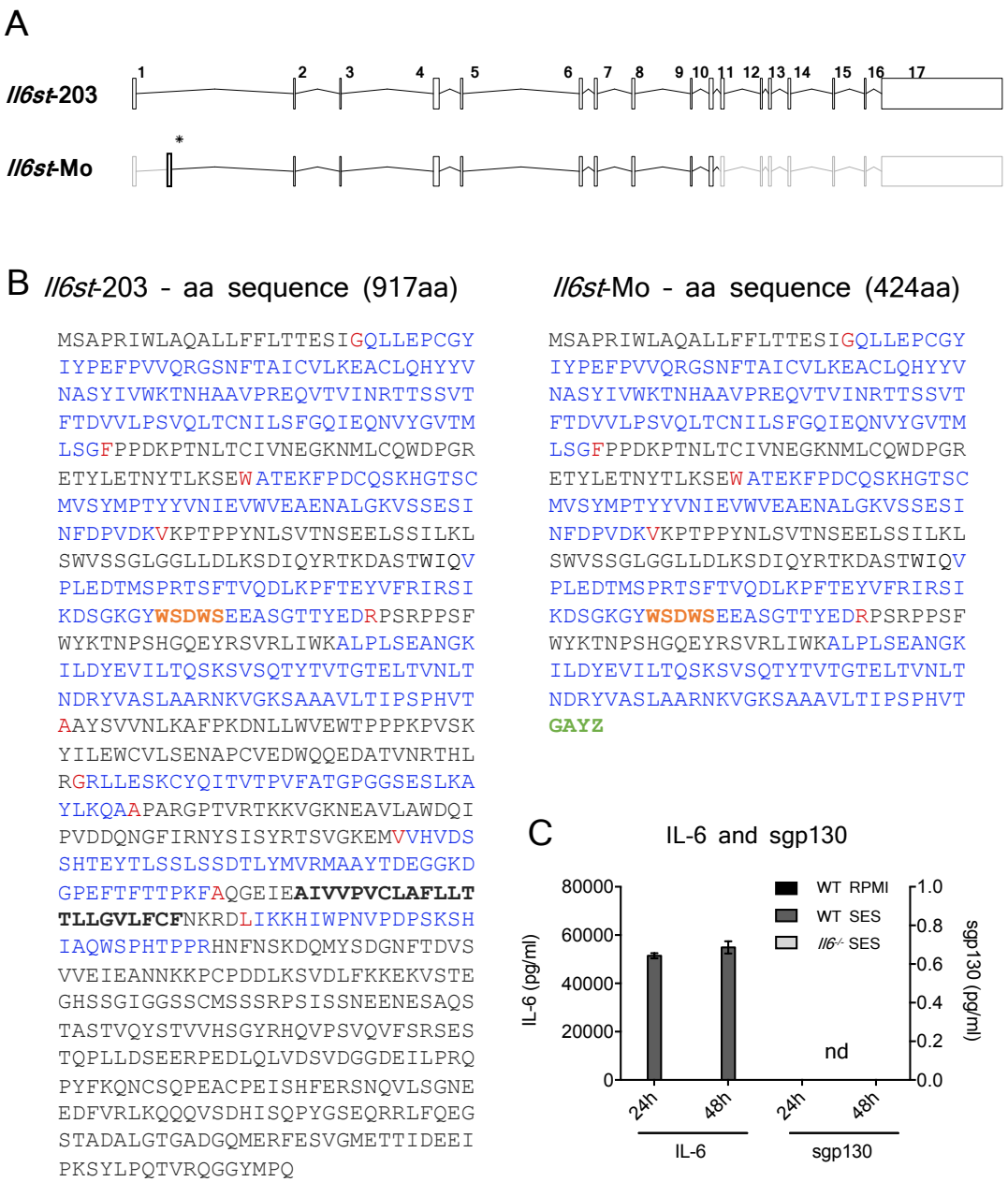

Figure 7.4. *De novo* assembly of *Il6st* gene transcripts. A. RNA-seq data derived from resident peritoneal macrophages isolated from zymosan treated mice were subjected to *de novo* transcript assembly. **B.** Amino acid sequence analysis of the potential novel transcript when compared with the reference sequence. **C.** Quantification of IL-6 and sgp130 in the culture supernatant of SES-stimulated resident peritoneal monocytic cells by ELISA (n = 2 mice). nd, not detected.

Translation of this gene sequence predicted a protein of 424 amino acids, which includes the WSXSW motif (Figure 7.4B). However, analysis of conditioned media from *ex vivo* SES stimulated resident peritoneal monocytic cells (*Section 2.4.2*) could not detect the secretion of this protein (Figure 7.4C).

7.3.4. Purification of sgp130 from peritoneal lavage

Experiments next aimed to purify sgp130 from the peritoneal cavity by affinity chromatography. Peritoneal lavage samples from WT mice at 3 h after SES stimulation were used. The purity and identity of the putative sgp130 isolated was verified by silver staining of PAGE-SDS gels (Figure 7.5A). The eluted monomeric protein had a predicted molecular mass of approximately 97 kDa (Figure 7.5A). However, the identity of this protein could not be confirmed by Western blot using the same polyclonal anti-gp130 antibody utilised during the purification (Figure 7.5B). Here, protein standards for sIL-6R and sgp130 were used as negative and positive control, (Table 2.3). It is proposed that the low yield of the purification, together with the low specificity of the polyclonal anti-gp130, made detection of sgp130 challenging.

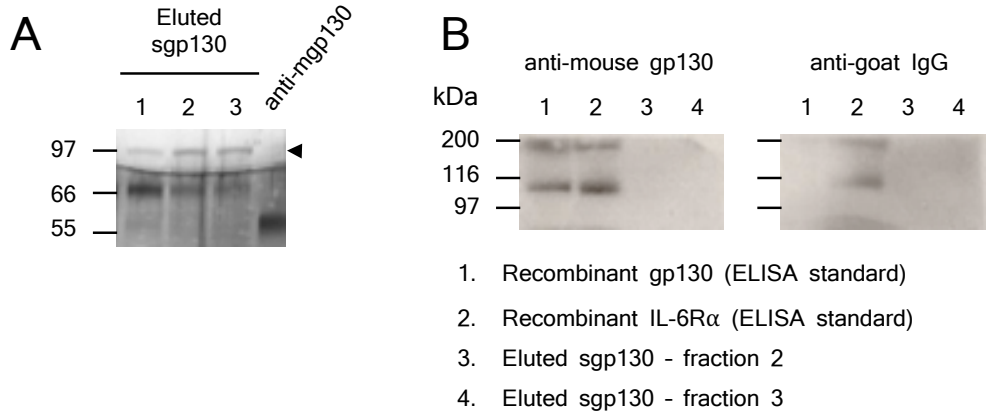

Figure 7.5. Purification of sgp130. A. Sgp130 was purified by column affinity, and eluted fractions (1, 2 and 3) loaded in an SDS-PAGE gel prior protein detection by silver staining. Goat anti-mouse gp130 antibody was used as a control. **B.** Western blot of sgp130 eluted fractions (lane 3: eluted fraction 2; lane 4: eluted fraction 3) using anti-mouse gp130 (left) or anti-goat IgG (right) as primary probes. Recombinant sgp130 obtained from the standard of gp130 ELISA (R&D; lane 1) and recombinant IL-6Rα obtained from the standard of IL-6R ELISA (R&D; lane 2) were used as positive and negative controls, respectively.

7.4. Discussion

Glycoprotein 130 is the common signal transducing receptor for all IL-6-related cytokines [48]. Several forms of soluble gp130 have been identified in humans that are generated through alternative splicing of the *Il6st* gene [285-288]. All forms retain a capacity to block IL-6 trans-signalling *in vivo* [78, 80]. Importantly, studies have shown that an engineered Fc-dimerized variant of sgp130 (sgp130-Fc) provides protection in several experimental models of inflammation and cancer [81-83]. In mice, a murine equivalent of human sgp130 has been previously identified [289]. However, the mechanisms of generating sgp130 in mice remain unclear.

De novo assembly was used to identify potential new transcripts for the *Il6st* gene in mice. This analysis relies on the combination of high quality sequencing data and complex computer algorithms to produce the most accurate assembly [227]. In the present study, *de novo* assembly was performed using next generation sequencing reads from two different platforms. RNA obtained from peritoneum samples after SES stimulation (Chapter 3) were sequenced using the Ion Torrent System (Life Technologies). This technology produces relatively long, singled-end (SE) reads. In contrast, data from peritoneal resident macrophages was obtained with the Illumina platform, which generates short paired-end sequencing reads (Table 7.2) [296-298]. In this regard, neither the Illumina nor the Ion Proton Systems provided optimal data for *de novo* transcript assembly. While the longer sequencing reads generated with the Ion Torrent System allows improved mapping of differential transcripts, the relative low depth of coverage and SE reads obtained in this experiment made the computational analysis for *de novo* discovery challenging. Conversely, data from zymosan-stimulated peritoneal resident macrophages, albeit produced with higher coverage and PE reads, was only available from a single experimental sample. Here, the putative transcript identified in datasets derived from peritoneal macrophages was predicted to extend through exon 10. Recently, Garbers et *al*. identified a human sg130 variant (termed sgp130-E10) that terminates in exon 10 as a consequence of alternative polyadenylation [288]. However, mice lack an alternative polyadenylation site in intron 10 [288]. In addition, culture of peritoneal resident cells with SES did not produce a

detectable form of sgp130 in the culture supernatants. In conclusion, while the data generated is interesting and will be investigated further, based on current analyses only speculative conclusions can be drawn.

Table 7.1. Characteristics of the sequencing platforms relative to *de novo* assembly

	Ion Torrent	Illumina
End sequencing	Singled-End	Paired-End
Read length	120 bp	50-75 bp
Replicates	3	1

Although the identification of a sgp130 variant in mice has been elusive at the transcript level, a putative form of sgp130 could be isolated from the peritoneal lavage of WT mice stimulated with SES, with or without Th1 cell co-transfer. The eluted putative protein had an approximate molecular mass of 97 kDa, which resembles to the only form of murine sgp130 previously described in the literature [289]. In addition, a sgp130 of similar molecular mass has been identified in human serum [285].

The purification of sgp130 encountered several challenges. First, purification required several rounds of incubation between the sample and the resin-linked polyclonal anti-mouse gp130 antibody to obtain a sufficient yield that could be detected by silver staining. Second, the eluting conditions had to rely on a lower pH than that recommended in the manufacturers' instructions (GlycoLink Micro Immobilization Kit affinity columns; Thermo Fisher Scientific). This led to partial damage of the conjugated antibody, and was identified in the sgp130 elute fractions (Figure 7.5A). Finally, the detection of sgp130 by silver staining relied on fixation in 50% ethanol and 10% acetic acid overnight in order to minimize the

background due to the long exposure time during detection. Unfortunately, western blotting was unable to detect sgp130 due to antibody affinity or cross-reactivity with other proteins.

In conclusion, while a soluble form of gp130 has long been identified in mice [289], the mechanism by which it is produced remains to be elucidated. In the context of peritoneal inflammation, we proposed that alternative splicing in the *Il6st* gene occurring in the peritoneal membrane might account for the sgp130 detected in peritoneal lavage. However, further studies are needed to determine the precise sequence of the transcript that encodes this form of sgp130, as well as to determine whether other forms of sgp130 are generated in mice.

Chapter 8. General Discussion

8.1. Introduction

Research conducted in this thesis aimed to evaluate how inflammatory responses elicited with the peritoneal membrane contribute to the control of competent host-defence, and inflammation-induced tissue damage. Combining RNA-seq analysis and bioinformatic pathway analysis, studies explored the interplay between stromal tissue and infiltrating leukocytes in an acute model of resolving inflammation. These investigations contributed to some new and exciting findings relevant to the biological activity of IL-6 in infection.

8.2. Relative activities of STAT1 and STAT3 ultimately define the transcriptional profile of the peritoneal membrane during inflammation

The transcriptome is a complex "dynamic entity" that is constantly being modified and adjusted to deliver specific responses that shape the outcome of inflammation. Understanding these dynamics requires a systematic evaluation of these broad changes [299, 300]. The novelty of this thesis, thus, resides in the use of a holistic approach to investigate the course of inflammation and the mechanisms that determine an effective immune response.

Studies focused on the changes that occur in the peritoneum during acute resolving inflammation, and in a setting that promotes a more pro-fibrotic outcome. In our model of peritoneal inflammation, both situations rely on IL-6 and IFN-γ signalling through the Jak-STAT pathway, and a selective activation of the latent transcription factors STAT1 and STAT3 [21, 33, 95, 243]. Increased evidence over the last decade has shown that the ultimate transcriptional output associated to these transcription factors depends on the fine balance between their relative activities [301, 302]. They frequently oppose each other. For example, STAT1 and STAT3 depict opposing roles in IL-21 signalling in $CD4^+$ T cells [303]. Similarly, genetic mutations that limit the activity of one of these transcription factors is often associated with increased activity of the other [90, 264, 304, 305]. This is especially relevant in situations where cytokines that signal through STAT1

and STAT3 dictate opposite outcomes. For example, STAT3 and STAT1 have contrary roles in regulating survival, proliferation, motility and immune tolerance, and their cross-regulation affects tumor expansion, survival and metastasis [301, 306]. During peritonitis, our data shows that pro-fibrotic Th1-driven STAT1 activity in the membrane triggers a more robust and sustained response than that observed during acute inflammation, where STAT3 activity was predominant in WT mice (Figure 8.1). Current studies in our laboratory are in line with these findings. Here, preliminary data from chromatin immuno-precipitation and next-generation sequencing (ChIP-seq) of peritoneal samples after inflammation show an increase in the number of peaks controlled by STAT1 as compared to STAT3-associated peaks (Dr David Millrine, unpublished observations). Conversely, studies assessing the impact of IL-6 or IL-27 signalling in T cells have shown that STAT3 contributes to the overall transcription output associated with both cytokines, whereas STAT1 is responsible for specificity [302]. These findings illustrate that the activities of STAT1 and STAT3 are closely aligned, and that the transcriptional output delivered by IL-6 and IL-27 illustrates the context-dependent nature of the cytokine receptor signal.

A major challenge posed by this thesis was to investigate how temporal changes in the transcriptome determine competent host defence, and the potential transition to inflammation associated tissue damage and fibrosis. Here, statistical analysis of the datasets proposed that changes in the peritoneal transcriptome are organised in three distinct and very defined patterns of gene expression. The importance of such approach resides in the idea that genes that are expressed together share common functions [226]. Indeed, analysis of the datasets in such a fashion allowed the identification of common and unique biological processes in WT and *Il6*$^{-/-}$ mice during acute inflammation and in a situation where pro-fibrotic Th1 cells drive tissue remodelling. Importantly, this approach demonstrated that IL-6 signalling has a broad impact on the overall transcriptional output seen is stromal tissue during acute resolving inflammation. This observation was illustrated by the degree of overlap in the overall transcriptional output between WT and *Il6*$^{-/-}$ mice during IL-6/STAT3 acute or IFN-γ/STAT1 pro-fibrotic setting (76% and

89%, respectively). This overlap was also striking when individual gene 'Behaviours' were studied.

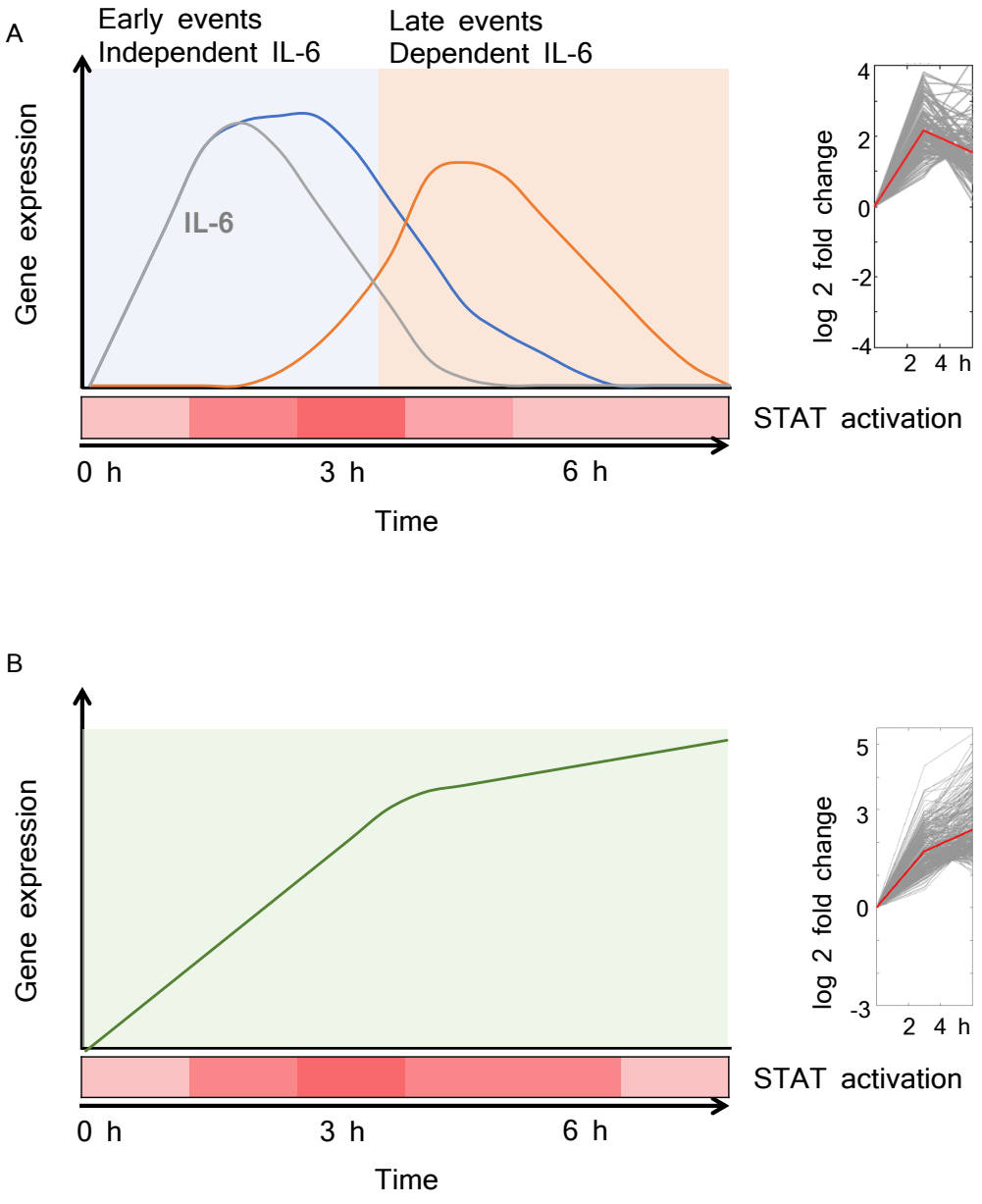

Figure 8.1. Temporal mechanisms of gene expression during acute resolving inflammation. During acute inflammation, genes can be divided in two phases: (1) those genes downstream TLR2, which are independent of IL-6 signalling, and (2) genes that are expressed as a consequence of IL-6 mediated STAT3 signalling in the peritoneum. **B.** IFN-γ-mediated STAT1 signalling in the peritoneal membrane induced changes in gene expression that were more robust and sustained over time than to those observed during acute resolving inflammation (**A**).

8.3. The balance between STAT1 and STAT3 activities determines host defence and the outcome of inflammation-induced tissue damage

The activation of STAT3 in non-hematopoietic stromal cells during acute inflammation suggests a regulatory role for this latent transcription factor in anti-microbial immunity. In this regard, IL-6/STAT3 signalling is essential for host defence against different pathogens [61-65, 252]. Importantly, mutations in the human or mouse *STAT3* gene result in hyper-immunoglobulin E syndrome and higher susceptibility of infection [307, 308]. In addition, STAT3 activation in endothelial cells is protective in endotoxin models of inflammation [309]. During acute bacterial peritonitis, IL-6/STAT3 activation in the peritoneal membrane coincides with neutrophil infiltration and bacterial clearance. Here, *Il6*$^{-/-}$ mice have a reduced capacity to contain the infection and present increased bacterial dissemination into the bloodstream. Studies presented in this thesis demonstrated that this defect is partly due to an impairment of effector characteristics of infiltrating neutrophils at the site of infection.

Importantly, IL-6 does not directly affect neutrophil activity [200, 278, 279]. It was therefore hypothesised that the impact of IL-6 on neutrophil effector functions was indirect, and mediated through responses governed by IL-6/STAT3 activity in stromal tissue cells. This hypothesis is in line with the idea that circulating neutrophils are "dormant" so as to prevent the release of ROS and proteolytic granules that could induce tissue injury [174, 310]. After infection, neutrophils rapidly migrate to the site of infection and become fully activated in response to several pro-inflammatory stimuli [174]. Thus, the nature and quality of the signals provided by the local inflamed microenvironment ultimately define the success of the inflammatory response. Here, we showed that IL-6 acting via STAT3 plays a major role in triggering these signals. For example, bioinformatic analysis linked the activation of STAT3 in the peritoneal membrane to enhanced anti-microbial activities in WT mice (Figure 8.2). In particular, IL-6-mediated activation of the peritoneal lining directs neutrophil priming and enhances phagocytosis. However, reconstitution of IL-6 trans-signalling in *Il6*$^{-/-}$ mice did not restore neutrophil respiratory burst activity, suggesting that both activities are regulated by different mechanism. This regulation may be akin to the control of neutrophil activities by

different neutrophil-activating chemokines [311]. Taken all together, we propose a model that outlines the interplay between stromal tissue and infiltrating leukocytes during acute infection (Figure 8.3).

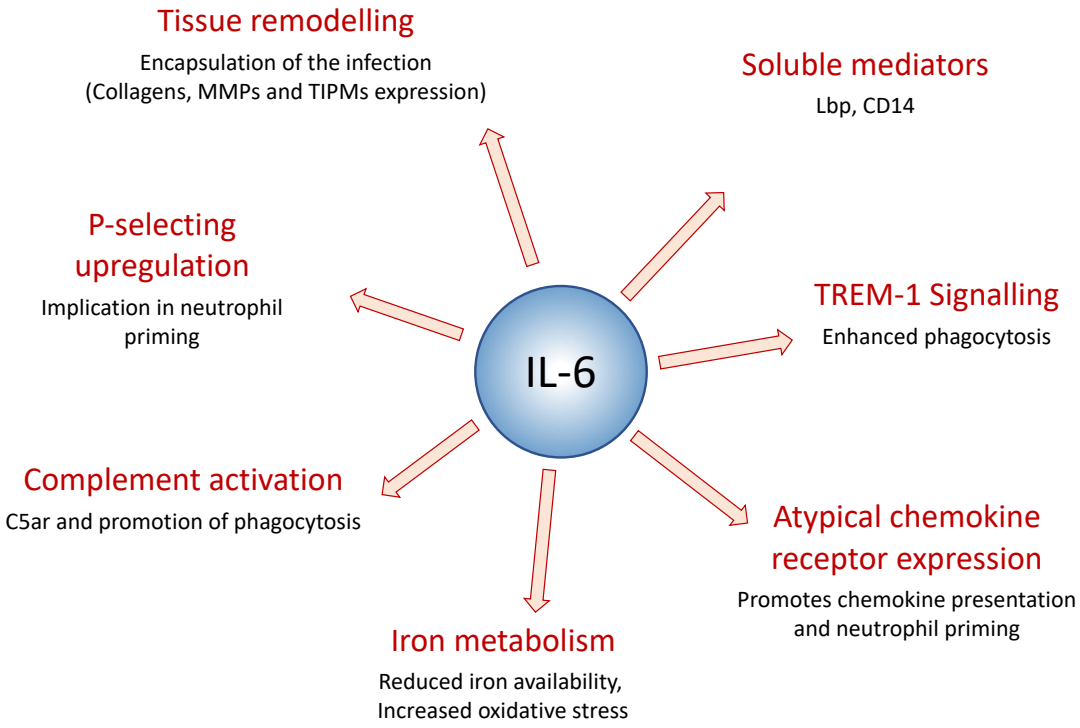

Figure 8.2. Novel mechanisms of IL-6 control of anti-microbial immunity. IL-6 signalling was associated with the upregulation of different genes that collectively ensure a successful host defence. These include complement molecules and soluble antimicrobial mediators, iron-chelating proteins, atypical chemokine receptors and adhesion molecules.

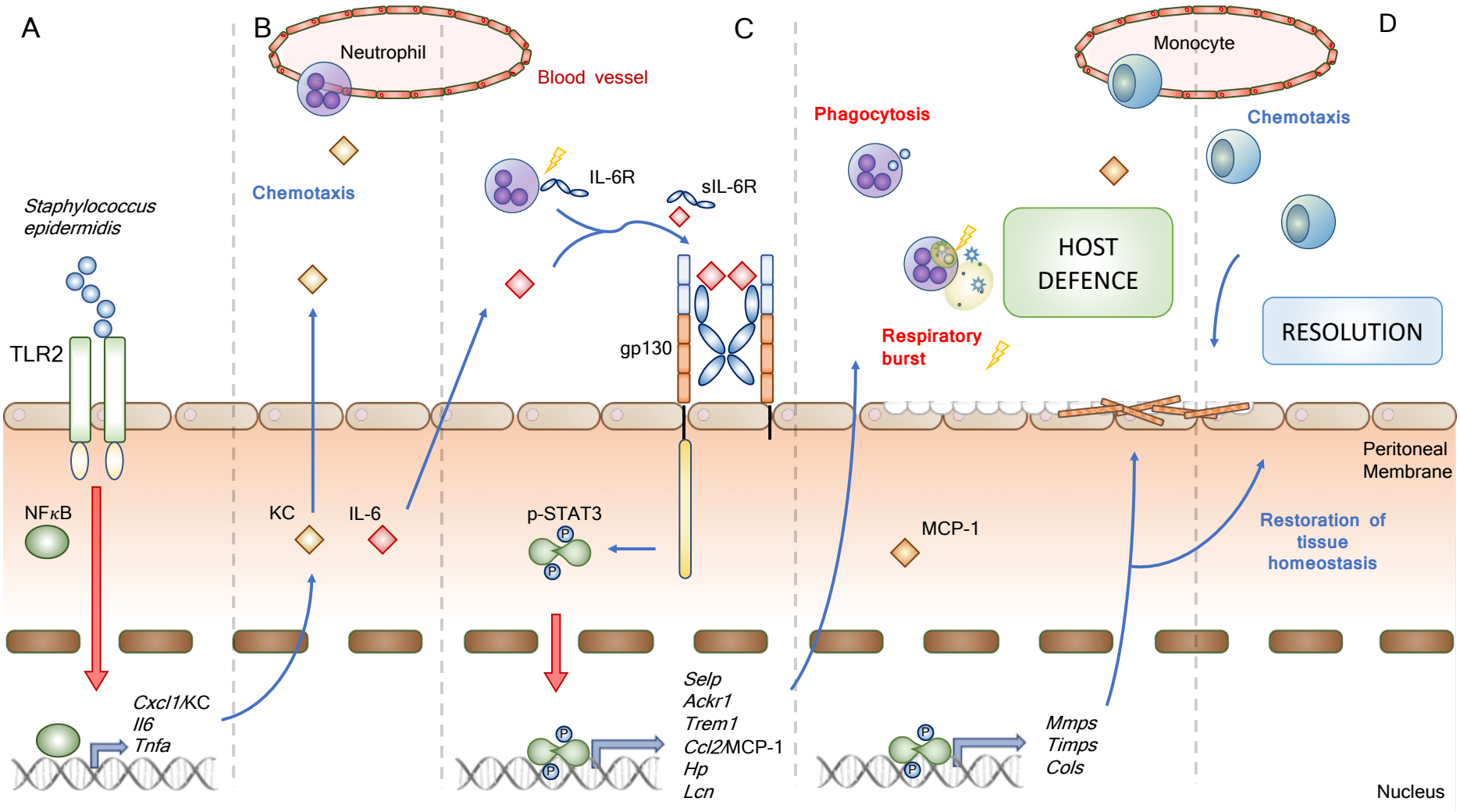
A
B
C
D
Neutrophil
Blood vessel
Monocyte
Chemotaxis
Chemotaxis
Phagocytosis
IL-6R
sIL-6R
Staphylococcus epidermidis
HOST DEFENCE
RESOLUTION
TLR2
gp130
Respiratory burst
Peritoneal Membrane
NFκB
KC
IL-6
p-STAT3
MCP-1
Restoration of tissue homeostasis
Cxcl1/KC
Il6
Tnfa
Selp
Ackr1
Trem1
Ccl2/MCP-1
Hp
Lcn
Mmps
Timps
Cols
Nucleus

Figure 8.3. Model of competent host defence. A. TLR2 activation by *S. epidermidis* induces the expression of several neutrophil chemokines, such as CXCL1, and cytokines, including IL-6 and IL-1β. **B**. CXCL1 mediates the recruitment of neutrophils to the peritoneal cavity. **C**. Upon transmigration, infiltrating neutrophils quickly shed their CD62L and IL-6R. The release of sIL-6R allows now the peritoneal lining to be responsive to IL-6 signalling. In this way, IL-6 acting *via* STAT3 induces the expression of several genes (i.e., atypical chemokine receptors, adhesion molecules, complement, soluble mediators, etc.). These molecules collectively enhance the immune response by different mechanisms, including neutrophil priming, ion sequestration, and an overall increase in oxidative stress. As a result, the host is capable to successfully clear the infection. **D**. Finally, the switch of chemokine expression mediated by IL-6 leads to apoptotic clearance of the infiltrating neutrophils and the recruitment of a monocyte population, which eventually leads to the correct resolution of the inflammatory response.

Transfer of $CD4^+$ Th1 cells into WT and *Il6*$^{-/-}$ mice was accompanied by an increase in STAT1 activity in the peritoneum [33]. Importantly, STAT1 activation compensated for the loss of STAT3 activity seen in *Il6*$^{-/-}$ mice during acute inflammation. In fact, restoration of the defects in host defence predicted in these mice was associated with a shift in the relative activities of STAT3 and STAT1 in the stromal tissue. In this regard, while the presence of Th1 cells only recovered 40% of the genes uniquely regulated by IL-6 in WT mice, these included genes linked with antimicrobial defence in this inflammatory context (e.g., *Selp, Lcn2, Saa1, Cdkn1a, Vcan, Il4ra, Hp, Fcgr1* and *Ccr5*) (Figure 8.4). These results support the idea that STAT1 and STAT3 have, to a certain extent, compensatory or overlapping roles [304, 305]. These observations also support a role of IFN-γ in innate immunity and host defence [263, 264], and highlight the correspondence in the activities elicited by both cytokines [25].

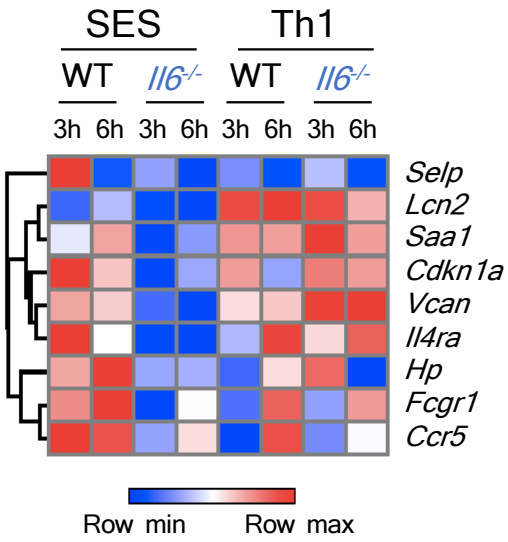

Figure 8.4. Genes unpaired in *Il6*$^{-/-}$ during acute resolving inflammation are rescued by the adoptive transfer of Th1 cells. This is relevant to the impact of Th1 recruitment in the peritoneal cavity as an adaptive immune response to support successful host defence.

While the adoptive transfer of CD4^{+} Th1 cells had a positive impact in the inflammatory response in the peritoneum, studies remain to understand the impact of these cells in the effector characteristics of infiltrating neutrophils. Studies in the literature have shown that, in contrast to IL-6, IFN-γ directly activates neutrophil effector functions [312, 313]. This is particularly relevant in the management of chronic granulomatous disease, where IFN-γ has been used as a therapy [314]. In the context of peritoneal infection, it would be interesting to investigate how IFN-γ/STAT1 signalling in the peritoneal membrane may influence neutrophil responses to infection. From our transcriptomic and pathway analysis, we predict that IFN-γ not only activates neutrophil function directly, but may also influence the stromal microenvironment to prime neutrophil responses locally.

On the other hand, STAT1 activity in the peritoneal membrane was also associated with an altered expression of molecules implicated in the physiological maintenance of the peritoneal lining. These included matrix proteases and their inhibitors, structural proteins and enzymes linked with immune homeostasis and tissue integrity. This is particularly relevant for the development of fibrosis after repetitive inflammation, where IFN-γ and STAT1 signalling disrupts the turnover of extracellular matrix by metalloproteases [33]. Importantly, fibrosis develops in response to recurrent episodes of inflammation through the IL-6-mediated proliferative expansion of Th1 cells [33]. Here, a memory recall to SES would be

expected to support antimicrobial immunity but inadvertently drives tissue damage. This may include the generation of SES targeted antibodies that are generated as a response to repeat peritoneal inflammation, and may lead to complement activation [33]. Consequently, peritoneal fibrosis may represent itself a component of anti-microbial host defence to encapsulate bacteria and prevent the dissemination of infection. [32]. Nevertheless, it is clear that the balance of STAT1 versus STAT3 activity ultimately determines the inflammatory outcome associated with infection control (Figure 8.5). This is akin to previous observations in several models of experimental hepatitis, where IFN-γ/STAT1 and IL-6/STAT3 signalling counteract each other. Here, STAT1 induces tissue injury, whereas STAT3 protects against inflammation induced tissue damage [152, 315].

In the present study, *ex vivo* expanded Th1 cells were adoptively transferred to WT and *Il6*$^{-/-}$ mice together with SES to mimic the pro-fibrotic setting observed after four rounds of acute resolving peritonitis [33]. While this approach provided an opportunity to assess the impact of these cells on the peritoneum to direct host defence, it is unclear whether this single challenge with SES and Th1 is sufficient to drive fibrosis. This seems unlikely for several reasons. First, although IFN-γ-driven STAT1 activation only occurs after the fourth episode of peritonitis, it seems obvious that inflammatory activation of the membrane during repetitive challenge will alter its responsiveness to subsequent stimuli. This may include epigenetic modifications or changes in surface receptors (e.g., IFNGR1 and IFNGR2) that determine the responsiveness of the peritoneal membrane to IFN-γ. Likewise, STAT3 associated activities observed during repetitive inflammation may become modified through changes in cooperative interactions with other transcription factors or transcriptional regulators (e.g., SP1, p300, glucocorticoid receptor) [316, 317]. These alterations may be particularly relevant at cis-regulatory modules or super-enhancer sites, where clustering of transcription factors have profound influences on gene expression [311]. In addition, studies in T cells have shown that STAT3 binding is required for the binding of STAT1 and subsequent STAT1-derived gene transduction [302]. Akin to these studies, repetitive STAT3 activation in the peritoneum may be required for the specific activity of STAT1 in the peritoneal membrane and the development of fibrosis. Thus, multiple mechanisms

may contribute to the transcriptional landscape seen in stromal tissue following inflammatory activation. In conclusion, future studies will need to determine whether the onset of fibrosis uniquely requires IFN-γ-driven STAT1 activation in the peritoneum, or whether recurrent episodes of inflammation are a prerequisite to prime the tissue for the development of fibrosis.

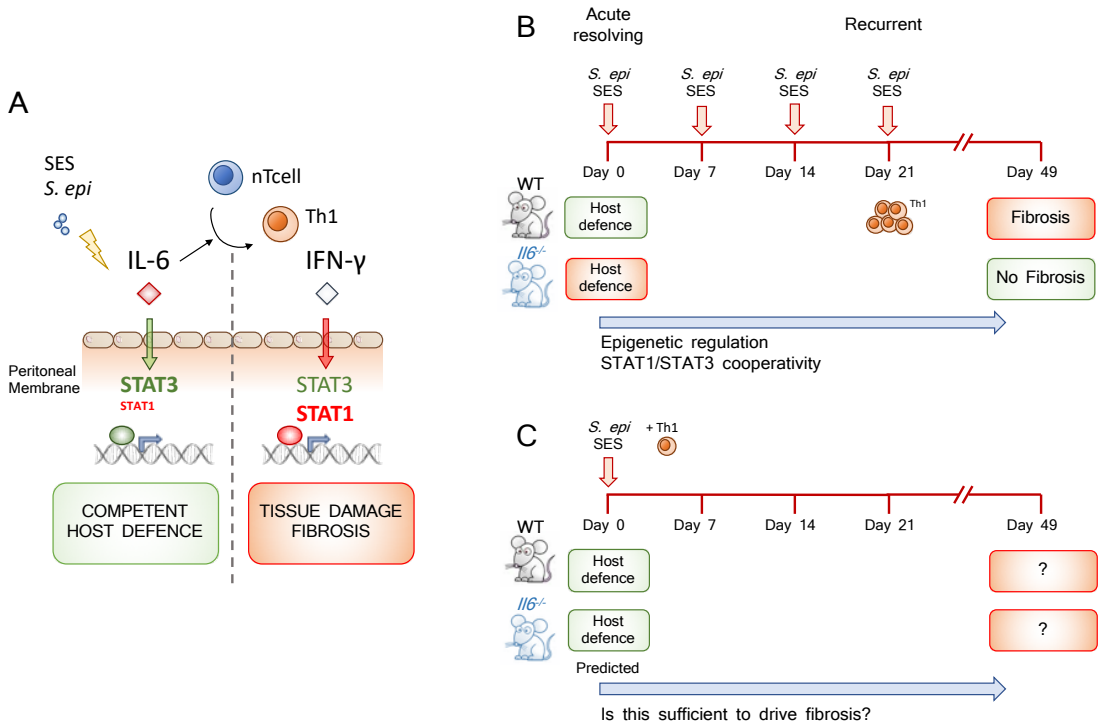

Figure 8.5. Balance between the relative activities of STAT1 and STAT3 in determining the outcome of inflammation. A. IL-6 is essential for the control of infection in a murine model of *S. epidermidis* induced peritonitis. Here, *Il6*$^{-/-}$ mice are less capable to contain the infection and present higher bacterial dissemination to the blood stream. This outcome is associated to a strong STAT3 activation in the peritoneal membrane. Conversely, during recurrent episodes of acute resolving sterile peritonitis (as produced by the repetitive (i.p.) challenge of *S. epidermidis* cell-free supernatant – SES), IL-6 promotes the proliferative expansion of CD4^{+} Th1 cells in the peritoneal cavity and the onset of fibrosis **(A & B)**. This outcome is associated to a strong IFN-γ-derived STAT1 activation in the membrane. **C.** Studies detailed in this thesis have explored the interplay between IL-6/STAT3 and IFN-γ/STAT1 signalling in the peritoneal membrane during acute inflammation by adoptively transferring *ex vivo* polarised Th1 cells together with SES into WT and *Il6*$^{-/-}$ mice. While this approach has provided exciting findings in the involvement of the peritoneal membrane in determining competent host defence versus inflammation-induced tissue damage, future studies need to elucidate whether the onset of fibrosis uniquely requires IFN-γ-driven STAT1 activation in the peritoneum, or whether recurrent episodes of inflammation are a prerequisite to prime the tissue for the development of fibrosis.

8.4. Future work

Data presented in this thesis provides an holistic view on the transcriptome changes occurring in episodes of acute resolving inflammation. Specifically, studies have considered the role of IL-6 and IFN-γ signalling and the activation of STAT1 and STAT3 in the peritoneum. Several mechanisms were unearthed through this approach, highlighting the role of Jak-STAT signalling in "educating" the immune response against infection. Future studies are however required to further investigate different issues.

- The balance in the relative activities of STAT1 and STAT3 ultimately define the effect of a given cytokine. Studies need to define the significance of STAT1-STAT3 crosstalk in the peritoneal membrane to determine the balance between successful host defence and inflammation-induced tissue injury. In this regard, our laboratory has recently conducted a ChIP-seq analysis of STAT1 and STAT3 activities in the inflamed peritoneum. This approach will provide valuable information on transcriptional crosstalk and potential cooperative interactions relevant to the control of gene expression.
- Repetitive episodes of acute resolving peritonitis led to the proliferative expansion of pro-fibrotic Th1 cells in the peritoneal cavity following recurrent inflammatory activation. Studies need to determine whether a single transfer of Th1 cells is sufficient to drive fibrosis. This approach will allow us to consider whether potential long-term changes in epigenetic mechanisms are involved in these processes.
- In line with the bullet points 1 and 2, studies will need to investigate the impact of epigenetic regulation in the stromal compartment as a prerequisite for the development of peritoneal fibrosis. These may include histone trimethylation and ATAC-seq (Assay for Transposase Accessible Chromatin with high-throughput sequencing) studies to evaluate chromatin accessibility to STAT1 and STAT3 during acute or repetitive inflammation.

In this regard, various transcription factors and co-activators are known to influence STAT-mediated gene transduction (e.g., p300, SP1, AP-1). Thus, their implication in host defence and fibrosis will need to be assessed.

- The effector function characteristics of infiltrating neutrophils are impaired as a result of IL-6 deficiency. However, the precise mechanism by which neutrophil phagocytosis and respiratory burst are primed needs further investigation. In particular, studies will need to investigate how candidate genes identified by RNA-seq affect neutrophil function.
- The assessment of the production of ROS depends on the quality of the sensors used for their detection. In this regard, APF only accounts for the detection of OH^-, NO_3^- and ClO^-, and does not illustrate the overall ROS production within the neutrophils. Thus, studies will require the use of alternative sensors or the combination of several techniques (e.g., APF staining and assessment of cytochrome B actives) to accurately reflect the respiratory burst status in neutrophils. The use of specific inhibitors for the enzymes SOD and MPO could also be used to determine the specific implication of NOX2 in the respiratory burst.
- Transcriptome analysis predicted that signatures relevant to the immune response (i.e. activation of leukocytes) were controlled by IL-6. Th1 cell adoptive transfer and IFN-γ signalling in the peritoneal membrane supplemented this level of control. Studies need to further investigate the impact of IFN-γ in directly or indirectly control neutrophil effector function during bacterial peritoniti

Bibliography

1. Abbas, A.K., A.H. Lichtman, and S. Pillai, *Cellular and molecular immunology*. 7th ed. 2012, Philadelphia: Elsevier/Saunders. x, 545 p.
2. Finlay, B.B. and G. McFadden, *Anti-immunology: evasion of the host immune system by bacterial and viral pathogens.* Cell, 2006. **124**(4): p. 767-82.
3. Medzhitov, R. and C.A. Janeway, Jr., *Innate immunity: the virtues of a nonclonal system of recognition.* Cell, 1997. **91**(3): p. 295-8.
4. Takeuchi, O. and S. Akira, *Pattern recognition receptors and inflammation.* Cell, 2010. **140**(6): p. 805-20.
5. Brubaker, S.W., et al., *Innate immune pattern recognition: a cell biological perspective.* Annu Rev Immunol, 2015. **33**: p. 257-90.
6. Serhan, C.N. and J. Savill, *Resolution of inflammation: the beginning programs the end.* Nat Immunol, 2005. **6**(12): p. 1191-7.
7. Roitt, I.M., J. Brostoff, and D.K. Male, *Immunology*. 6th ed. 2001, Edinburgh ; New York: Mosby. 480 p.
8. Artis, D. and H. Spits, *The biology of innate lymphoid cells.* Nature, 2015. **517**(7534): p. 293-301.
9. Jones, S.A., *Directing transition from innate to acquired immunity: defining a role for IL-6.* J Immunol, 2005. **175**(6): p. 3463-8.
10. Pancer, Z. and M.D. Cooper, *The evolution of adaptive immunity.* Annu Rev Immunol, 2006. **24**: p. 497-518.
11. Sadofsky, M.J., *The RAG proteins in V(D)J recombination: more than just a nuclease.* Nucleic Acids Res, 2001. **29**(7): p. 1399-409.
12. Sallusto, F., J. Geginat, and A. Lanzavecchia, *Central memory and effector memory T cell subsets: function, generation, and maintenance.* Annu Rev Immunol, 2004. **22**: p. 745-63.
13. McHeyzer-Williams, L.J. and M.G. McHeyzer-Williams, *Antigen-specific memory B cell development.* Annu Rev Immunol, 2005. **23**: p. 487-513.
14. Farber, D.L., et al., *Immunological memory: lessons from the past and a look to the future.* Nat Rev Immunol, 2016. **16**(2): p. 124-8.
15. Netea, M.G., et al., *A guiding map for inflammation.* Nat Immunol, 2017. **18**(8): p. 826-831.
16. Medzhitov, R., *Origin and physiological roles of inflammation.* Nature, 2008. **454**(7203): p. 428-35.

17. Topley, N., et al., *Activation of inflammation and leukocyte recruitment into the peritoneal cavity.* Kidney Int Suppl, 1996. **56**: p. S17-21.

18. Barton, G.M., *A calculated response: control of inflammation by the innate immune system.* J Clin Invest, 2008. **118**(2): p. 413-20.

19. Godson, C., et al., *Cutting edge: lipoxins rapidly stimulate nonphlogistic phagocytosis of apoptotic neutrophils by monocyte-derived macrophages.* J Immunol, 2000. **164**(4): p. 1663-7.

20. Hurst, S.M., et al., *Il-6 and its soluble receptor orchestrate a temporal switch in the pattern of leukocyte recruitment seen during acute inflammation.* Immunity, 2001. **14**(6): p. 705-14.

21. McLoughlin, R.M., et al., *IL-6 trans-signaling via STAT3 directs T cell infiltration in acute inflammation.* Proc Natl Acad Sci U S A, 2005. **102**(27): p. 9589-94.

22. Sadik, C.D. and A.D. Luster, *Lipid-cytokine-chemokine cascades orchestrate leukocyte recruitment in inflammation.* J Leukoc Biol, 2012. **91**(2): p. 207-15.

23. Romano, M., et al., *Role of IL-6 and its soluble receptor in induction of chemokines and leukocyte recruitment.* Immunity, 1997. **6**(3): p. 315-25.

24. Oh, J.W., et al., *Role of IL-6 and the soluble IL-6 receptor in inhibition of VCAM-1 gene expression.* J Immunol, 1998. **161**(9): p. 4992-9.

25. McLoughlin, R.M., et al., *Interplay between IFN-gamma and IL-6 signaling governs neutrophil trafficking and apoptosis during acute inflammation.* J Clin Invest, 2003. **112**(4): p. 598-607.

26. Basil, M.C. and B.D. Levy, *Specialized pro-resolving mediators: endogenous regulators of infection and inflammation.* Nat Rev Immunol, 2016. **16**(1): p. 51-67.

27. Gautier, E.L., et al., *Local apoptosis mediates clearance of macrophages from resolving inflammation in mice.* Blood, 2013. **122**(15): p. 2714-22.

28. Bellingan, G.J., et al., *In vivo fate of the inflammatory macrophage during the resolution of inflammation: inflammatory macrophages do not die locally, but emigrate to the draining lymph nodes.* J Immunol, 1996. **157**(6): p. 2577-85.

29. Golpon, H.A., et al., *Life after corpse engulfment: phagocytosis of apoptotic cells leads to VEGF secretion and cell growth.* FASEB J, 2004. **18**(14): p. 1716-8.

30. Casadevall, A. and L.A. Pirofski, *The damage-response framework of microbial pathogenesis.* Nat Rev Microbiol, 2003. **1**(1): p. 17-24.

31. Wynn, T.A., *Cellular and molecular mechanisms of fibrosis.* J Pathol, 2008. **214**(2): p. 199-210.

32. Ulrichs, T. and S.H. Kaufmann, *New insights into the function of granulomas in human tuberculosis.* J Pathol, 2006. **208**(2): p. 261-9.

33. Fielding, C.A., et al., *Interleukin-6 signaling drives fibrosis in unresolved inflammation.* Immunity, 2014. **40**(1): p. 40-50.

34. Davies, S.J., et al., *Longitudinal changes in peritoneal kinetics: the effects of peritoneal dialysis and peritonitis.* Nephrol Dial Transplant, 1996. **11**(3): p. 498-506.

35. Williams, J.D., et al., *Morphologic changes in the peritoneal membrane of patients with renal disease.* J Am Soc Nephrol, 2002. **13**(2): p. 470-9.

36. Davies, S.J., et al., *Peritoneal glucose exposure and changes in membrane solute transport with time on peritoneal dialysis.* J Am Soc Nephrol, 2001. **12**(5): p. 1046-51.

37. Vilcek, J. and M. Feldmann, *Historical review: Cytokines as therapeutics and targets of therapeutics.* Trends Pharmacol Sci, 2004. **25**(4): p. 201-9.

38. Dinarello, C.A., *Historical insights into cytokines.* Eur J Immunol, 2007. **37 Suppl 1**: p. S34-45.

39. Mosser, D.M. and X. Zhang, *Interleukin-10: new perspectives on an old cytokine.* Immunol Rev, 2008. **226**: p. 205-18.

40. Yoshida, H. and C.A. Hunter, *The immunobiology of interleukin-27.* Annu Rev Immunol, 2015. **33**: p. 417-43.

41. Hunter, C.A. and S.A. Jones, *IL-6 as a keystone cytokine in health and disease.* Nat Immunol, 2015. **16**(5): p. 448-57.

42. Rossi, D. and A. Zlotnik, *The biology of chemokines and their receptors.* Annu Rev Immunol, 2000. **18**: p. 217-42.

43. Jones, G.E., *Cellular signaling in macrophage migration and chemotaxis.* J Leukoc Biol, 2000. **68**(5): p. 593-602.

44. Hombria, J.C., et al., *Characterisation of Upd2, a Drosophila JAK/STAT pathway ligand.* Dev Biol, 2005. **288**(2): p. 420-33.

45. Brown, S., N. Hu, and J.C. Hombria, *Identification of the first invertebrate interleukin JAK/STAT receptor, the Drosophila gene domeless.* Curr Biol, 2001. **11**(21): p. 1700-5.

46. Kingsolver, M.B. and R.W. Hardy, *Making connections in insect innate immunity.* Proc Natl Acad Sci U S A, 2012. **109**(46): p. 18639-40.

47. Fielding, C.A., et al., *Viral IL-6 blocks neutrophil infiltration during acute inflammation.* J Immunol, 2005. **175**(6): p. 4024-9.

48. Heinrich, P.C., et al., *Principles of interleukin (IL)-6-type cytokine signalling and its regulation.* Biochem J, 2003. **374**(Pt 1): p. 1-20.

49. Weissenbach, J., et al., *Two interferon mRNAs in human fibroblasts: in vitro translation and Escherichia coli cloning studies.* Proc Natl Acad Sci U S A, 1980. **77**(12): p. 7152-6.

50. Yasukawa, K., et al., *Structure and expression of human B cell stimulatory factor-2 (BSF-2/IL-6) gene.* EMBO J, 1987. **6**(10): p. 2939-45.

51. Haegeman, G., et al., *Structural analysis of the sequence coding for an inducible 26-kDa protein in human fibroblasts.* Eur J Biochem, 1986. **159**(3): p. 625-32.

52. Ritchie, D.G. and G.M. Fuller, *Hepatocyte-stimulating factor: a monocyte-derived acute-phase regulatory protein.* Ann N Y Acad Sci, 1983. **408**: p. 490-502.

53. Sehgal, P.B., et al., *Human beta 2 interferon and B-cell differentiation factor BSF-2 are identical.* Science, 1987. **235**(4790): p. 731-2.

54. Akira, S., T. Taga, and T. Kishimoto, *Interleukin-6 in biology and medicine.* Adv Immunol, 1993. **54**: p. 1-78.

55. Tanaka, T., M. Narazaki, and T. Kishimoto, *IL-6 in Inflammation, Immunity, and Disease.* Cold Spring Harbor Perspectives in Biology, 2014. **6**(10).

56. Colmont, C.S., et al., *Human peritoneal mesothelial cells respond to bacterial ligands through a specific subset of Toll-like receptors.* Nephrol Dial Transplant, 2011. **26**(12): p. 4079-90.

57. Klimpel, G.R., *Soluble factor(s) from LPS-activated macrophages induce cytotoxic T cell differentiation from alloantigen-primed spleen cells.* J Immunol, 1980. **125**(3): p. 1243-9.

58. Hirano, T., et al., *Complementary DNA for a novel human interleukin (BSF-2) that induces B lymphocytes to produce immunoglobulin.* Nature, 1986. **324**(6092): p. 73-6.

59. Andus, T., et al., *Recombinant human B cell stimulatory factor 2 (BSF-2/IFN-beta 2) regulates beta-fibrinogen and albumin mRNA levels in Fao-9 cells.* FEBS Lett, 1987. **221**(1): p. 18-22.

60. Heinrich, P.C., J.V. Castell, and T. Andus, *Interleukin-6 and the acute phase response.* Biochem J, 1990. **265**(3): p. 621-36.

61. Kopf, M., et al., *Impaired immune and acute-phase responses in interleukin-6-deficient mice.* Nature, 1994. **368**(6469): p. 339-42.

62. Ladel, C.H., et al., *Lethal tuberculosis in interleukin-6-deficient mutant mice.* Infect Immun, 1997. **65**(11): p. 4843-9.

63. van der Poll, T., et al., *Interleukin-6 gene-deficient mice show impaired defense against pneumococcal pneumonia.* J Infect Dis, 1997. **176**(2): p. 439-44.

64. Lee, S.W., et al., *IL-6 induces long-term protective immunity against a lethal challenge of influenza virus.* Vaccine, 1999. **17**(5): p. 490-6.

65. Gao, W. and M.A. Pereira, *Interleukin-6 is required for parasite specific response and host resistance to Trypanosoma cruzi.* Int J Parasitol, 2002. **32**(2): p. 167-70.

66. Cronstein, B.N., *Interleukin-6--a key mediator of systemic and local symptoms in rheumatoid arthritis.* Bull NYU Hosp Jt Dis, 2007. **65 Suppl 1**: p. S11-5.

67. Mudter, J. and M.F. Neurath, *Il-6 signaling in inflammatory bowel disease: pathophysiological role and clinical relevance.* Inflamm Bowel Dis, 2007. **13**(8): p. 1016-23.

68. Hodge, D.R., E.M. Hurt, and W.L. Farrar, *The role of IL-6 and STAT3 in inflammation and cancer.* Eur J Cancer, 2005. **41**(16): p. 2502-12.

69. Paonessa, G., et al., *Two distinct and independent sites on IL-6 trigger gp 130 dimer formation and signalling.* EMBO J, 1995. **14**(9): p. 1942-51.

70. Heinrich, P.C., et al., *Interleukin-6-type cytokine signalling through the gp130/Jak/STAT pathway.* Biochem J, 1998. **334 (Pt 2)**: p. 297-314.

71. Matthews, V., et al., *Cellular cholesterol depletion triggers shedding of the human interleukin-6 receptor by ADAM10 and ADAM17 (TACE).* J Biol Chem, 2003. **278**(40): p. 38829-39.

72. Jones, S.A., et al., *C-reactive protein: a physiological activator of interleukin 6 receptor shedding.* J Exp Med, 1999. **189**(3): p. 599-604.

73. Marin, V., et al., *Chemotactic agents induce IL-6Ralpha shedding from polymorphonuclear cells: involvement of a metalloproteinase of the TNF-alpha-converting enzyme (TACE) type.* Eur J Immunol, 2002. **32**(10): p. 2965-70.

74. McLoughlin, R.M., et al., *Differential regulation of neutrophil-activating chemokines by IL-6 and its soluble receptor isoforms.* J Immunol, 2004. **172**(9): p. 5676-83.

75. Marin, V., et al., *The IL-6-soluble IL-6Ralpha autocrine loop of endothelial activation as an intermediate between acute and chronic inflammation: an experimental model involving thrombin.* J Immunol, 2001. **167**(6): p. 3435-42.

76. Modur, V., et al., *Retrograde inflammatory signaling from neutrophils to endothelial cells by soluble interleukin-6 receptor alpha.* J Clin Invest, 1997. **100**(11): p. 2752-6.

77. Heink, S., et al., *Trans-presentation of IL-6 by dendritic cells is required for the priming of pathogenic TH17 cells.* Nat Immunol, 2017. **18**(1): p. 74-85.

78. Wolf, J., et al., *Different Soluble Forms of the Interleukin-6 Family Signal Transducer gp130 Fine-tune the Blockade of Interleukin-6 Trans-signaling.* J Biol Chem, 2016. **291**(31): p. 16186-96.

79. Mullberg, J., et al., *Differential shedding of the two subunits of the interleukin-6 receptor.* FEBS Lett, 1993. **332**(1-2): p. 174-8.

80. Jostock, T., et al., *Soluble gp130 is the natural inhibitor of soluble interleukin-6 receptor transsignaling responses.* Eur J Biochem, 2001. **268**(1): p. 160-7.

81. Chalaris, A., et al., *The soluble Interleukin 6 receptor: generation and role in inflammation and cancer.* Eur J Cell Biol, 2011. **90**(6-7): p. 484-94.

82. Waetzig, G.H. and S. Rose-John, *Hitting a complex target: an update on interleukin-6 trans-signalling.* Expert Opin Ther Targets, 2012. **16**(2): p. 225-36.

83. Jones, S.A., J. Scheller, and S. Rose-John, *Therapeutic strategies for the clinical blockade of IL-6/gp130 signaling.* J Clin Invest, 2011. **121**(9): p. 3375-83.

84. O'Shea, J.J. and R. Plenge, *JAK and STAT signaling molecules in immunoregulation and immune-mediated disease.* Immunity, 2012. **36**(4): p. 542-50.

85. Rawlings, J.S., K.M. Rosler, and D.A. Harrison, *The JAK/STAT signaling pathway.* J Cell Sci, 2004. **117**(Pt 8): p. 1281-3.

86. Schaper, F., et al., *Activation of the protein tyrosine phosphatase SHP2 via the interleukin-6 signal transducing receptor protein gp130 requires tyrosine kinase Jak1 and limits acute-phase protein expression.* Biochem J, 1998. **335 (Pt 3)**: p. 557-65.

87. Ernst, M. and B.J. Jenkins, *Acquiring signalling specificity from the cytokine receptor gp130.* Trends Genet, 2004. **20**(1): p. 23-32.

88. Taniguchi, K., et al., *A gp130-Src-YAP module links inflammation to epithelial regeneration.* Nature, 2015. **519**(7541): p. 57-62.

89. Bohmer, F.D. and K. Friedrich, *Protein tyrosine phosphatases as wardens of STAT signaling.* JAKSTAT, 2014. **3**(1): p. e28087.

90. Villarino, A.V., Y. Kanno, and J.J. O'Shea, *Mechanisms and consequences of Jak-STAT signaling in the immune system.* Nat Immunol, 2017. **18**(4): p. 374-384.

91. Palvimo, J.J., *PIAS proteins as regulators of small ubiquitin-related modifier (SUMO) modifications and transcription.* Biochem Soc Trans, 2007. **35**(Pt 6): p. 1405-8.

92. Croker, B.A., et al., *SOCS3 negatively regulates IL-6 signaling in vivo.* Nat Immunol, 2003. **4**(6): p. 540-5.

93. Lang, R., et al., *SOCS3 regulates the plasticity of gp130 signaling.* Nat Immunol, 2003. **4**(6): p. 546-50.

94. Topley, N., et al., *Human peritoneal mesothelial cells synthesize interleukin-6: induction by IL-1 beta and TNF alpha.* Kidney Int, 1993. **43**(1): p. 226-33.

95. Fielding, C.A., et al., *IL-6 regulates neutrophil trafficking during acute inflammation via STAT3.* J Immunol, 2008. **181**(3): p. 2189-95.

96. Catar, R., et al., *IL-6 Trans-Signaling Links Inflammation with Angiogenesis in the Peritoneal Membrane.* J Am Soc Nephrol, 2017. **28**(4): p. 1188-1199.

97. Chen, Q., et al., *Fever-range thermal stress promotes lymphocyte trafficking across high endothelial venules via an interleukin 6 trans-signaling mechanism.* Nat Immunol, 2006. **7**(12): p. 1299-308.

98. Schindler, R., et al., *Correlations and interactions in the production of interleukin-6 (IL-6), IL-1, and tumor necrosis factor (TNF) in human blood mononuclear cells: IL-6 suppresses IL-1 and TNF.* Blood, 1990. **75**(1): p. 40-7.

99. Tilg, H., et al., *Interleukin-6 (IL-6) as an anti-inflammatory cytokine: induction of circulating IL-1 receptor antagonist and soluble tumor necrosis factor receptor p55.* Blood, 1994. **83**(1): p. 113-8.

100. Jones, G.W., et al., *Loss of CD4+ T cell IL-6R expression during inflammation underlines a role for IL-6 trans signaling in the local maintenance of Th17 cells.* J Immunol, 2010. **184**(4): p. 2130-9.

101. Korn, T., et al., *IL-17 and Th17 Cells.* Annu Rev Immunol, 2009. **27**: p. 485-517.

102. Onogawa, T., *Local delivery of soluble interleukin-6 receptors to improve the outcome of alpha-toxin producing Staphylococcus aureus infection in mice.* Immunobiology, 2005. **209**(9): p. 651-60.

103. Hirano, T., et al., *Excessive production of interleukin 6/B cell stimulatory factor-2 in rheumatoid arthritis.* Eur J Immunol, 1988. **18**(11): p. 1797-801.

104. Grossman, R.M., et al., *Interleukin 6 is expressed in high levels in psoriatic skin and stimulates proliferation of cultured human keratinocytes.* Proc Natl Acad Sci U S A, 1989. **86**(16): p. 6367-71.

105. Yamamoto, M., et al., *IL-6 is required for the development of Th1 cell-mediated murine colitis.* J Immunol, 2000. **164**(9): p. 4878-82.

106. de Benedetti, F., et al., *Correlation of serum interleukin-6 levels with joint involvement and thrombocytosis in systemic juvenile rheumatoid arthritis.* Arthritis Rheum, 1991. **34**(9): p. 1158-63.

107. Nowell, M.A., et al., *Soluble IL-6 receptor governs IL-6 activity in experimental arthritis: blockade of arthritis severity by soluble glycoprotein 130.* J Immunol, 2003. **171**(6): p. 3202-9.

108. Ohshima, S., et al., *Interleukin 6 plays a key role in the development of antigen-induced arthritis.* Proc Natl Acad Sci U S A, 1998. **95**(14): p. 8222-6.

109. Samoilova, E.B., et al., *IL-6-deficient mice are resistant to experimental autoimmune encephalomyelitis: roles of IL-6 in the activation and differentiation of autoreactive T cells.* J Immunol, 1998. **161**(12): p. 6480-6.

110. Scheller, J., et al., *The pro- and anti-inflammatory properties of the cytokine interleukin-6.* Biochim Biophys Acta, 2011. **1813**(5): p. 878-88.

111. Atreya, R., et al., *Blockade of interleukin 6 trans signaling suppresses T-cell resistance against apoptosis in chronic intestinal inflammation: evidence in crohn disease and experimental colitis in vivo.* Nat Med, 2000. **6**(5): p. 583-8.

112. Rose-John, S., *The Soluble Interleukin 6 Receptor: Advanced Therapeutic Options in Inflammation.* Clin Pharmacol Ther, 2017. **102**(4): p. 591-598.

113. Williams, J.D., et al., *The natural course of peritoneal membrane biology during peritoneal dialysis.* Kidney Int Suppl, 2003(88): p. S43-9.

114. Ealick, S.E., et al., *Three-dimensional structure of recombinant human interferon-gamma.* Science, 1991. **252**(5006): p. 698-702.

115. Frucht, D.M., et al., *IFN-gamma production by antigen-presenting cells: mechanisms emerge.* Trends Immunol, 2001. **22**(10): p. 556-60.

116. Trinchieri, G., *Interleukin-12: a proinflammatory cytokine with immunoregulatory functions that bridge innate resistance and antigen-specific adaptive immunity.* Annu Rev Immunol, 1995. **13**: p. 251-76.

117. Schroder, K., et al., *Interferon-gamma: an overview of signals, mechanisms and functions.* J Leukoc Biol, 2004. **75**(2): p. 163-89.

118. Boehm, U., et al., *Cellular responses to interferon-gamma.* Annu Rev Immunol, 1997. **15**: p. 749-95.

119. Beretta, L., et al., *Expression of the protein kinase PKR in modulated by IRF-1 and is reduced in 5q- associated leukemias.* Oncogene, 1996. **12**(7): p. 1593-6.

120. Robson, R.L., et al., *Differential regulation of chemokine production in human peritoneal mesothelial cells: IFN-gamma controls neutrophil migration across the mesothelium in vitro and in vivo.* J Immunol, 2001. **167**(2): p. 1028-38.

121. Randal, M. and A.A. Kossiakoff, *The structure and activity of a monomeric interferon-gamma:alpha-chain receptor signaling complex.* Structure, 2001. **9**(2): p. 155-63.

122. Darnell, J.E., Jr., I.M. Kerr, and G.R. Stark, *Jak-STAT pathways and transcriptional activation in response to IFNs and other extracellular signaling proteins.* Science, 1994. **264**(5164): p. 1415-21.

123. Ni Cheallaigh, C., et al., *A Common Variant in the Adaptor Mal Regulates Interferon Gamma Signaling.* Immunity, 2016. **44**(2): p. 368-79.

124. Uddin, S., et al., *Interaction of p59fyn with interferon-activated Jak kinases.* Biochem Biophys Res Commun, 1997. **235**(1): p. 83-8.

125. Smyth, D., et al., *Interferon-gamma-induced increases in intestinal epithelial macromolecular permeability requires the Src kinase Fyn.* Lab Invest, 2011. **91**(5): p. 764-77.

126. Schreiber, R.D. and M.A. Farrar, *The biology and biochemistry of interferon-gamma and its receptor.* Gastroenterol Jpn, 1993. **28 Suppl 4**: p. 88-94; discussion 95-6.

127. Starr, R., et al., *A family of cytokine-inducible inhibitors of signalling.* Nature, 1997. **387**(6636): p. 917-21.

128. You, M., D.H. Yu, and G.S. Feng, *Shp-2 tyrosine phosphatase functions as a negative regulator of the interferon-stimulated Jak/STAT pathway.* Mol Cell Biol, 1999. **19**(3): p. 2416-24.

129. ten Hoeve, J., et al., *Identification of a nuclear Stat1 protein tyrosine phosphatase.* Mol Cell Biol, 2002. **22**(16): p. 5662-8.

130. Duffield, J.S., et al., *Host responses in tissue repair and fibrosis.* Annu Rev Pathol, 2013. **8**: p. 241-76.

131. Desmouliere, A., et al., *Transforming growth factor-beta 1 induces alpha-smooth muscle actin expression in granulation tissue myofibroblasts and in quiescent and growing cultured fibroblasts.* J Cell Biol, 1993. **122**(1): p. 103-11.

132. Sime, P.J., et al., *Adenovector-mediated gene transfer of active transforming growth factor-beta1 induces prolonged severe fibrosis in rat lung.* J Clin Invest, 1997. **100**(4): p. 768-76.

133. Nightingale, J., et al., *Oncostatin M, a cytokine released by activated mononuclear cells, induces epithelial cell-myofibroblast transdifferentiation via Jak/Stat pathway activation.* J Am Soc Nephrol, 2004. **15**(1): p. 21-32.

134. Hinz, B., et al., *The myofibroblast: one function, multiple origins.* Am J Pathol, 2007. **170**(6): p. 1807-16.

135. Peyrol, S., et al., *Lysyl oxidase gene expression in the stromal reaction to in situ and invasive ductal breast carcinoma.* Am J Pathol, 1997. **150**(2): p. 497-507.

136. Olsen, K.C., et al., *Transglutaminase 2 and its role in pulmonary fibrosis.* Am J Respir Crit Care Med, 2011. **184**(6): p. 699-707.

137. Mozaffarian, A., et al., *Mechanisms of oncostatin M-induced pulmonary inflammation and fibrosis.* J Immunol, 2008. **181**(10): p. 7243-53.

138. Wynn, T.A. and L. Barron, *Macrophages: master regulators of inflammation and fibrosis.* Semin Liver Dis, 2010. **30**(3): p. 245-57.

139. Pesce, J.T., et al., *Arginase-1-expressing macrophages suppress Th2 cytokine-driven inflammation and fibrosis.* PLoS Pathog, 2009. **5**(4): p. e1000371.

140. Hashimoto, S., et al., *IL-4 and IL-13 induce myofibroblastic phenotype of human lung fibroblasts through c-Jun NH2-terminal kinase-dependent pathway.* J Allergy Clin Immunol, 2001. **107**(6): p. 1001-8.

141. Oriente, A., et al., *Interleukin-13 modulates collagen homeostasis in human skin and keloid fibroblasts.* J Pharmacol Exp Ther, 2000. **292**(3): p. 988-94.

142. Hesse, M., et al., *Differential regulation of nitric oxide synthase-2 and arginase-1 by type 1/type 2 cytokines in vivo: granulomatous pathology is shaped by the pattern of L-arginine metabolism.* J Immunol, 2001. **167**(11): p. 6533-44.

143. Vaillant, B., et al., *Regulation of hepatic fibrosis and extracellular matrix genes by the th response: new insight into the role of tissue inhibitors of matrix metalloproteinases.* J Immunol, 2001. **167**(12): p. 7017-26.

144. Wang, S. and R. Hirschberg, *BMP7 antagonizes TGF-beta -dependent fibrogenesis in mesangial cells.* Am J Physiol Renal Physiol, 2003. **284**(5): p. F1006-13.

145. Ma, L.J., et al., *Transforming growth factor-beta-dependent and -independent pathways of induction of tubulointerstitial fibrosis in beta6(-/-) mice.* Am J Pathol, 2003. **163**(4): p. 1261-73.

146. Wynn, T.A., *Fibrotic disease and the T(H)1/T(H)2 paradigm.* Nat Rev Immunol, 2004. **4**(8): p. 583-94.

147. Wynn, T.A., et al., *An IL-12-based vaccination method for preventing fibrosis induced by schistosome infection.* Nature, 1995. **376**(6541): p. 594-6.

148. Gurujeyalakshmi, G. and S.N. Giri, *Molecular mechanisms of antifibrotic effect of interferon gamma in bleomycin-mouse model of lung fibrosis: downregulation of TGF-beta and procollagen I and III gene expression.* Exp Lung Res, 1995. **21**(5): p. 791-808.

149. Keane, M.P., et al., *IL-12 attenuates bleomycin-induced pulmonary fibrosis.* Am J Physiol Lung Cell Mol Physiol, 2001. **281**(1): p. L92-7.

150. Poynard, T., et al., *Viral hepatitis C.* Lancet, 2003. **362**(9401): p. 2095-100.

151. Oldroyd, S.D., et al., *Interferon-gamma inhibits experimental renal fibrosis.* Kidney Int, 1999. **56**(6): p. 2116-27.

152. Hong, F., et al., *Opposing roles of STAT1 and STAT3 in T cell-mediated hepatitis: regulation by SOCS.* J Clin Invest, 2002. **110**(10): p. 1503-13.

153. Chinen, T., et al., *Suppressor of cytokine signaling-1 regulates inflammatory bowel disease in which both IFNgamma and IL-4 are involved.* Gastroenterology, 2006. **130**(2): p. 373-88.

154. Wen, J., et al., *Interactions between Th1 cells and Tregs affect regulation of hepatic fibrosis in biliary atresia through the IFN-gamma/STAT1 pathway.* Cell Death Differ, 2017. **24**(6): p. 997-1006.

155. Chugh, S., et al., *Peritoneal Membrane Injury and Peritoneal Dialysis.* Advances in Nephrology, 2014. **2014**: p. 10.

156. Coles, G.A. and J.D. Williams, *What is the place of peritoneal dialysis in the integrated treatment of renal failure?* Kidney Int, 1998. **54**(6): p. 2234-40.

157. Tokgoz, B., *Clinical advantages of peritoneal dialysis.* Perit Dial Int, 2009. **29 Suppl 2**: p. S59-61.

158. Devuyst, O., P.J. Margetts, and N. Topley, *The pathophysiology of the peritoneal membrane.* J Am Soc Nephrol, 2010. **21**(7): p. 1077-85.

159. Gonzalez-Mateo, G.T., et al., *[Animal models of peritoneal dialysis: relevance, difficulties, and future].* Nefrologia, 2008. **28 Suppl 6**: p. 17-22.

160. Nikitidou, O., et al., *Animal models in peritoneal dialysis.* Front Physiol, 2015. **6**: p. 244.

161. Hoff, C.M., *Experimental animal models of encapsulating peritoneal sclerosis.* Perit Dial Int, 2005. **25 Suppl 4**: p. S57-66.

162. Pawlaczyk, K., et al., *Animal Models of Peritoneal Dialysis: Thirty Years of Our Own Experience.* Biomed Res Int, 2015. **2015**: p. 261813.

163. Gonzalez-Mateo, G.T., et al., *Chronic exposure of mouse peritoneum to peritoneal dialysis fluid: structural and functional alterations of the peritoneal membrane.* Perit Dial Int, 2009. **29**(2): p. 227-30.

164. Ferrantelli, E., et al., *A Novel Mouse Model of Peritoneal Dialysis: Combination of Uraemia and Long-Term Exposure to PD Fluid.* Biomed Res Int, 2015. **2015**: p. 106902.

165. Pillay, J., et al., *In vivo labeling with 2H2O reveals a human neutrophil lifespan of 5.4 days.* Blood, 2010. **116**(4): p. 625-7.

166. Tsuda, Y., et al., *Three different neutrophil subsets exhibited in mice with different susceptibilities to infection by methicillin-resistant Staphylococcus aureus.* Immunity, 2004. **21**(2): p. 215-26.

167. Ley, K., et al., *Getting to the site of inflammation: the leukocyte adhesion cascade updated.* Nat Rev Immunol, 2007. **7**(9): p. 678-89.

168. Kansas, G.S., *Selectins and their ligands: current concepts and controversies.* Blood, 1996. **88**(9): p. 3259-87.

169. Marshall, B.T., et al., *Direct observation of catch bonds involving cell-adhesion molecules.* Nature, 2003. **423**(6936): p. 190-3.

170. Simon, S.I., et al., *Neutrophil tethering on E-selectin activates beta 2 integrin binding to ICAM-1 through a mitogen-activated protein kinase signal transduction pathway.* J Immunol, 2000. **164**(8): p. 4348-58.

171. Sligh, J.E., Jr., et al., *Inflammatory and immune responses are impaired in mice deficient in intercellular adhesion molecule 1.* Proc Natl Acad Sci U S A, 1993. **90**(18): p. 8529-33.

172. Phillipson, M., et al., *Intraluminal crawling of neutrophils to emigration sites: a molecularly distinct process from adhesion in the recruitment cascade.* J Exp Med, 2006. **203**(12): p. 2569-75.

173. Cinamon, G., et al., *Chemoattractant signals and beta 2 integrin occupancy at apical endothelial contacts combine with shear stress signals to promote transendothelial neutrophil migration.* J Immunol, 2004. **173**(12): p. 7282-91.

174. Mayadas, T.N., X. Cullere, and C.A. Lowell, *The multifaceted functions of neutrophils.* Annu Rev Pathol, 2014. **9**: p. 181-218.

175. Summers, C., et al., *Neutrophil kinetics in health and disease.* Trends Immunol, 2010. **31**(8): p. 318-24.

176. Jones, S.A., et al., *Different functions for the interleukin 8 receptors (IL-8R) of human neutrophil leukocytes: NADPH oxidase and phospholipase D are activated through IL-8R1 but not IL-8R2.* Proc Natl Acad Sci U S A, 1996. **93**(13): p. 6682-6.

177. Condliffe, A.M., E. Kitchen, and E.R. Chilvers, *Neutrophil priming: pathophysiological consequences and underlying mechanisms.* Clin Sci (Lond), 1998. **94**(5): p. 461-71.

178. Guthrie, L.A., et al., *Priming of neutrophils for enhanced release of oxygen metabolites by bacterial lipopolysaccharide. Evidence for increased activity of the superoxide-producing enzyme.* J Exp Med, 1984. **160**(6): p. 1656-71.

179. Underhill, D.M. and A. Ozinsky, *Phagocytosis of microbes: complexity in action.* Annu Rev Immunol, 2002. **20**: p. 825-52.

180. Swanson, J.A. and A.D. Hoppe, *The coordination of signaling during Fc receptor-mediated phagocytosis.* J Leukoc Biol, 2004. **76**(6): p. 1093-103.

181. Fallman, M., R. Andersson, and T. Andersson, *Signaling properties of CR3 (CD11b/CD18) and CR1 (CD35) in relation to phagocytosis of complement-opsonized particles.* J Immunol, 1993. **151**(1): p. 330-8.

182. Hirsch, J.G. and Z.A. Cohn, *Degranulation of polymorphonuclear leucocytes following phagocytosis of microorganisms.* J Exp Med, 1960. **112**: p. 1005-14.

183. Segal, A.W. and A. Abo, *The biochemical basis of the NADPH oxidase of phagocytes.* Trends Biochem Sci, 1993. **18**(2): p. 43-7.

184. Hampton, M.B., A.J. Kettle, and C.C. Winterbourn, *Inside the neutrophil phagosome: oxidants, myeloperoxidase, and bacterial killing.* Blood, 1998. **92**(9): p. 3007-17.

185. Panday, A., et al., *NADPH oxidases: an overview from structure to innate immunity-associated pathologies.* Cell Mol Immunol, 2015. **12**(1): p. 5-23.

186. Segal, A.W., *The NADPH oxidase and chronic granulomatous disease.* Mol Med Today, 1996. **2**(3): p. 129-35.

187. Rae, J., et al., *X-Linked chronic granulomatous disease: mutations in the CYBB gene encoding the gp91-phox component of respiratory-burst oxidase.* Am J Hum Genet, 1998. **62**(6): p. 1320-31.

188. Noack, D., et al., *Autosomal recessive chronic granulomatous disease caused by defects in NCF-1, the gene encoding the phagocyte p47-phox: mutations not arising in the NCF-1 pseudogenes.* Blood, 2001. **97**(1): p. 305-11.

189. Roos, D., et al., *Mutations in the X-linked and autosomal recessive forms of chronic granulomatous disease.* Blood, 1996. **87**(5): p. 1663-81.

190. Lacy, P., *Mechanisms of degranulation in neutrophils.* Allergy Asthma Clin Immunol, 2006. **2**(3): p. 98-108.

191. Toonen, R.F. and M. Verhage, *Vesicle trafficking: pleasure and pain from SM genes.* Trends Cell Biol, 2003. **13**(4): p. 177-86.

192. Burgoyne, R.D. and A. Morgan, *Secretory granule exocytosis.* Physiol Rev, 2003. **83**(2): p. 581-632.

193. Segal, A.W., J. Dorling, and S. Coade, *Kinetics of fusion of the cytoplasmic granules with phagocytic vacuoles in human polymorphonuclear leukocytes. Biochemical and morphological studies.* J Cell Biol, 1980. **85**(1): p. 42-59.

194. Briggs, R.T., et al., *Superoxide production by polymorphonuclear leukocytes. A cytochemical approach.* Histochemistry, 1986. **84**(4-6): p. 371-8.

195. Bianchi, M., et al., *Restoration of anti-Aspergillus defense by neutrophil extracellular traps in human chronic granulomatous disease after gene therapy is calprotectin-dependent.* J Allergy Clin Immunol, 2011. **127**(5): p. 1243-52 e7.

196. Byrd, A.S., et al., *An extracellular matrix-based mechanism of rapid neutrophil extracellular trap formation in response to Candida albicans.* J Immunol, 2013. **190**(8): p. 4136-48.

197. Papayannopoulos, V. and A. Zychlinsky, *NETs: a new strategy for using old weapons.* Trends Immunol, 2009. **30**(11): p. 513-21.

198. Clark, S.R., et al., *Platelet TLR4 activates neutrophil extracellular traps to ensnare bacteria in septic blood.* Nat Med, 2007. **13**(4): p. 463-9.

199. Hakkim, A., et al., *Impairment of neutrophil extracellular trap degradation is associated with lupus nephritis.* Proc Natl Acad Sci U S A, 2010. **107**(21): p. 9813-8.

200. Rice, C.M., *Interleukin-6 control of neutrophil effector function*, in *School of Medicine*. 2014, Cardiff University.

201. Schmittgen, T.D. and K.J. Livak, *Analyzing real-time PCR data by the comparative C(T) method.* Nat Protoc, 2008. **3**(6): p. 1101-8.

202. Livak, K.J. and T.D. Schmittgen, *Analysis of relative gene expression data using real-time quantitative PCR and the 2(-Delta Delta C(T)) Method.* Methods, 2001. **25**(4): p. 402-8.

203. Fenwick, N., G. Griffin, and C. Gauthier, *The welfare of animals used in science: how the "Three Rs" ethic guides improvements.* Can Vet J, 2009. **50**(5): p. 523-30.

204. Metzker, M.L., *Sequencing technologies - the next generation.* Nat Rev Genet, 2010. **11**(1): p. 31-46.

205. Wang, Z., M. Gerstein, and M. Snyder, *RNA-Seq: a revolutionary tool for transcriptomics.* Nat Rev Genet, 2009. **10**(1): p. 57-63.

206. Ozsolak, F. and P.M. Milos, *RNA sequencing: advances, challenges and opportunities.* Nat Rev Genet, 2011. **12**(2): p. 87-98.

207. Pennisi, E., *Genomics. Semiconductors inspire new sequencing technologies.* Science, 2010. **327**(5970): p. 1190.

208. Rusk, N., *Torrents of sequence.* Nat Meth, 2011. **8**(1): p. 44-44.

209. Imbeaud, S., et al., *Towards standardization of RNA quality assessment using user-independent classifiers of microcapillary electrophoresis traces.* Nucleic Acids Res, 2005. **33**(6): p. e56.

210. Schroeder, A., et al., *The RIN: an RNA integrity number for assigning integrity values to RNA measurements.* BMC Mol Biol, 2006. **7**: p. 3.

211. Baker, S.C., et al., *The External RNA Controls Consortium: a progress report.* Nat Methods, 2005. **2**(10): p. 731-4.

212. Dobin, A., et al., *STAR: ultrafast universal RNA-seq aligner.* Bioinformatics, 2013. **29**(1): p. 15-21.

213. Langmead, B. and S.L. Salzberg, *Fast gapped-read alignment with Bowtie 2.* Nat Methods, 2012. **9**(4): p. 357-9.

214. Andrews, S. *FastQC: a quality control tool for high throughput sequence data.* 2010; Available from: http://www.bioinformatics.babraham.ac.uk/projects/fastqc.

215. Parekh, S., et al., *The impact of amplification on differential expression analyses by RNA-seq.* Sci Rep, 2016. **6**: p. 25533.

216. Li, X., et al., *Quality control of RNA-seq experiments.* Methods Mol Biol, 2015. **1269**: p. 137-46.

217. Griffith, M., et al., *Informatics for RNA Sequencing: A Web Resource for Analysis on the Cloud.* PLoS Comput Biol, 2015. **11**(8): p. e1004393.

218. Williams, A.G., et al., *RNA-seq Data: Challenges in and Recommendations for Experimental Design and Analysis.* Curr Protoc Hum Genet, 2014. **83**: p. 11 13 1-20.

219. Sayols, S., D. Scherzinger, and H. Klein, *dupRadar: a Bioconductor package for the assessment of PCR artifacts in RNA-Seq data.* BMC Bioinformatics, 2016. **17**(1): p. 428.

220. Love, M.I., W. Huber, and S. Anders, *Moderated estimation of fold change and dispersion for RNA-seq data with DESeq2.* Genome Biol, 2014. **15**(12): p. 550.

221. Rousseeuw, P.J., *Silhouettes: A graphical aid to the interpretation and validation of cluster analysis.* Journal of Computational and Applied Mathematics, 1987. **20**(November): p. 12.

222. Gove, R. *Using the elbow method to determine the optimal number of clusters for k-means clustering*. December 26, 2017; Available from: https://bl.ocks.org/rpgove/0060ff3b656618e9136b.

223. Robert Tibshirani, G.W.a.T.H., *Estimating the number of clusters in a data set via the gap statistic.* Journal of the Royal Statistical Society, 2000. **63**(63): p. 12.

224. Hartigan, J.A., *Clustering algorithms*. Wiley series in probability and mathematical statistics. 1975, New York,: Wiley. xiii, 351 p.

225. Ensembl. *Glossary, TSL (Transcript Support Level)*. Available from: http://www.ensembl.org/Help/Glossary?id=492.

226. Eisen, M.B., et al., *Cluster analysis and display of genome-wide expression patterns.* Proc Natl Acad Sci U S A, 1998. **95**(25): p. 14863-8.

227. Conesa, A., et al., *A survey of best practices for RNA-seq data analysis.* Genome Biol, 2016. **17**: p. 13.

228. Hoebe, K., E. Janssen, and B. Beutler, *The interface between innate and adaptive immunity*. Nat Immunol, 2004. **5**(10): p. 971-4.

229. Kobayashi, Y., *The role of chemokines in neutrophil biology*. Front Biosci, 2008. **13**: p. 2400-7.

230. *GENE-E*. Available from: https://software.broadinstitute.org/GENE-E/.

231. *Morpheus*. Available from: https://software.broadinstitute.org/morpheus/.

232. *Venn Diagram*. Available from: http://bioinformatics.psb.ugent.be/webtools/Venn/.

233. Wickham, H., *Ggplot2 : elegant graphics for data analysis*. Use R! 2009, New York: Springer. viii, 212 p.

234. Fasano, G. and A. Franceschini, *A multidimensional version of the Kolmogorov–Smirnov test*. Monthly Notices of the Royal Astronomical Society, 1987. **225**(1): p. 155-170.

235. He, F., et al., *Non-parametric MANOVA approaches for non-normal multivariate outcomes with missing values*. Communications in Statistics - Theory and Methods, 2017. **46**(14): p. 7188-7200.

236. *Ingenuity Pathway Analysis*. Available from: https://www.qiagenbioinformatics.com/products/ingenuity-pathway-analysis.

237. Jaccard, P., *Etude de la distribution florale dans une portion des Alpes et du Jura*. Vol. 37. 1901. 547-579.

238. Strunk, T., et al., *TLR2 mediates recognition of live Staphylococcus epidermidis and clearance of bacteremia*. PLoS One, 2010. **5**(4): p. e10111.

239. Kolaczkowska, E. and P. Kubes, *Neutrophil recruitment and function in health and inflammation*. Nat Rev Immunol, 2013. **13**(3): p. 159-75.

240. Mouw, J.K., G. Ou, and V.M. Weaver, *Extracellular matrix assembly: a multiscale deconstruction*. Nat Rev Mol Cell Biol, 2014. **15**(12): p. 771-85.

241. Hediger, M.A., et al., *The ABCs of membrane transporters in health and disease (SLC series): introduction*. Mol Aspects Med, 2013. **34**(2-3): p. 95-107.

242. Schaible, U.E. and S.H. Kaufmann, *Iron and microbial infection*. Nat Rev Microbiol, 2004. **2**(12): p. 946-53.

243. Greenhill, C.J., et al., *IL-6 trans-signaling modulates TLR4-dependent inflammatory responses via STAT3*. J Immunol, 2011. **186**(2): p. 1199-208.

244. Arts, R.J., et al., *TREM-1: intracellular signaling pathways and interaction with pattern recognition receptors*. J Leukoc Biol, 2013. **93**(2): p. 209-15.

245. Bleharski, J.R., et al., *A role for triggering receptor expressed on myeloid cells-1 in host defense during the early-induced and adaptive phases of the immune response*. J Immunol, 2003. **170**(7): p. 3812-8.

246. Roe, K., S. Gibot, and S. Verma, *Triggering receptor expressed on myeloid cells-1 (TREM-1): a new player in antiviral immunity?* Front Microbiol, 2014. **5**: p. 627.

247. McDermid, J.M. and A.M. Prentice, *Iron and infection: effects of host iron status and the iron-regulatory genes haptoglobin and NRAMP1 (SLC11A1) on host-pathogen interactions in tuberculosis and HIV.* Clin Sci (Lond), 2006. **110**(5): p. 503-24.

248. Goetz, D.H., et al., *The neutrophil lipocalin NGAL is a bacteriostatic agent that interferes with siderophore-mediated iron acquisition.* Mol Cell, 2002. **10**(5): p. 1033-43.

249. Chan, Y.R., et al., *Lipocalin 2 is required for pulmonary host defense against Klebsiella infection.* J Immunol, 2009. **182**(8): p. 4947-56.

250. Peyssonnaux, C., et al., *HIF-1alpha expression regulates the bactericidal capacity of phagocytes.* J Clin Invest, 2005. **115**(7): p. 1806-15.

251. Dienz, O. and M. Rincon, *The effects of IL-6 on CD4 T cell responses.* Clin Immunol, 2009. **130**(1): p. 27-33.

252. Longhi, M.P., et al., *Interleukin-6 is crucial for recall of influenza-specific memory CD4 T cells.* PLoS Pathog, 2008. **4**(2): p. e1000006.

253. Rochman, I., W.E. Paul, and S.Z. Ben-Sasson, *IL-6 increases primed cell expansion and survival.* J Immunol, 2005. **174**(8): p. 4761-7.

254. Shoulders, M.D. and R.T. Raines, *Collagen structure and stability.* Annu Rev Biochem, 2009. **78**: p. 929-58.

255. Orgel, J.P., T.J. Wess, and A. Miller, *The in situ conformation and axial location of the intermolecular cross-linked non-helical telopeptides of type I collagen.* Structure, 2000. **8**(2): p. 137-42.

256. Lucero, H.A. and H.M. Kagan, *Lysyl oxidase: an oxidative enzyme and effector of cell function.* Cell Mol Life Sci, 2006. **63**(19-20): p. 2304-16.

257. Frantz, C., K.M. Stewart, and V.M. Weaver, *The extracellular matrix at a glance.* J Cell Sci, 2010. **123**(Pt 24): p. 4195-200.

258. Prehm, P., *Hyaluronate is synthesized at plasma membranes.* Biochem J, 1984. **220**(2): p. 597-600.

259. Prehm, P., *Release of hyaluronate from eukaryotic cells.* Biochem J, 1990. **267**(1): p. 185-9.

260. Mills, K.H., et al., *Cell-mediated immunity to Bordetella pertussis: role of Th1 cells in bacterial clearance in a murine respiratory infection model.* Infect Immun, 1993. **61**(2): p. 399-410.

261. Akhiani, A.A., et al., *Protection against Helicobacter pylori infection following immunization is IL-12-dependent and mediated by Th1 cells.* J Immunol, 2002. **169**(12): p. 6977-84.

262. Salgame, P., *Host innate and Th1 responses and the bacterial factors that control Mycobacterium tuberculosis infection.* Curr Opin Immunol, 2005. **17**(4): p. 374-80.

263. Meraz, M.A., et al., *Targeted disruption of the Stat1 gene in mice reveals unexpected physiologic specificity in the JAK-STAT signaling pathway.* Cell, 1996. **84**(3): p. 431-42.

264. Durbin, J.E., et al., *Targeted disruption of the mouse Stat1 gene results in compromised innate immunity to viral disease.* Cell, 1996. **84**(3): p. 443-50.

265. Kuo, H.J., et al., *Type VI collagen anchors endothelial basement membranes by interacting with type IV collagen.* J Biol Chem, 1997. **272**(42): p. 26522-9.

266. Nareyeck, G., et al., *Differential interactions of decorin and decorin mutants with type I and type VI collagens.* Eur J Biochem, 2004. **271**(16): p. 3389-98.

267. Campo, G.M., et al., *TNF-alpha, IFN-gamma, and IL-1beta modulate hyaluronan synthase expression in human skin fibroblasts: synergistic effect by concomital treatment with FeSO4 plus ascorbate.* Mol Cell Biochem, 2006. **292**(1-2): p. 169-78.

268. Slevin, M., et al., *Hyaluronan-mediated angiogenesis in vascular disease: uncovering RHAMM and CD44 receptor signaling pathways.* Matrix Biol, 2007. **26**(1): p. 58-68.

269. Jiang, D., J. Liang, and P.W. Noble, *Hyaluronan as an immune regulator in human diseases.* Physiol Rev, 2011. **91**(1): p. 221-64.

270. Khan, T., et al., *Metabolic dysregulation and adipose tissue fibrosis: role of collagen VI.* Mol Cell Biol, 2009. **29**(6): p. 1575-91.

271. Martinez-Hernandez, A. and P.S. Amenta, *The hepatic extracellular matrix. II. Ontogenesis, regeneration and cirrhosis.* Virchows Arch A Pathol Anat Histopathol, 1993. **423**(2): p. 77-84.

272. Veidal, S.S., et al., *MMP mediated degradation of type VI collagen is highly associated with liver fibrosis--identification and validation of a novel biochemical marker assay.* PLoS One, 2011. **6**(9): p. e24753.

273. Stickel, F., et al., *Serum collagen type VI and XIV and hyaluronic acid as early indicators for altered connective tissue turnover in alcoholic liver disease.* Dig Dis Sci, 2001. **46**(9): p. 2025-32.

274. Freise, C., et al., *The alpha 2 chain of collagen type VI sequesters latent proforms of matrix-metalloproteinases and modulates their activation and activity.* Matrix Biol, 2009. **28**(8): p. 480-9.

275. Kaplanski, G., et al., *IL-6: a regulator of the transition from neutrophil to monocyte recruitment during inflammation.* Trends Immunol, 2003. **24**(1): p. 25-9.

276. Xing, Z., et al., *IL-6 is an antiinflammatory cytokine required for controlling local or systemic acute inflammatory responses.* J Clin Invest, 1998. **101**(2): p. 311-20.

277. Chalaris, A., et al., *Apoptosis is a natural stimulus of IL6R shedding and contributes to the proinflammatory trans-signaling function of neutrophils.* Blood, 2007. **110**(6): p. 1748-55.

278. Wright, H.L., et al., *Effects of IL-6 and IL-6 blockade on neutrophil function in vitro and in vivo.* Rheumatology (Oxford), 2014. **53**(7): p. 1321-31.

279. Mullen, P.G., et al., *Tumor necrosis factor-alpha and interleukin-6 selectively regulate neutrophil function in vitro.* J Surg Res, 1995. **58**(2): p. 124-30.

280. Venturi, G.M., et al., *Leukocyte migration is regulated by L-selectin endoproteolytic release.* Immunity, 2003. **19**(5): p. 713-24.

281. Kishimoto, T.K., M.A. Jutila, and E.C. Butcher, *Identification of a human peripheral lymph node homing receptor: a rapidly down-regulated adhesion molecule.* Proc Natl Acad Sci U S A, 1990. **87**(6): p. 2244-8.

282. Dewald, B., M. Thelen, and M. Baggiolini, *Two transduction sequences are necessary for neutrophil activation by receptor agonists.* J Biol Chem, 1988. **263**(31): p. 16179-84.

283. Woolley, J.F., J. Stanicka, and T.G. Cotter, *Recent advances in reactive oxygen species measurement in biological systems.* Trends Biochem Sci, 2013. **38**(11): p. 556-65.

284. Pelletier, M.G., et al., *Characterization of neutrophils and macrophages from ex vivo-cultured murine bone marrow for morphologic maturation and functional responses by imaging flow cytometry.* Methods, 2017. **112**: p. 124-146.

285. Narazaki, M., et al., *Soluble forms of the interleukin-6 signal-transducing receptor component gp130 in human serum possessing a potential to inhibit signals through membrane-anchored gp130.* Blood, 1993. **82**(4): p. 1120-6.

286. Tanaka, M., et al., *Cloning of novel soluble gp130 and detection of its neutralizing autoantibodies in rheumatoid arthritis.* J Clin Invest, 2000. **106**(1): p. 137-44.

287. Zhang, J.G., et al., *Identification and characterization of two distinct truncated forms of gp130 and a soluble form of leukemia inhibitory factor receptor alpha-chain in normal human urine and plasma.* J Biol Chem, 1998. **273**(17): p. 10798-805.

288. Sommer, J., et al., *Alternative intronic polyadenylation generates the interleukin-6 trans-signaling inhibitor sgp130-E10.* J Biol Chem, 2014. **289**(32): p. 22140-50.

289. Matsuda, T. and T. Hirano, *Establishment of the ELISA for murine soluble gp130, a signal transducer for the IL-6 family cytokine, and its detection in the ascitic fluids*

of tumor-bearing mice. Biochem Biophys Res Commun, 1994. **202**(1): p. 637-42.

290. Yates, A., et al., *Ensembl 2016.* Nucleic Acids Res, 2016. **44**(D1): p. D710-6.

291. Anders, S., A. Reyes, and W. Huber, *Detecting differential usage of exons from RNA-seq data.* Genome Res, 2012. **22**(10): p. 2008-17.

292. Trapnell, C., et al., *Transcript assembly and quantification by RNA-Seq reveals unannotated transcripts and isoform switching during cell differentiation.* Nat Biotechnol, 2010. **28**(5): p. 511-5.

293. Saito, M., et al., *Molecular cloning of a murine IL-6 receptor-associated signal transducer, gp130, and its regulated expression in vivo.* J Immunol, 1992. **148**(12): p. 4066-71.

294. Dagil, R., et al., *The WSXWS motif in cytokine receptors is a molecular switch involved in receptor activation: insight from structures of the prolactin receptor.* Structure, 2012. **20**(2): p. 270-82.

295. Yoshimura, A., et al., *Mutations in the Trp-Ser-X-Trp-Ser motif of the erythropoietin receptor abolish processing, ligand binding, and activation of the receptor.* J Biol Chem, 1992. **267**(16): p. 11619-25.

296. Katz, Y., et al., *Analysis and design of RNA sequencing experiments for identifying isoform regulation.* Nat Methods, 2010. **7**(12): p. 1009-15.

297. Labaj, P.P., et al., *Characterization and improvement of RNA-Seq precision in quantitative transcript expression profiling.* Bioinformatics, 2011. **27**(13): p. i383-91.

298. Garber, M., et al., *Computational methods for transcriptome annotation and quantification using RNA-seq.* Nat Methods, 2011. **8**(6): p. 469-77.

299. Baliga, N. *What is Systems Biology*. Available from: https://www.systemsbiology.org/about/what-is-systems-biology/.

300. Chuang, H.Y., M. Hofree, and T. Ideker, *A decade of systems biology.* Annu Rev Cell Dev Biol, 2010. **26**: p. 721-44.

301. Avalle, L., et al., *STAT1 and STAT3 in tumorigenesis: A matter of balance.* JAKSTAT, 2012. **1**(2): p. 65-72.

302. Hirahara, K., et al., *Asymmetric Action of STAT Transcription Factors Drives Transcriptional Outputs and Cytokine Specificity.* Immunity, 2015. **42**(5): p. 877-89.

303. Wan, C.K., et al., *Opposing roles of STAT1 and STAT3 in IL-21 function in CD4+ T cells.* Proc Natl Acad Sci U S A, 2015. **112**(30): p. 9394-9.

304. Costa-Pereira, A.P., et al., *Mutational switch of an IL-6 response to an interferon-gamma-like response.* Proc Natl Acad Sci U S A, 2002. **99**(12): p. 8043-7.

305. Qing, Y. and G.R. Stark, *Alternative activation of STAT1 and STAT3 in response to interferon-gamma.* J Biol Chem, 2004. **279**(40): p. 41679-85.

306. Regis, G., et al., *Ups and downs: the STAT1:STAT3 seesaw of Interferon and gp130 receptor signalling.* Semin Cell Dev Biol, 2008. **19**(4): p. 351-9.

307. Steward-Tharp, S.M., et al., *A mouse model of HIES reveals pro- and anti-inflammatory functions of STAT3.* Blood, 2014. **123**(19): p. 2978-87.

308. Holland, S.M., et al., *STAT3 mutations in the hyper-IgE syndrome.* N Engl J Med, 2007. **357**(16): p. 1608-19.

309. Kano, A., et al., *Endothelial cells require STAT3 for protection against endotoxin-induced inflammation.* J Exp Med, 2003. **198**(10): p. 1517-25.

310. El-Benna, J., et al., *Priming of the neutrophil respiratory burst: role in host defense and inflammation.* Immunol Rev, 2016. **273**(1): p. 180-93.

311. Vahedi, G., et al., *Super-enhancers delineate disease-associated regulatory nodes in T cells.* Nature, 2015. **520**(7548): p. 558-62.

312. Ellis, T.N. and B.L. Beaman, *Interferon-gamma activation of polymorphonuclear neutrophil function.* Immunology, 2004. **112**(1): p. 2-12.

313. Shalaby, M.R., et al., *Activation of human polymorphonuclear neutrophil functions by interferon-gamma and tumor necrosis factors.* J Immunol, 1985. **135**(3): p. 2069-73.

314. Marciano, B.E., et al., *Long-term interferon-gamma therapy for patients with chronic granulomatous disease.* Clin Infect Dis, 2004. **39**(5): p. 692-9.

315. Ogata, H., et al., *Deletion of the SOCS3 gene in liver parenchymal cells promotes hepatitis-induced hepatocarcinogenesis.* Gastroenterology, 2006. **131**(1): p. 179-93.

316. Loeffler, S., et al., *Interleukin-6 induces transcriptional activation of vascular endothelial growth factor (VEGF) in astrocytes in vivo and regulates VEGF promoter activity in glioblastoma cells via direct interaction between STAT3 and Sp1.* Int J Cancer, 2005. **115**(2): p. 202-13.

317. Zhang, Z., et al., *STAT3 acts as a co-activator of glucocorticoid receptor signaling.* J Biol Chem, 1997. **272**(49): p. 30607-10.